NASA Contractor Report 191111

A Model of Concurrent Flow Flame Spread Over a Thin Solid Fuel

Paul V. Ferkul
Case Western Reserve University
Cleveland, Ohio

Prepared for
Lewis Research Center
Under Grant NAG3-1046

National Aeronautics and Space Administration

A MODEL OF CONCURRENT FLOW FLAME SPREAD OVER A THIN SOLID FUEL

Paul Vincent Ferkul
Case Western Reserve University
Cleveland, Ohio 44106

Abstract

A numerical model is developed to examine laminar flame spread and extinction over a thin solid fuel in low-speed concurrent flows. The model provides a more precise fluid-mechanical description of the flame by incorporating an elliptic treatment of the upstream flame stabilization zone near the fuel burnout point. Parabolic equations are used to treat the downstream flame, which has a higher flow Reynolds number. The parabolic and elliptic regions are coupled smoothly by an appropriate matching of boundary conditions. The solid phase consists of an energy equation with surface radiative loss and a surface pyrolysis relation. Steady spread with constant flame and pyrolysis lengths is found possible for thin fuels and this facilitates the adoption of a moving coordinate system attached to the flame with the flame spread rate being an eigenvalue. Calculations are performed in purely forced flow in a range of velocities which are lower than those induced in a normal gravity buoyant environment. Both quenching and

blowoff extinction are observed. The results show that as flow velocity or oxygen percentage is reduced, the flame spread rate, the pyrolysis length, and the flame length all decrease, as expected. The flame standoff distance from the solid and the reaction zone thickness, however, first increase with decreasing flow velocity, but eventually decrease very near the quenching extinction limit. The short, diffuse flames observed at low flow velocities and oxygen levels are consistent with available experimental data. The maximum flame temperature decreases slowly at first as flow velocity is reduced, then falls more steeply close to the quenching extinction limit. Low velocity quenching occurs as a result of heat loss. At low velocities, surface radiative loss becomes a significant fraction of the total combustion heat release. In addition, the shorter flame length causes an increase in the fraction of conduction downstream compared to conduction to the fuel. These heat losses lead to lower flame temperatures, and ultimately, extinction. This extinction mechanism differs from that of blowoff, where the flame is unable to be stabilized due to the high flow velocity.

Table of Contents

List of Figures

Nomenclature

$\overline{A}_s$	Solid Phase Pre-Exponential Factor (3.8×10^7 cm/s)
$\overline{B}_g$	Gas Phase Pre-Exponential Factor (1.0×10^{13} cm^3/g/s)
$\overline{C}_p$	Gas Phase Specific Heat (0.33 cal/g/K)
$\overline{C}_s$	Solid Phase Specific Heat (0.30 cal/g/K)
Da	Damkohler Number, $\overline{\alpha}^* \overline{\rho}^* \overline{B}_g / \overline{U}_R^2$
D_i	Diffusion Coefficient of i (i = F or O), $\overline{D}_i / \overline{D}_i^* = (\overline{T}/\overline{T}^*)^2$
$\overline{D}_i^*$	Reference Diffusion Coeffient (2.13 cm^2/s)
$\overline{E}_g$	Gas Phase Activation Energy (2.7×10^4 cal/gmol)
E_g	$\overline{E}_g / \overline{R} / \overline{T}_\infty$ (45.3)
$\overline{E}_s$	Solid Phase Activation Energy (3.0×10^4 cal/gmol)
E_s	$\overline{E}_s / \overline{R} / \overline{T}_\infty$ (50.3)
f	Oxygen/Fuel Stoichiometric Mass Ratio (1.185)
$\overline{g}$	Gravity Level (0.0 cm/s^2)
Gr	Grashof Number, $\overline{\alpha}^* \overline{g} / \overline{U}_R^3$ (0.0)
h	Solid Thickness, $\overline{h} / \overline{x}_R$
$\overline{L}$	Latent Heat of Fuel (-180 cal/g)
L	$\overline{L} / \overline{C}_s / \overline{T}_\infty$ (-2.00)
Le_i	Lewis Number of i (i = F or O), $\overline{\alpha}^* / \overline{D}_i^*$ (1.0)
$\dot{m}$	Mass Flux from Fuel, $\dot{m} / \overline{\rho}^* / \overline{U}_R$
P	Pressure, $(\overline{P} - \overline{P}_\infty) / \overline{\rho}^* / \overline{U}_R^2$
$\overline{P}_\infty$	Ambient Pressure (1 atm)
Pr	Prandtl Number, $\overline{\nu}^* / \overline{\alpha}^*$ (0.7)
$\overline{Q}$	Heat of Combustion (4.00×10^3 cal/g)
Q	$\overline{Q} / \overline{C}_p / \overline{T}_\infty$ (40.4)
$\dot{Q}$	Energy Source Term, $-Q\dot{\omega}_F$
q_y	Heat Flux to Solid, $\kappa (\partial T / \partial y)_w$
$\overline{R}$	Ideal Gas Constant (1.989 cal/gmol/K)
s	Distance Along Fuel Surface, $\overline{s} / \overline{x}_R$
T	Temperature, $\overline{T} / \overline{T}_\infty$
$\overline{T}_\infty$	Ambient Temperature (300 K)
$\overline{T}^*$	Reference Temperature (1250 K)
T^*	$\overline{T}^* / \overline{T}_\infty$ (4.167)

$\overline{T}_F$ Adiabatic Flame Temperature (2200 K)

$\overline{T}_L$ Temperature at which $\overline{L}$ is given (300 K)

T_L $\overline{T}_L/\overline{T}_\infty$ (1.0)

$\overline{T}_s$ Solid Temperature

T_s $\overline{T}_s/\overline{T}_\infty$

u Velocity in x-direction, $\overline{u}/\overline{U}_R$

$\overline{U}_B$ Reference Buoyant Velocity, $(\overline{\alpha}^*\overline{g})^{1/3}$

$\overline{U}_R$ Reference Velocity, $\overline{U}_\infty + \overline{U}_B - \overline{V}_F$

$\overline{U}_\infty$ Forced Flow Velocity

v Velocity in y-direction, $\overline{v}/\overline{U}_R$

$\overline{V}_F$ Flame Spread Rate

x x-coordinate, $\overline{x}/\overline{x}_R$

$\overline{x}_R$ Reference Length, $\overline{\alpha}^*/\overline{U}_R$

y y-coordinate, $\overline{y}/\overline{x}_R$

Y_F Fuel Mass Fraction

Y_O Oxygen Mass Fraction

$Y_{O,\infty}$ Ambient Oxygen Mass Fraction

$\overline{\alpha}^*$ Reference Thermal Diffusivity ($2.13\ cm^2/s$)

Γ Solid Phase Radiation Parameter, $\overline{\sigma}\varepsilon\overline{T}_\infty^3/(\overline{\rho}^*\overline{C}_P\overline{U}_R)$

ε Solid Emissivity (1.0)

κ Gas Thermal Conductivity, $\overline{\kappa}/\overline{\kappa}^* = \overline{T}/\overline{T}^*$

$\overline{\kappa}^*$ Reference Thermal Conductivity (1.93×10^{-4} cal/cm/s/K)

μ Gas Viscosity, $\overline{\mu}/\overline{\mu}^* = \overline{T}/\overline{T}^*$

$\overline{\mu}^*$ Reference Gas Viscosity (4.10×10^{-4} g/cm/s)

Ξ Solid Phase Parameter, $\overline{\rho}_s\overline{V}_F\overline{C}_s/\overline{\rho}^*/\overline{U}_R/\overline{C}_P$

ρ Gas Density, $\overline{\rho}/\overline{\rho}^*$

$\overline{\rho}^*$ Reference Density (2.75×10^{-4} g/cm^3)

$\overline{\rho}_\infty$ Ambient Density (1.15×10^{-3} g/cm^3)

ρ_∞ Density, $\overline{\rho}_\infty/\overline{\rho}^*$ (4.167)

$\overline{\rho}_s$ Solid Density (0.263 g/cm^3)

$\overline{\sigma}$ Stefan-Boltzmann Constant (1.356×10^{-12} cal/cm^2/K^4/s)

$\overline{\tau}$ Fuel Half-Thickness (0.0038 cm)

$\dot{\omega}_F$ Fuel Source Term, $-Da\rho^2Y_FY_O\exp(-E_g/T)$

$\dot{\omega}_O$ Oxygen Source Term, $f\dot{\omega}_F$

Subscripts

B	Buoyant
f	Flame
F	Fuel or Flame
g	Gas Phase
h	Heat up
i	Species i = F or O
L	Refers to Latent Heat
max	Maximum
min	Minimum
O	Oxygen
P	Pyrolysis, Pressure
par	Refers to parabolic region
prod	Products
R	Reference
s	Solid Phase
S	Stand-off
T	Thickness
w	Value at Fuel Surface
y	Along the y-direction
∞	Value at Far Field

Superscripts

*	Evaluated at T*

Note: A bar above a variable indicates that it is a dimensional quantity.

Chapter 1. Introduction

The study of combustion in a microgravity environment offers a chance to examine aspects of flames without the complicating influence of natural convection.[1] Recently, interest in microgravity combustion has been steadily increasing. This is due in large part to experiments already performed in microgravity, each of which has revealed new and exciting combustion phenomena.[2]

While the body of scientific knowledge of microgravity combustion has been getting larger, there is still an ever increasing series of new questions which arise. Therefore, the demand for microgravity facilities (such as the Space Shuttle, drop towers, and Keplerian trajectory aircraft) has increased considerably.

In addition to the scientific reasons, a practical concern of studying combustion in microgravity is spacecraft fire safety. In a recent paper detailing past and present fire safety practices aboard spacecraft, it is concluded, among other things, that "the microgravity research community has much to offer advanced spacecraft fire safety."[3]

As is true with any scientific research effort, an experiment should be complemented by a theoretical investigation. The theoretical side of the research is often guided by the experiment, but likewise can aid in the

selection of the experiment. When seen in this light, the theoretical effort is simply the formalization and expansion of the knowledge obtained in the experiment.

Additionally, a sound theory is useful in predicting results when an experiment is infeasible. This is especially evident in microgravity studies. Any earthbound facility is limited in its ability to provide a microgravity environment, and of course a space experiment is very costly. Thus, a capable theory becomes a valuable tool both in understanding and predicting the physics of the problem.

1.1. Classes of Solid Combustion

Solid combustion is a broad field. Its study is made tractable by dividing it into several classes. First, almost all common fires are composed of diffusion flames. A diffusion flame initially separates the fuel and oxidizer, which diffuse into the flame zone and react, hence the name.*

Flames can be stationary or spreading. A stationary flame is established when only a fixed area is exposed to the flame. On the other hand, a spreading flame, which is of more practical concern, greatly depends on the rate at

---

*In a premixed flame, on the other hand, the fuel and oxidizer are initially mixed. The combustion of a double-base solid propellant is an example.

which the solid fuel can be heated up to its pyrolysis temperature. Thus, any prediction of a spreading flame needs to consider the solid phase.

A further division is made by considering the direction of the oxidizer flow relative to the direction of flame spread, shown in fig. 1. In opposed flow flame spread, the flame spreads in the direction opposite the flow (fig. 1a), while in concurrent flow flame spread, the flame spreads in the same direction as the flow (fig. 1b). The oxidizer stream can consist of forced flow, buoyant flow, or a combination of the two. On earth, a hot flame generates buoyant flow up. Thus, a flame spreading downward spreads in opposed flow mode, and a flame spreading upward spreads in concurrent flow mode.

Concurrent flow flame spread has received much attention, since fires of practical interest are most hazardous in this configuration. Many experiments and analytic studies have been performed on concurrent flow flame spread. Detailed numerical predictions have been somewhat hindered by the complicated nature of the problem, since the flames are often large, turbulent, and radiant.

Whether opposed flow or concurrent flow, certain fundamental mechanisms apply. The flame transfers heat to the solid by conduction and radiation. This heat causes the solid to gasify, and the gaseous fuel then flows toward

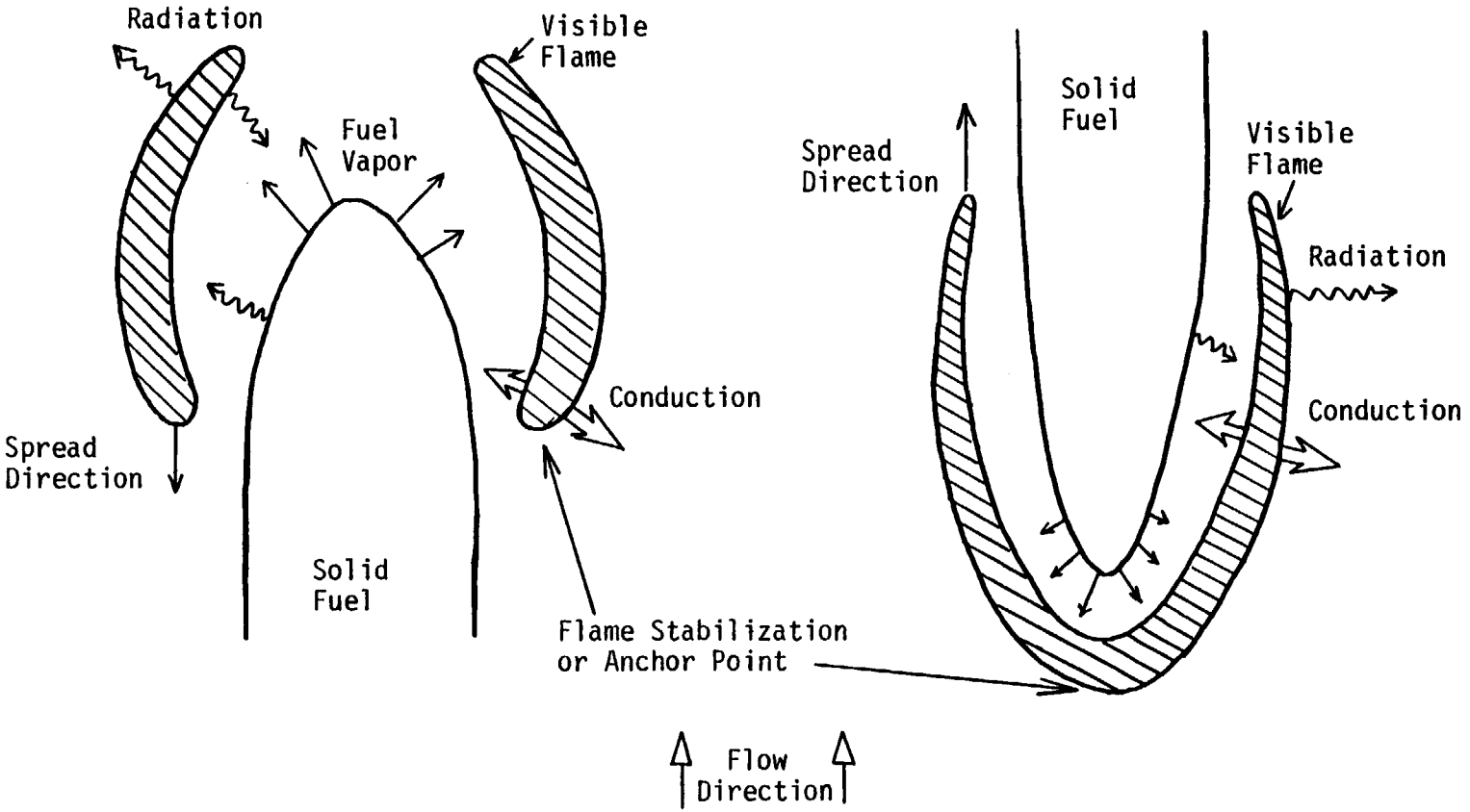

(a) Opposed flow flame spread

(b) Concurrent flow flame spread

Figure 1. Flame spread over solids.

the flame. In the flame zone, fuel and oxygen come together, react, and sustain the flame. The flame is stabilized in a position that balances the complicated flows of heat and mass.

To get a complete understanding of these flames, we are interested not only in their structure and spread characteristics, but also in extinction (or how they go out). Everyone is familiar to some degree with the effect of flow velocity on flames. For example, gently blowing on a weak fire usually intensifies it. However, blow too hard, and the fire will go out. This "blowoff" is due to the fact that too much oxygen is supplied to the flame. The reaction rate in the flame zone simply cannot keep pace with the high flow rate of oxygen, and the flame is literally blown away. Blowoff extinction has been studied extensively.

On the other side of the coin, what would happen to a flame if the flow of oxygen were reduced steadily, perhaps all the way to zero? In the gravitational field of earth, we cannot answer this question, since buoyant flows (on the order of tens of centimeters per second) will always accompany any flame. By studying flames in microgravity, we can endeavor to answer this and other questions. Will the flame burn continuously, or will it eventually go out? Why? What is the effect of low-speed flow on the flame?

A theoretical model[4] suggests that the flame will eventually go out as the flow velocity is reduced. The reason is that heat loss becomes important. The heat loss reduces the flame temperature below the point that combustion can be sustained.

In this effort, concurrent-flow flame spread over a thin fuel in zero gravity* is to be studied. The flow field is generated by purely forced convection. (There is no buoyant flow since gravity is assumed to be zero.) Whenever we say "thin fuel" we mean hydrodynamically and thermally thin. Hydrodynamically thin means that the thickness of the fuel is always much smaller than the distance of the flame from the fuel surface (or, equivalently, the gas phase length scale). Thermally thin means that the rate of conduction in depth of the solid fuel is much faster than the heat up rate of the gas phase along the fuel surface (effectively, this means that the temperature is constant across the fuel thickness).

Before proceeding with a detailed explanation of the problem, a brief presentation of earlier related work on solid phase flame spread is given below. The following discussion is not intended to be an exhaustive review, but

---

*In a spacecraft, a microgravity environment exists. We consider strictly zero gravity, however, as a starting point. To model microgravity effects, buoyant and inertial forces should be considered.

instead outlines the historical framework which provided the motivation for this work.

1.2. Solid Phase Combustion Modelling Techniques

The earliest models relied on heat transfer arguments to obtain expressions for global parameters (e.g., spread rate) in terms of other known quantities. Despite their simplicity, trends were predicted fairly well. (Today, more sophisticated analytical predictions of piloted ignition and flame spread using fuel and environment parameters as inputs are used to try to cover a wide range of conditions.[5])

More sophisticated models solved conservation equations to obtain a better understanding of the flames. The earliest of these solved parabolic (or boundary layer type) equations. Sometimes, similarity solutions existed. Otherwise, these equations could be solved by a numerical marching scheme, i.e., given an initial profile, the downstream profile at the next grid point could be found immediately. Furthermore, the "flame sheet" approximation was made. This assumed that as soon as the fuel and oxidizer met, they reacted (infinitely fast). This neglected the detailed chemical reaction effects.

Later models began to include real, finite-rate chemical reaction effects. The added difficulty was in the evaluation of highly non-linear Arrhenius rate relations.

Finally, models included the complete (elliptic) conservation equations, together with finite-rate reaction expressions. The solution of elliptic equations is considerably more difficult than parabolic equations, since any point in the domain is, in general, affected by all surrounding points, not only upstream points. Early models of this type assumed a velocity field, but eventually, even the full Navier-Stokes equations were solved.

Some studies of flames above solid fuels were simplified by considering the case where the flame was stationary. How is a stationary flame established? The trick is to allow only a small area of fuel to be exposed, and assume the rate of fuel regression (or burnout) is small. A good simulation of such a flame is made by considering a flame over a fuel soaked wick, or a flame above a porous burner through which fuel is forced. In either case, of course, no burnout can occur. Stationary flame studies are well-suited to examining the flame structure as a function of environmental parameters, but cannot examine flame growth and spread. In the following discussion, both stationary flame and flame spread models will be presented.

1.3. Overview of Early Relevant Solid Combustion Models

An approximately chronological summary of combustion modelling research relevant to this work is presented. As was mentioned previously, only a cursory overview is given.

The reader is advised to examine several review articles[6,7] for a more complete early history, as well as a more recent review.[8]

An early work[9] examined the stationary flame structure of a fuel soaked wick both with an experiment and a numerical model. In the model, laminar, boundary layer type equations were solved to obtain the flame structure in the flame and thermal plume. The initial profile for the equations was provided by a similarity solution which exists over the region where pyrolysis was occurring (i.e., above the wick). Infinitely fast kinetics (flame sheet approximation) were assumed. While the prediction approximated the experimental results fairly accurately, the model was simple by today's standards. Yet, by the authors' own admission, it was too awkward to use for direct flame spread analysis, given their computational capabilities.

A predictive model of flame spread in concurrent flow in several different geometries (floor, ceiling, and wall, e.g.) was produced.[10] The solid phase was unsteady, and the gas phase quasi-steady, i.e., the gas phase response time was much shorter than the characteristic solid time. The gas phase equations were two-dimensional, laminar, and parabolic (boundary layer type). Radiation was neglected, and a flame sheet approximation was made. Using various assumptions, the solid and gas phase equations were

decoupled and a similarity solution was found for all equations except for the species equation downstream of the pyrolysis zone (a similarity solution for the ceiling configuration was not found, however).

One of the limitations of these works was the neglection of finite-rate chemical kinetic effects. Since a flame is a complicated reacting system, the inclusion of an improved chemical model is necessary. The effects of temperature, fuel and oxidizer concentration, flow velocity, and mass diffusion then can be seen to influence flame spread and extinction characteristics through the flame chemistry. Including finite-rate chemistry, the elliptic two-dimensional, quasi-steady gas phase energy and species equations were solved.[11] The flow field was assumed uniform, thus eliminating the need to solve the complicated Navier-Stokes equations. The solid fuel equation neglected conduction ahead of the flame, but included an Arrhenius type pyrolysis relation and unsteady solid phase heat up. Opposed flow flame spread over a thin solid fuel was examined. By considering opposed flow flame spread, the problem is immediately simplified because the flame is not only shorter*, but the spread process only depends on the flame structure at the anchor point, whereas in concurrent

*The shorter flame can make the effects of radiation and turbulence less important.

flow, the entire flame and thermal plume should be considered to predict spread rate. Flame spread and blowoff extinction were obtained, in good agreement with experiment. This model provided the basis for many of the more recent ones, including this work, which are able to utilize improved computer capability and performance.

Another attempt to go beyond the flame sheet assumption was made.[12] A stationary flame calculation, which solved the laminar boundary layer equations for velocity, temperature, and species, included a finite-rate chemical reaction term. As done in earlier work, the initial profile was provided by the similarity solution which exists in the pyrolysis zone. The finite rate chemistry effects led to a shorter flame length and fuel preheat distance. In addition, there was the possibility of fuel vapor escaping from the flame zone unreacted (escaped pyrolyzates or incomplete combustion), which could be quantified.

Modelling continued to move toward a more thorough formulation. The complete elliptic set of equations, including the Navier-Stokes equations, were used to examine the mixed flow* combustion of a vertical fuel plate imbedded in an inert substrate.[13] Laminar, steady flow was

*Mixed flow includes any combination of buoyant and forced flow.

assumed. The fuel plate was 4 centimeters long, and the inert substrate extended 1 centimeter in front of the fuel. Fuel burnout was assumed to be negligible, so a stationary flame existed. The small fixed length of the fuel permitted computation, since a fuel of longer extent would require a prohibitively large computational time. A simple energy balance was used to model the rate of production of pyrolysis products from the fuel. The equations were solved in dimensional form, and results demonstrated the importance of the pressure field in controlling the flow near the flame stabilization point.

A similar examination of a stationary flame stabilized at the leading edge of a fuel plate was carried out.[14] The main difference from the previous work was the fact that the fuel began immediately (i.e., there was no inert plate extension) and the fuel plate extended all the way downstream. Again, the full two-dimensional laminar elliptic equations were solved (here, in nondimensional form) including finite-rate chemical reaction. The effect of flow velocity on the structure of the flame was examined (buoyant flow was neglected). At first, the flame enveloped the fuel completely, but as the flow velocity was increased, the flame retreated downstream, and was eventually blown out of the computational domain. The importance of using elliptic equations to model the stabilization of

the flame was demonstrated. Furthermore, at arbitrarily low flow velocities, a flame which was dimensionally small but kinetically strong was found to exist. This was because, with the neglection of any heat loss mechanism, the flame had plenty of time for the combustion reactions to proceed, but merely reduced its size.

A concurrent flow flame spread model examined the combustion of a thin fuel.[15] This laminar, unsteady formulation was able to predict the initial transitory flame growth period followed by steady flame propagation. The laminar, two-dimensional, elliptic energy and species conservation equations were solved numerically. A simple finite-rate chemical reaction was assumed. Solution of the Navier-Stokes equations was avoided by prescribing a velocity field, in this case, a constant property Hagen-Poiseuille flow. Relatively high velocity forced flows (i.e., 60 cm/s and up) were studied. Some agreement with experimental data was obtained, all the way up to the blowoff limit.

1.4. Microgravity Combustion of Solids: Modelling and Experiments

Up to this point, the discussion has presented work which was not necessarily interested in the effects of microgravity. If gravity was neglected in a work, a high forced flow velocity was substituted. In ref. 14, there

were hints of the utility of studying that type of combustion in a reduced gravity environment. At low forced flow velocities (sub-buoyant), the flame was very small, and could be more susceptible to heat loss effects. Thus, the solid fuel was allowed to lose heat through black body radiation.[16] Now, as the flow velocity was decreased, the flame eventually went out due to the increased relative importance of heat loss. Thus, both quenching and blowoff extinction were observed.

At this time, the importance of an elliptic treatment of the flame stabilization zone was recognized.[17] This is due to the fact that in the stabilization zone, the thermal length is the appropriate scale (meaning the product of the Reynolds and Prandtl numbers is unity, or $Re_x Pr=1$), and thus the Reynolds number in the flame stabilization zone was order unity*. When the Reynolds number is order unity, diffusion of mass, momentum, and heat in both the streamwise and cross-stream directions is important. Thus, elliptic type equations result. A unified presentation of quenching and blowoff extinction for several flame systems was made.

---

*The Prandtl number is order unity for most common gases. It is a measure of the rate of diffusion of momentum to the rate of conduction of heat for a given fluid.

In more concrete terms, the thermal length is found by considering a simple convection/conduction balance. As the cold oxygen stream flows into the flame and is warmed to the flame temperature, its rate of change of energy is given by the expression $\rho u C_p (T_f - T_\infty)$, where ρ, u, and C_p are the gas density, velocity and specific heat respectively. T_f is the flame temperature, and T_∞ is the ambient temperature. This flow is heated by conduction from the flame, given approximately as $\kappa(T_f - T_\infty)/x$, where κ is the thermal conductivity of the gas and x is thermal length. Equating the two expressions yields the thermal length, $x = \kappa/(\rho u C_p)$. Then, defining a Reynolds number based on x, this last expression is equivalent to $Re_x Pr = 1$.

The experimental efforts examining flame spread over solid fuels in microgravity began to expand. Quiescent flame spread over a thin fuel in microgravity* was studied.[18] Experiments were conducted at atmospheric pressure over a range of oxygen percentages from pure oxygen down to the limiting value. Among the findings, quenching extinction was observed in microgravity. It was found to be quite different from blowoff extinction encountered in normal gravity. The flame structure and low flow veloci-

*A flame spreading in a quiescent, microgravity environment spreads in opposed flow mode. This is clear in a flame-fixed coordinate system, where the oxidizer feeds into the flame in the opposed flow configuration.

ties verify the need for an elliptic system of equations to model the problem in that the Reynolds number and Peclet number are order unity. This is especially true for slow flames in microgravity, where the flame stabilization region is a large percentage of the overall flame zone.

The previous results were combined with a study examining the effect of low speed flow on these flames spreading in microgravity[19] to clarify the role of convection on opposed flow flame spread and extinction.[20] An extinction boundary was generated. Another more recent investigation[21] filled in additional data. For a flame burning at a given oxygen percentage, as the characteristic velocity* was increased, the flame would eventually be blown off and as the characteristic velocity was decreased, the flame eventually was quenched. Between the two limits, there was a point where the flame would spread fastest. This point could be at a velocity below that due to normal gravity buoyant flow. Hence, the most hazardous condition from a fire safety standpoint could happen if buoyancy is completely removed and a small forced flow is applied. In

*The characteristic velocity represents the rate at which oxygen is convected into the flame zone. It is best visualized in flame-fixed coordinates. For example, for quiescent opposed flow flame spread, the characteristic velocity is the flame spread rate. For a downward burning flame in a gravitational environment, the characteristic velocity is the magnitude of the buoyant flow at the flame stabilization point, plus the spread rate.

a spacecraft, therefore, ventilation currents may establish this scenario. The importance of further work was clear.

On the modelling front, a sophisticated prediction of opposed flow flame spread characteristics at microgravity was made.[22] Imposed flow velocities from zero (no flow, quiescent spread) all the way up to the blowoff limit, were studied. This steady, laminar, two-dimensional model numerically solved the full Navier-Stokes equations together with elliptic energy and species concentration equations. Radiation from the gas and solid phase, and their interaction, was modelled. Sample flame structures and radiation profiles were given. It was found that flames in microgravity are radiatively controlled, a phenomenon that would be masked in normal gravity. Specifically, results showed that including gas phase radiation greatly changed the flame structure in that a cooler, smaller flame results. Although, by including only surface radiation (and neglecting gas phase radiation completely) flame spread rates and extinction trends were largely unchanged. This suggests that the important aspects of low-speed flame spread modelling can be captured without including the very difficult gas phase radiation treatment, but instead only the essential heat loss mechanism given simply by solid phase radiation. However, it is clear that gas phase radiation is necessary to complete the task of quantita-

tively predicting flames, when detailed chemistry and soot production need to be included.

Very recently, the last model has been upgraded to examine unsteady opposed flow flame spread over thermally thick solid fuels.[23] All of the features were retained, with the exception that a simplified treatment of the gas-phase radiation was made, since computation otherwise would be too slow.

Another current research effort[24] has examined the ignition and spread of a flame in a zero gravity environment. This unsteady model is mainly different from others in the assumption that the velocity field can be calculated using potential flow, relaxing the no-slip boundary condition on the fuel surface. Initial results considered the axisymmetric case of quiescent spread. The case of imposing a slow flow on the flame is under development. Here, a three-dimensional computation is required.

1.5. Combustion Experiments in Space

Finally, some mention of the ultimate microgravity environment will be made. Ideally, we would like to have unlimited time, space, and accessibility to carry out microgravity combustion experiments. The best we can achieve today, with respect to duration and quality of microgravity, is provided by spacecraft such as the Space Shuttle. However because of the large amount of time and

money required to build and perform a space experiment, the study of combustion in a spacecraft environment has been severely limited. In fact, up until a few years ago, only one set of experiments had been performed. In the 1970's, the combustion characteristics of various practical solid materials were examined aboard Skylab.[25] The objectives were very simple, in that only visual observations were made on whether and how the various materials burned, and in some cases, extinguished, in quiescent environments. Motion picture photography enabled measurement of spread rate. In general, the flames were reported as being weaker than their normal gravity counterparts. However, while venting the chamber to extinguish the flame, combustion would first intensify due to the generation of air currents. This hinted at the importance of flow on combustion in microgravity.

Within the last two years, the second set of experiments, examining the combustion characteristics of thin paper samples, was performed aboard the Space Shuttle.[23] Several successful runs at different oxygen percentages and pressures have been carried out in a quiescent chamber. Thermocouple readouts as well as film photography were utilized. Results demonstrated that the flames were in general weaker, more diffuse, less yellow, and larger than their counterparts in normal gravity. The appearance of

the flames suggests an extinction mechanism caused by a drop in flame temperature due to heat loss. This heat loss mechanism has been proposed in an earlier theoretical model.[4]

In mid-1992, several small scale combustion experiments were performed aboard the shuttle within a glovebox module.[26] Three experiments examining candle flames, wire insulation flammability, and smoldering combustion were successfully performed. Motion picture photography, still photography, and thermocouples were used. Results are preliminary, but the microgravity environment has once again produced new and interesting phenomena.

The preceding paragraphs represent the entire history of spacecraft-based combustion experiments. While additional combustion experiments are slated for spacecraft in this decade, by and large, most of the effort has relied on earth-based facilities such as drop towers, Keplerian trajectory aircraft, and computational studies.

1.6. Summary

The brief presentation above shows the current direction of flame spread modelling. Clearly, work continues to be guided by increased computational power. Earliest work focused on obtaining simple heat transfer based expressions. Then, similarity solutions were employed. Eventually, parabolic equations were solved

numerically to capture the downstream region of flames. As computational power increased, elliptic computations first started to appear. The first of these assumed a flow field. Ultimately even the fully elliptic Navier-Stokes equations were solved to capture small flames or flame stabilization regions.

The scope of this work then becomes evident as an attempt to further our understanding by studying concurrent flow flames with the complete equations. Elliptic equations are used in the flame stabilization region. Downstream, parabolic equations are used to capture the relatively long preheat region, where the hot gases heat the unburnt fuel. The entire preheat history of the solid needs to be considered, since the rate at which the fuel is heated affects the flame spread rate.

Chapter 2. Theoretical Formulation

The problem considered in this work can be described as steady, concurrent flow flame spread over a thin solid fuel in low-speed forced flow. More specifically, "concurrent" means that the flame spreads in the same direction as the flow velocity. "Thin" means that the fuel is both hydrodynamically and thermally thin. Hydrodynamically thin means that the thickness of the fuel is always much smaller than the distance of the flame from the fuel surface (or, equivalently, the gas phase length scale). Thermally thin means that the rate of conduction in depth of the solid fuel is much faster than the heat up rate of the gas phase along the fuel surface (effectively, this means that the temperature is constant across the fuel thickness). Furthermore, the fuel is considered thin enough that it burns out before the flame becomes too large (e.g. turbulent). Low-speed forced flows are considered, at strictly zero gravity.

The geometry is shown schematically in fig. 2. Here, the flame is shown stabilized over the fuel, which burns out completely at x=0. A steady* formulation is allowed

*For flame spread over thick fuels, the ignition method can affect subsequent flame spread and extinction. Thus, an unsteady formulation is needed. For thin fuels, the ignition method shouldn't matter as long as a steady solution exists.

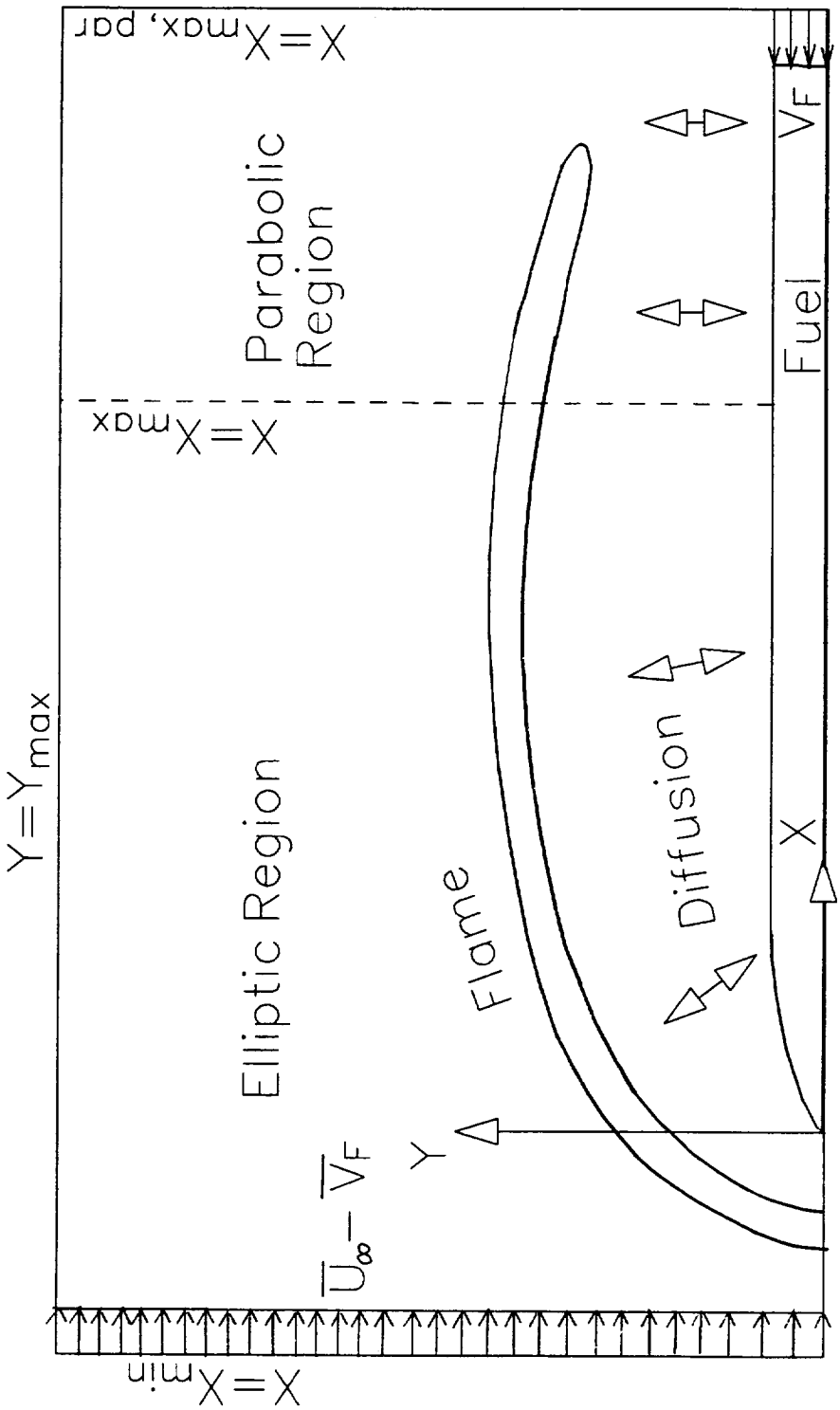

Figure 2. Schematic of problem showing elliptic and parabolic regions.

by solving the equations in "flame-fixed" coordinates. The coordinate system is attached to the burnout point of the solid fuel. A transformation between laboratory and flame-fixed coordinates is given simply by considering the rate of flame spread. In flame-fixed coordinates, the forced convective stream feeds in from the left at the rate $\overline{U}_\infty$ diminished by the flame spread rate $\overline{V}_F$, which is an unknown eigenvalue. In addition the fuel feeds in from the right at the flame spread rate.

The model employs two-dimensional, steady conservation equations. The domain is divided into an "elliptic region" and a "parabolic region" as shown in fig. 2. These regions get their name from the nature of the equations being solved there. In the elliptic region, diffusion in both coordinate directions is considered and boundary conditions are required around the entire boundary of the region. In the parabolic region, diffusion in the stream-wise direction is assumed to be small compared to diffusion in the cross-stream direction. Thus, boundary conditions are only needed on two sides of the domain (the top and bottom). The parabolic region also requires an initial profile specification.

One might ask why the parabolic region is necessary at all if the elliptic region captures the flame stabilization zone. The answer lies in the solution of the solid phase

equations. The solid begins to be heated far downstream of the flame stabilization zone. Therefore, it is wise to treat this long region with the more economical parabolic formulation as soon as the Reynolds number (or more appropriately, the Peclet number) is large enough.

The elliptic region is considerably more difficult to solve both because the equations are more complicated and since boundary conditions are required around the whole region. Our goal has been to make use of the parabolic equations where appropriate to save computation time, while at the same time using the full elliptic equations to accurately model the flame stabilization region where diffusion in both coordinate directions is important. The two regions are described in detail below.

2.1. Elliptic Region

2.1.1. Flow Field Equations

The flow field is solved using the full Navier-Stokes equations. The continuity equation is needed for closure. Stokes' hypothesis is assumed, and is a good approximation for air.[27] In two dimensions, the equations are:

Continuity:
$$\frac{\partial(\bar{\rho}\bar{u})}{\partial(\bar{x})} + \frac{\partial(\bar{\rho}\bar{v})}{\partial(\bar{y})} = 0 \qquad (1)$$

Conservation of momentum in x-direction:
$$\bar{\rho}\bar{u}\frac{\partial\bar{u}}{\partial\bar{x}} + \bar{\rho}\bar{v}\frac{\partial\bar{u}}{\partial\bar{y}} = -\frac{\partial\bar{P}}{\partial\bar{x}} + \frac{\partial}{\partial\bar{x}}\left\{\bar{\mu}\left[2\frac{\partial\bar{u}}{\partial\bar{x}} - \frac{2}{3}\left(\frac{\partial\bar{u}}{\partial\bar{x}} + \frac{\partial\bar{v}}{\partial\bar{y}}\right)\right]\right\} + \frac{\partial}{\partial\bar{y}}\left[\bar{\mu}\left(\frac{\partial\bar{u}}{\partial\bar{y}} + \frac{\partial\bar{v}}{\partial\bar{x}}\right)\right] + \bar{g}\,(\bar{\rho}_{\infty} - \bar{\rho}) \qquad (2)$$

Conservation of momentum in y-direction:

$$\overline{\rho}\overline{u}\frac{\partial\overline{v}}{\partial\overline{x}} + \overline{\rho}\overline{v}\frac{\partial\overline{v}}{\partial\overline{y}} = -\frac{\partial\overline{P}}{\partial\overline{y}} + \frac{\partial}{\partial\overline{y}}\left\{\overline{\mu}\left[2\frac{\partial\overline{v}}{\partial\overline{y}} - \frac{2}{3}\left(\frac{\partial\overline{u}}{\partial\overline{x}} + \frac{\partial\overline{v}}{\partial\overline{y}}\right)\right]\right\} + \frac{\partial}{\partial\overline{x}}\left[\overline{\mu}\left(\frac{\partial\overline{u}}{\partial\overline{y}} + \frac{\partial\overline{v}}{\partial\overline{x}}\right)\right] \qquad (3)$$

Please note that a bar above a variable indicates that it is a dimensional quantity.

The inertia terms are on the left hand side of the momentum equations and represent the acceleration of a fluid element as a result of the applied forces, which appear on the right side of the equations. The first term is the pressure gradient, the second set of terms represent the viscous shear stress, and the last term in the x-momentum equation is the force due to buoyancy. This buoyant term takes the convenient form as shown after the hydrostatic pressure distribution (which would occur in a quiescent fluid) is subtracted. In this form, it is evident that a *density difference* leads to flow. The hydrostatic pressure field due to the body force term is not of interest. (However, for all calculations in this work, it is assumed that $\overline{g} = 0$.)

Since the density of the fluid changes substantially in a flame, the equations are written in compressible form. The density is evaluated by using the equation of state:

$$\overline{P} = \overline{\rho}\overline{R}\overline{T} \qquad (4)$$

The temperature dependence of viscosity is assumed to be

given simply as:

$$\overline{\mu} \propto \overline{T} \qquad (5)$$

In reality, viscosity (and other transport coefficients presented later) are a weaker function of temperature than the assumed linear relation given in eq. (5). However for simplicity, we use this expression, and do not expect any qualitative trends in our results to be affected.

2.1.2. Flow Field Boundary Conditions

As described earlier, boundary conditions need to be specified over the entire region. Please refer to fig. 2 for the complete picture.

Inflow ($\overline{x} = \overline{x}_{min}$): $\overline{u} = \overline{U}_\infty - \overline{V}_F$, $\overline{v} = 0$ (6, 7)

Top ($\overline{y} = \overline{y}_{max}$): $\overline{u} = \overline{U}_\infty - \overline{V}_F$, $\partial\overline{v}/\partial\overline{y} = 0$ (8, 9)

Outflow ($\overline{x} = \overline{x}_{max}$): $\partial\overline{u}/\partial\overline{x}$ and $\partial\overline{v}/\partial\overline{x}$ are given by the parabolic solution, which is described later.

Bottom ($\overline{y} = 0$):

$\overline{x} < 0$: $\partial\overline{u}/\partial\overline{y} = 0$, $\overline{v} = 0$ (10, 11)

$\overline{x} \geq 0$: $\overline{u} = -\overline{V}_F$, $\overline{v} = \overline{v}_w$ (12, 13)

The spread rate $\overline{V}_F$ is an eigenvalue which is found as part of the solution. It is updated at each iteration, and is found in the solution of the solid phase equations, described in a later section. The velocity $\overline{v}_w$ is also determined by the solid phase equations. Basically, the mass flux from the fuel depends only on the temperature of the fuel. Knowing the mass flux, we can calculate $\overline{v}_w$.

Since the velocity is given at the inflow and bottom of the domain, pressure is not known here. Because very low speed flows are considered, pressure varies only slightly from the ambient value of 1 atm. For this problem, it is sufficient to set pressure to 1 atm. at an arbitrary point in the domain. The upper left corner is chosen.

These boundary conditions assume that the flow is perfectly aligned with the fuel plate. While in a spacecraft environment the recirculation currents are quite random, the sensitivity of the flame to angle of flow velocity was outside the scope of this effort.

Through these boundary conditions, one of the principal parameters of interest is varied, namely the free stream velocity $\overline{U}_\infty$. The last boundary conditions, eqs. (12) and (13), are given by the solution of the solid phase equations. From the point of view of the gas-phase equations, the coupling between the gas and solid phases is made through these boundary conditions.

2.1.3. Nondimensional Equations and Boundary Conditions

There are several reasons for using nondimensional equations. A proper choice of scaling parameters simplifies numerical computation. Consider an example where we

use a length scale*, L_0, to nondimensionalize the spatial coordinates in the governing equations. We want to ensure that L_0 is the smallest scale of importance in the physical solution of the problem, so that we know that taking ten grid points in that scale, for example, should be sufficient to accurately solve the problem. Thus, much of the guesswork in choosing a grid is eliminated as other parameters in the problem are changed. Another important reason to nondimensionalize is to capture the important parameters in the problem, for example, the Reynolds number. Finally, from a practical point of view, nondimensional variables are good to work with since their values should be order unity. Otherwise, it is sometimes clumsy to deal with very small or very large numbers in the same problem, and can make the presentation of results in such cases somewhat confusing.

Velocity is nondimensionalized by the characteristic relative velocity $\overline{U}_R = \overline{U}_\infty + \overline{U}_B - \overline{V}_F$. The three components represent a contribution from forced flow, buoyant flow, and flow due to the rate of flame spread, respectively. $\overline{U}_R$ is a measure of the net velocity near the flame stabilization region due to these three terms.

---

*The length scale is a function of other parameters in the problem, and thus can change with these parameters for different cases.

The coordinates $\bar{x}$ and $\bar{y}$ are nondimensionalized by the thermal length, given as $\bar{x}_R = \bar{\alpha}^* / \bar{U}_R$. The thermal length is found by considering a conduction-convection balance, and is a good measure of the flame standoff distance and the flame thickness in the stabilization zone. The asterisk indicates that the property is evaluated at the temperature $\bar{T}^*$, which is the mean of the adiabatic flame temperature and the ambient temperature. For convenience, we use $\bar{T}^* = 1250\,K$ in all cases.

The property values are based on air, which is a good approximation to the dominant component in the gas phase. While certain property values depend greatly on composition (e.g., large heavy fuel molecules behave quite differently than air), a detailed specification of property values based on composition is not attempted at this time. One reason for this is that the chemistry assumed is rather simplified, so any prediction based on the chemistry would be very limited.

Density and viscosity are nondimensionalized by their values at the reference temperature $\bar{T}^*$. Pressure is referenced to the ambient value of 1 atm. and is nondimensionalized as $P = (\bar{P} - \bar{P}_\infty) / \bar{\rho}^* \bar{u}_R^2$. These (and all) nondimensional parameters are also listed in the nomenclature list. Using these quantities, the equations become:

Continuity: $$\frac{\partial(\rho u)}{\partial(x)} + \frac{\partial(\rho v)}{\partial(y)} = 0 \qquad (14)$$

Conservation of momentum in x-direction:

$$\rho u\frac{\partial u}{\partial x} + \rho v\frac{\partial u}{\partial y} = -\frac{\partial P}{\partial x} + Pr\,\frac{\partial}{\partial x}\left\{\mu\left[2\frac{\partial u}{\partial x} - \frac{2}{3}\left(\frac{\partial u}{\partial x} + \frac{\partial v}{\partial y}\right)\right]\right\} + Pr\,\frac{\partial}{\partial y}\left[\mu\left(\frac{\partial u}{\partial y} + \frac{\partial v}{\partial x}\right)\right] + Gr\,(\rho_\infty - \rho) \qquad (15)$$

Conservation of momentum in y-direction:

$$\rho u\frac{\partial v}{\partial x} + \rho v\frac{\partial v}{\partial y} = -\frac{\partial P}{\partial y} + Pr\,\frac{\partial}{\partial y}\left\{\mu\left[2\frac{\partial v}{\partial y} - \frac{2}{3}\left(\frac{\partial u}{\partial x} + \frac{\partial v}{\partial y}\right)\right]\right\} + Pr\,\frac{\partial}{\partial x}\left[\mu\left(\frac{\partial u}{\partial y} + \frac{\partial v}{\partial x}\right)\right] \qquad (16)$$

In these equations, the Prandtl number, Pr, appears. This is the result of choosing the thermal length as the characteristic length scale. For all cases, Pr is assumed constant and equal to 0.7. The Reynolds number based on x, Re_x, is given simply as x/Pr, and similarly, Re_y=y/Pr. Equivalently, x and y represent Peclet numbers based on x and y respectively. The boundary conditions become:

Inflow ($x = x_{min}$): $u = (\overline{U}_\infty - \overline{V}_F)/\overline{U}_R$, $v = 0$ (17, 18)

Top ($y = y_{max}$): $u = (\overline{U}_\infty - \overline{V}_F)/\overline{U}_R$, $\partial v/\partial y = 0$ (19, 20)

Outflow ($x = x_{max}$): $\partial u/\partial x$ and $\partial v/\partial x$ are given by the parabolic solution, which is described later.

Bottom ($y = 0$):

$x < 0$: $\partial u/\partial y = 0$, $v = 0$ (21, 22)

$x \geq 0$: $u = -\overline{V}_F/\overline{U}_R$, $v = v_w$ (23, 24)

Note that for purely forced flow, $(\overline{U}_\infty - \overline{V}_F)/\overline{U}_R = 1$.

2.1.4. Energy Equation

By assuming the specific heat of the gas is constant,

conservation of energy enables us to write an equation for temperature as follows:

$$\overline{\rho}\overline{u}\overline{C_p}\frac{\partial\overline{T}}{\partial x}+\overline{\rho}\overline{v}\overline{C_p}\frac{\partial\overline{T}}{\partial y}=\frac{\partial}{\partial x}\left(\overline{\kappa}\frac{\partial\overline{T}}{\partial x}\right)+\frac{\partial}{\partial y}\left(\overline{\kappa}\frac{\partial\overline{T}}{\partial y}\right)+\overline{\dot{Q}} \qquad (25)$$

The left hand side of the equation represents the convection of heat. The right hand side is the heat conduction term and the source term due to the chemical reaction. The heat release due to viscous dissipation and compressive work are neglected since they are small compared to the combustion heat release. The specific heat, $\overline{C}_p$, is assumed constant. The conductivity is assumed to vary according to:

$$\overline{\kappa}\propto\overline{T} \qquad (26)$$

The form of the energy source term is:

$$\overline{\dot{Q}}=\overline{Q}\,\overline{B}_g\,\overline{\rho}^2 Y_F Y_O \exp(-\overline{E}_g/\overline{RT}) \qquad (27)$$

This finite rate expression is for a one-step, second order reaction.

2.1.5. Energy Equation Boundary Conditions

The boundary conditions for the energy equation resemble those for the momentum equation, since they are both elliptic in nature:

Inflow ($\overline{x}=\overline{x}_{min}$): $\overline{T}=\overline{T}_\infty$ (28)

Top ($\overline{y}=\overline{y}_{max}$): $\overline{T}=\overline{T}_\infty$ (29)

Outflow ($\overline{x}=\overline{x}_{max}$): $\partial\overline{T}/\partial\overline{x}$ is given by the parabolic solution, which is described later.

Bottom ($\bar{y}=0$):

$$\bar{x} < 0: \qquad \partial\bar{T}/\partial\bar{y} = 0 \qquad (30)$$

$$\bar{x} \geq 0: \qquad \bar{T} = \bar{T}_s \qquad (31)$$

The relation given in eq. (31) is determined by solution of the solid phase equations, which is described shortly.

2.1.6. Nondimensional Energy Equation and Boundary Conditions

Temperature is nondimensionalized by the ambient temperature, $\bar{T}_\infty$, and conductivity is nondimensionalized by its value at $\bar{T}^*$ (of these two reference temperatures, the former is useful in presenting results, while the latter is appropriate for evaluating property values). The equation becomes:

$$\rho u \frac{\partial T}{\partial x} + \rho v \frac{\partial T}{\partial y} = \frac{\partial}{\partial x}\left(\kappa \frac{\partial T}{\partial x}\right) + \frac{\partial}{\partial y}\left(\kappa \frac{\partial T}{\partial y}\right) + \dot{Q} \qquad (32)$$

where

$$\dot{Q} = Da\, Q\, \rho^2 Y_F\, Y_O \exp(-E/T) \qquad (33)$$

Note the appearance of the Damkohler number, Da, in the last equation ($Da = \bar{\alpha}^* \bar{\rho}^* \bar{B}_g / \bar{U}_R^2$). The Damkohler number is the ratio of the characteristic flow time over the chemical reaction time in one thermal length. It varies inversely as the square of relative velocity. The boundary conditions are:

Inflow ($x = x_{min}$): $T = 1$ (34)

Top ($y = y_{max}$): $T = 1$ (35)

Outflow ($x = x_{max}$): $\partial T/\partial x$ is given by the parabolic

solution, which is described later.

Bottom (y = 0):

$$x < 0: \qquad \partial T/\partial y = 0 \qquad (36)$$

$$x \geq 0: \qquad T = T_s \qquad (37)$$

In eq. (37), T_s is determined by solution of the solid phase equations.

2.1.7. Fuel and Oxygen Species Conservation Equations

The species conservation equations are:

$$\overline{\rho u}\frac{\partial Y_F}{\partial x} + \overline{\rho v}\frac{\partial Y_F}{\partial y} = \frac{\partial}{\partial x}\left(\overline{\rho}\,\overline{D}_F\frac{\partial Y_F}{\partial x}\right) + \frac{\partial}{\partial y}\left(\overline{\rho}\,\overline{D}_F\frac{\partial Y_F}{\partial y}\right) + \overline{\omega_F} \qquad (38)$$

$$\overline{\rho u}\frac{\partial Y_O}{\partial x} + \overline{\rho v}\frac{\partial Y_O}{\partial y} = \frac{\partial}{\partial x}\left(\overline{\rho}\,\overline{D}_O\frac{\partial Y_O}{\partial x}\right) + \frac{\partial}{\partial y}\left(\overline{\rho}\,\overline{D}_O\frac{\partial Y_O}{\partial y}\right) + \overline{\omega_O} \qquad (39)$$

The left hand side of the equations represents the convective term. The right hand side is the mass diffusion term and the sink term due to the chemical reaction. The diffusion coefficient, $\overline{\rho}\,\overline{D}_i$, is assumed to vary as follows:

$$(\overline{\rho}\,\overline{D}_i) \propto \overline{T} \qquad (40)$$

The form of the species sink terms is:

$$\overline{\omega_F} = -\overline{B}_g\,\overline{\rho}^2 Y_F Y_O \exp(-\overline{E}_g/\overline{R}\,\overline{T}), \quad \overline{\omega_O} = f\,\overline{\omega_F} \qquad (41, 42)$$

where f is the stoichiometric oxidizer/fuel mass ratio.

2.1.8. Fuel and Oxygen Species Boundary Conditions

Again, the boundary conditions resemble those in preceding sections since the equations are elliptic:

$$\text{Inflow } (\overline{x} = \overline{x}_{min}): \qquad Y_F = 0, \; Y_O = Y_{O,\infty} \qquad (43, 44)$$

Top ($\overline{y} = \overline{y}_{max}$): $Y_F = 0$, $Y_O = Y_{O,\infty}$ (45, 46)

Outflow ($\overline{x} = \overline{x}_{max}$): $\partial Y_F/\partial \overline{x}$ and $\partial Y_O/\partial \overline{x}$ are given by the parabolic solution, which is described later.

Bottom ($\overline{y} = 0$):

$\overline{x} < 0$: $\partial Y_F/\partial \overline{y} = 0$, $\partial Y_O/\partial \overline{y} = 0$ (47, 48)

$\overline{x} > 0$: $\overline{m} Y_{F,w} = \overline{m} + \overline{\rho}\overline{D}_F (\partial Y_F/\partial \overline{y})_w$ (49)

$\overline{m} Y_{O,w} = \overline{\rho}\overline{D}_O (\partial Y_O/\partial \overline{y})_w$ (50)

2.1.9. Nondimensional Species Equations and Boundary Conditions

The terms $\overline{\rho}\overline{D}_i$ are nondimensionalized by their value at $\overline{T}^*$. The equations become:

$$\rho u \frac{\partial Y_F}{\partial x} + \rho v \frac{\partial Y_F}{\partial y} = \frac{1}{Le_F}\left[\frac{\partial}{\partial x}\left(\rho D_F \frac{\partial Y_F}{\partial x}\right) + \frac{\partial}{\partial y}\left(\rho D_F \frac{\partial Y_F}{\partial y}\right)\right] + \dot{\omega}_F \qquad (51)$$

$$\rho u \frac{\partial Y_O}{\partial x} + \rho v \frac{\partial Y_O}{\partial y} = \frac{1}{Le_O}\left[\frac{\partial}{\partial x}\left(\rho D_O \frac{\partial Y_O}{\partial x}\right) + \frac{\partial}{\partial y}\left(\rho D_O \frac{\partial Y_O}{\partial y}\right)\right] + \dot{\omega}_O \qquad (52)$$

Where: $\dot{\omega}_F = -Da\,\rho^2 Y_F Y_O \exp(-E_g/T)$, $\dot{\omega}_O = f\,\dot{\omega}_F$ (53, 54)

The boundary conditions are:

Inflow ($x = x_{min}$): $Y_F = 0$, $Y_O = Y_{O,\infty}$ (55, 56)

Top ($y = y_{max}$): $Y_F = 0$, $Y_O = Y_{O,\infty}$ (57, 58)

Outflow ($x = x_{max}$): $\partial Y_F/\partial x$ and $\partial Y_O/\partial x$ are given by the parabolic solution, which is described later.

Bottom ($y = 0$):

$x < 0$: $\partial Y_F/\partial y = 0$, $\partial Y_O/\partial y = 0$ (59, 60)

$x \geq 0$: $\dot{m} Y_{F,w} = \dot{m} + (\rho D_F/Le_F)(\partial Y_F/\partial y)_w$ (61)

$\dot{m} Y_{O,w} = (\rho D_O/Le_O)(\partial Y_O/\partial y)_w$ (62)

2.2. Parabolic Region

The equations for the parabolic region are identical to those in the elliptic region except for the neglection of the stream-wise diffusion terms. In addition, in deriving the flow field equations, the y-momentum equation drops out completely, and, in this case, the pressure gradient term in the x-momentum equation is zero. The equations have the well-known form of boundary layer flow over a flat plate. They are presented below.

2.2.1. Nondimensional Parabolic Region Equations

Continuity:
$$\frac{\partial(\rho u)}{\partial(x)} + \frac{\partial(\rho v)}{\partial(y)} = 0 \qquad (63)$$

X-Momentum:
$$\rho u \frac{\partial u}{\partial x} + \rho v \frac{\partial u}{\partial y} = Pr \frac{\partial}{\partial y}\left(\mu \frac{\partial u}{\partial y}\right) + Gr\,(\rho_\infty - \rho) \qquad (64)$$

Energy:
$$\rho u \frac{\partial T}{\partial x} + \rho v \frac{\partial T}{\partial y} = \frac{\partial}{\partial y}\left(\kappa \frac{\partial T}{\partial y}\right) + \dot{Q} \qquad (65)$$

Species:

Fuel:
$$\rho u \frac{\partial Y_F}{\partial x} + \rho v \frac{\partial Y_F}{\partial y} = \frac{1}{Le_F} \frac{\partial}{\partial y}\left(\rho D_F \frac{\partial Y_F}{\partial y}\right) + \dot{\omega}_F \qquad (66)$$

Oxygen:
$$\rho u \frac{\partial Y_O}{\partial x} + \rho v \frac{\partial Y_O}{\partial y} = \frac{1}{Le_O} \frac{\partial}{\partial y}\left(\rho D_O \frac{\partial Y_O}{\partial y}\right) + \dot{\omega}_O \qquad (67)$$

2.2.2. Nondimensional Parabolic Region Boundary Conditions

The parabolic region requires boundary conditions only on the top and bottom of the domain, as well as an initial profile specification. The initial profile is given by the values obtained at the outflow ($x = x_{max}$) of the elliptic

solution. Thus, velocity, temperature, and the species concentrations are given. The boundary conditions on the top and bottom of the domain are identical to those presented in previous sections.*

2.3. Coupling Between Elliptic and Parabolic Regions

The coupling between the elliptic and parabolic regions is best understood by considering the solution algorithm. First, the elliptic equations are used for several iterations to get an updated elliptic field. Then, the values of the variables (u, v, T, Y_F, and Y_O) at the outflow of the elliptic region are used as the initial profile for the parabolic equations. After sweeping through the parabolic region and the solid phase equations, the elliptic region is again calculated. This time, however, the boundary conditions at the outflow for the elliptic equations are based on the parabolic solution, by evaluating derivatives with respect to x in the parabolic region at the interface between the two regions, and using these derivative boundary conditions for the elliptic region.

In previous elliptic computations of this sort, the outflow boundary conditions are given simply as a zero-

---

*One exception is the boundary condition for v-velocity. Since the y-momentum equation drops out, v needs to be specified only on the bottom of the domain.

gradient normal to the boundary (e.g., ref. 14). This is because information beyond the boundary is unknown. A result is that the solution near the boundary is not as accurate as the solution away from the boundary. In our case, we can use the actual (non-zero) gradient as given by the first step of the parabolic computation, as described above. Upon iteration, the converged solution provides a much smoother transition between the elliptic and parabolic domains.

This is shown in fig. 3. In fig. 3a, zero gradient boundary conditions for the outflow of the elliptic region are used. In the elliptic region, the isotherm near the boundary levels off due to the zero-gradient condition. Thus, a slight dip is evident.

In fig. 3b, the results of the method used in this work are shown. Now, there is a smooth transition between the two regions.

2.4. Solid Phase Equations

The solid phase is solved by considering the conservation of mass and energy together with a pyrolysis relation. The flame spread rate, $\overline{V}_F$, appears as an eigenvalue. The geometry of the solid fuel is shown in fig. 4. The density of the solid is assumed constant while the thickness is allowed to decrease due to pyrolysis. In fig. 4 dimensions are greatly exaggerated. As far as the gas phase is

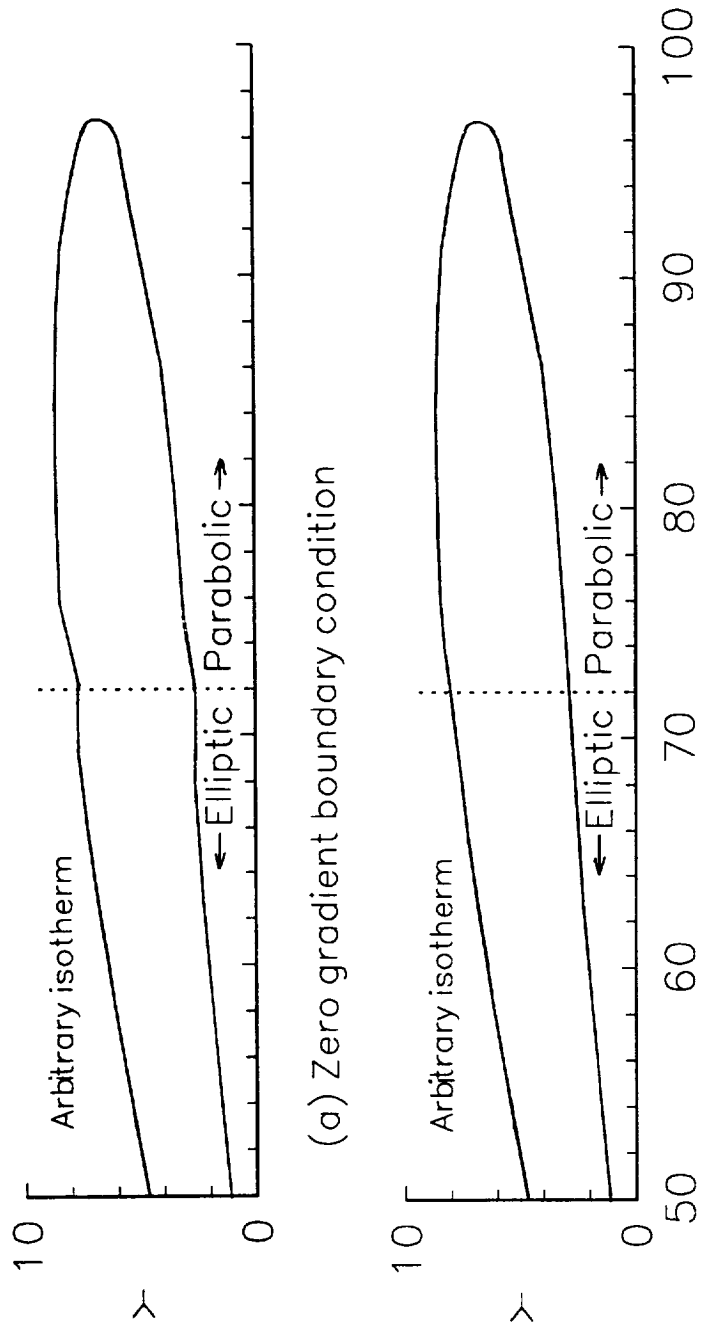

Figure 3. Elliptic/parabolic matching boundary conditions.

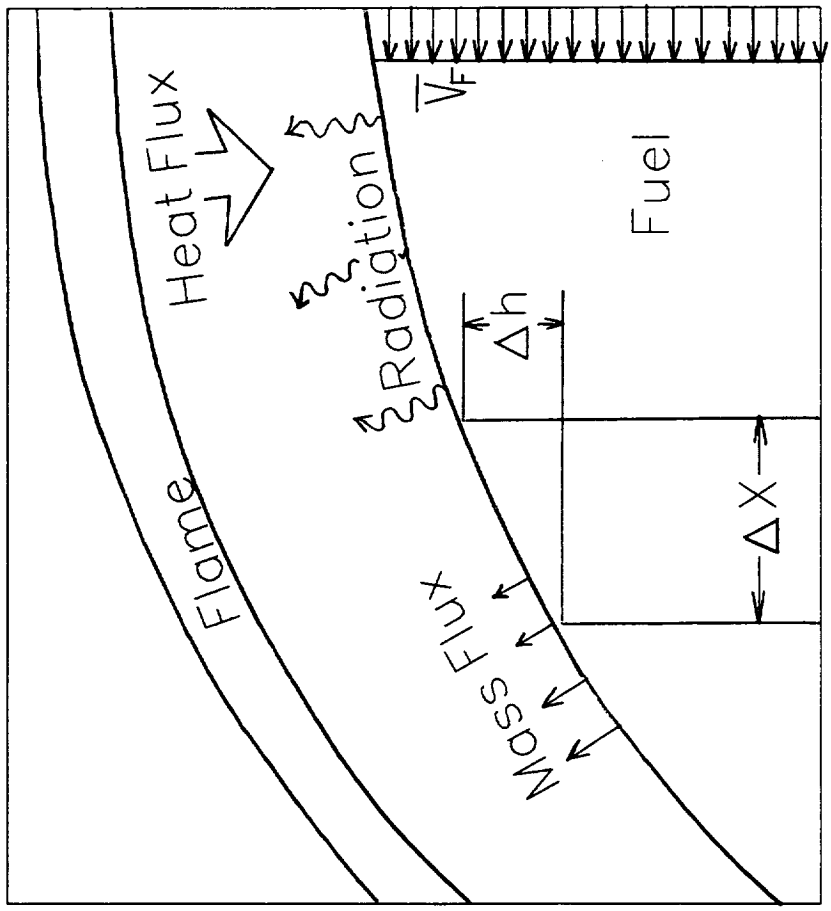

Figure 4. Geometry of Solid Fuel.

concerned, the solid is infinitesimally thin, meaning that the flame stand-off distance is much larger than the fuel thickness. In deriving these equations, it is assumed that:

$$\sqrt{1 + (d\bar{h}/d\bar{x})^2} \approx 1 \qquad (68)$$

This is an excellent assumption for all cases studied. The solid phase equation is:

$$\bar{q}_y + \bar{\rho}_s \bar{V}_F \bar{C}_s \frac{d(\bar{h}\bar{T}_s)}{d\bar{x}} = \sigma \epsilon (\bar{T}_s^4 - \bar{T}_\infty^4) + \bar{\rho}_s \bar{V}_F \frac{d\bar{h}}{d\bar{x}} [(\bar{C}_s - \bar{C}_p)\bar{T}_L + (-\bar{L}) + \bar{C}_p \bar{T}_s] \qquad (69)$$

On the left side, the first term, $\bar{q}_y$, is the conductive heat flux incident on the solid from the gas phase. It is given as $\bar{q}_y = [\bar{\kappa}(\partial\bar{T}/\partial\bar{y})]_{g,w}$. This term represents the coupling between the gas and solid phase from the point of view of the solid equations. The solid phase spans both the elliptic and parabolic regions. The second term represents the convection of heat due to flux of fuel. As described earlier, in the flame-fixed coordinate system used, the fuel feeds into the domain at the speed $\bar{V}_F$. It may be clearer for the reader to examine this term in laboratory coordinates. In laboratory coordinates, it is simply the unsteady bulk heat up term.

On the right side, the first term is the surface radiative heat loss term. The second term is the energy

change due to the latent heat of vaporization of the fuel. $\overline{L}$ is the latent heat of the fuel, which is specified at the temperature $\overline{T}_L$ ($\overline{T}_L = 300\,K$ in this problem).

The pyrolyzed gases constitute blowing from the wall. The pyrolysis law chosen specifies that the rate of pyrolysis depends only on the temperature of the fuel (zeroth-order pyrolysis). It is:

$$\overline{\dot{m}} = \overline{A}_s \overline{\rho}_s \exp(-\overline{E}_s/\overline{RT}_s) \qquad (70)$$

Using eq. (70), the blowing velocity $\overline{v}_w$ can be found, since the density of the gas is known at the wall. Remember that the solid density, $\overline{\rho}_s$, is constant. This is different from other models[11,15,22] which assumed the thickness of the fuel was constant, but the density was decreased as pyrolysis occurred, making the pyrolysis relation first-order. The reason for using a zeroth-order pyrolysis relation is that complete fuel burnout is possible. A first-order pyrolysis law requires an arbitrary (but non-zero) specification of unburnt solid char, at which point burnout is said to occur.

When combined with the conservation of mass for the solid fuel, the pyrolysis relation becomes:

$$\frac{d\overline{h}}{d\overline{x}} = \frac{\overline{A}_s}{\overline{V}_F} \exp(-\overline{E}_s/\overline{RT}_s) \qquad (71)$$

Equations (70) and (71) are solved with the following

boundary conditions:

$$\text{At } \bar{x} = \bar{x}_{max,\,par}: \qquad \bar{T} = \bar{T}_\infty,\ \bar{h} = \bar{\tau} \qquad (72,\ 73)$$

The flame spread rate $\bar{V}_F$ is an eigenvalue and is solved for iteratively. In solving the solid phase equations, the conductive heat flux distribution from the gas phase is known as a function of x. The spread rate, $\bar{V}_F$, is guessed. If this guess is too high, the fuel moves too fast for complete burnout to occur. If the guess is too low, burnout occurs too soon (i.e. at $\bar{x} > 0$). The spread rate is adjusted using a simple bisection method until burnout occurs at $\bar{x} = 0$.

Using $\bar{x}_R$, $\bar{\rho}^* \bar{C}_p \bar{U}_R \bar{T}_\infty$, and $\bar{C}_s$ to nondimensionalize $\bar{h}$, $\bar{q}_y$, and $\bar{C}_p$ respectively, the equations and boundary conditions become:

$$q_y + \Xi \frac{d(hT)}{dx} = \Gamma (T^4 - 1) + \Xi \frac{dh}{dx} [(1 - C_p) T_L + (-L) + C_p T] \qquad (74)$$

$$\text{At } x = x_{max,\,par}: \qquad T = 1,\ h = \bar{\tau}/\bar{x}_R \qquad (75,\ 76)$$

In eq. (74), $\Xi = \bar{\rho}_s \bar{V}_F \bar{C}_s / \bar{\rho}^* / \bar{U}_R / \bar{C}_p$, and $\Gamma = \bar{\sigma} \varepsilon \bar{T}_\infty^3 / \bar{\rho}^* / \bar{C}_p / \bar{U}_R$. The last term, Γ, is the non-dimensional surface radiative heat loss parameter. It varies inversely with relative velocity.

Chapter 3. Numerical Model

The problem is analyzed by writing the finite-difference representation of the equations and solving them using the CRAY X-MP supercomputer at NASA Lewis Research Center. The algorithm used is called SIMPLER (Semi-Implicit Method for Pressure-Linked Equations Revised). This algorithm is presented in detail in a textbook,[28] and so only the unique features are presented here. The computer program, which was written based on this algorithm specifically for this problem, appears in the appendix, along with parameter values.

In any finite-difference method, the domain is broken up into a grid structure. The equations are written for an individual control volume (or grid square) by considering its interaction with neighboring control volumes. The solution can be thought of as equivalent to finding the parameters of interest at the interfaces of adjacent control volumes by an appropriate interpolation method, and then calculating the quantities at all control volumes using some matrix inversion technique. Finite-difference methods vary according to how they determine interface quantities. Simple interpolation methods require less computational complexity, but suffer in accuracy.

As can be seen in the Theoretical Formulation chapter, the equations are quite complex. Both first and second

derivative terms appear. In addition, the equations are non-linear. These attributes lead to several complications.

3.1. Discretization of Convective Terms

The terms such as $\rho u(\partial T/\partial x)$ representing convection, are somewhat troublesome. The problem lies in writing the *appropriate* finite difference representation for a given control volume. The physical meaning of such a term should be considered when deriving the finite difference form. If we assume that temperature, T, represents the energy of the fluid, then $\rho u(\partial T/\partial x)$ is the rate of energy transfer to the control volume due to the fluid flowing at velocity u. This is of course why it is called a convective term -- the energy is convected by the velocity. Clearly, anything in a stream of fluid is generally affected more by the upstream than the downstream flow. In writing the discretization equations, then, it is important to weight the upstream quantity. It is the directional character of velocity which drives this consideration. One common approach is to use the upwind-difference scheme (or donor-cell method). In this method, the value of a variable (say, temperature) at the interface of a control volume is set equal to the value on the upwind side of the interface. This is perhaps the simplest possible weighting function.

While the upwind-difference scheme captures the essential elements of a convective-diffusive transport problem, there are instances when the method becomes less accurate. Specifically, as the grid Peclet number*, Pe, becomes large, conduction is overestimated. This is because while at an interface, the value of temperature is correctly given as described above, the conduction is assumed based on a linear profile between the two points on either side of the interface. In actuality, the conduction at the interface is close to zero, but the upwind scheme predicts a value much larger.

To overcome this difficulty, the exact solution of the convective-diffusive equation

$$\rho u C_p \frac{\partial T}{\partial x} = \frac{\partial}{\partial x}\left(\kappa \frac{\partial T}{\partial x}\right) \qquad (77)$$

is determined for adjacent control volumes. This solution determines the value of temperature, T, to use at the interface of the control volumes. Consider two adjacent control volumes separated by Δx. Let T_L and T_R be the temperature of the two control volumes. the exact solution of eq. (77) (assuming ρu is constant for the control volumes) is then:

---

*The grid Peclet number is a measure of the relative strength of convective to conductive transport in an individual control volume.

$$\frac{(T(x) - T_L)}{(T_R - T_L)} = \frac{[\exp(\rho u C_p x/\kappa) - 1]}{[\exp(\rho u C_p \Delta x/\kappa) - 1]} \qquad (78)$$

and the value at the interface between the two control volumes is readily given. Since exponential terms are relatively costly to compute, an approximating polynomial (fifth order in x) is used instead. The approximation is very close to the exact solution, enabling accuracy for any grid Peclet number.

While eq. (77) is one-dimensional, the same idea is used to solve the two-dimensional equations in this work. The convective-diffusive transfer is simply considered along each coordinate direction.

3.2. Treatment of Source Terms

In the SIMPLER algorithm, all terms other than convective and diffusive ones are lumped together and called source terms*. The rules governing their discretization follow.

Suppose the equation of interest is the conservation of energy, for which temperature is the dependent variable. The source term is in general a function of T, derivatives of T, and other variables in the problem. The key is to

---

*The only exception to this is in the solution of the Navier-Stokes equations where the pressure gradient terms are handled individually. This will be described subsequently.

linearize the source term as

$$S = S_c + S_p T \qquad (79)$$

and ensure that S_p is always less than zero. In eq. (79), T represents the temperature of a given control volume, which is to be calculated. The coefficients S_c and S_p may be functions of any number of variables in the problem (including a value of T that is guessed or taken from a previous iteration). This specification guarantees that the source term will not lead to instability, even for the highly non-linear Arrhenius rate expressions of combustion in this problem.

3.3. Staggered Grid System

In developing the finite difference form of many equations, it is generally a good idea to use the same grid structure for each dependent variable to minimize the complexity in bookkeeping all of the grid locations and interpolation between grids. However, there is nothing wrong with using different grid structures for different equations. It only makes sense to do this if some benefit can be derived. In the SIMPLER algorithm, a staggered grid is used to eliminate problems brought on by the appearance of first derivative terms, such as pressure gradient terms or terms appearing in the continuity equation.

A very coarse grid structure is shown for demonstration purposes in fig. 5. The grid is generated by first

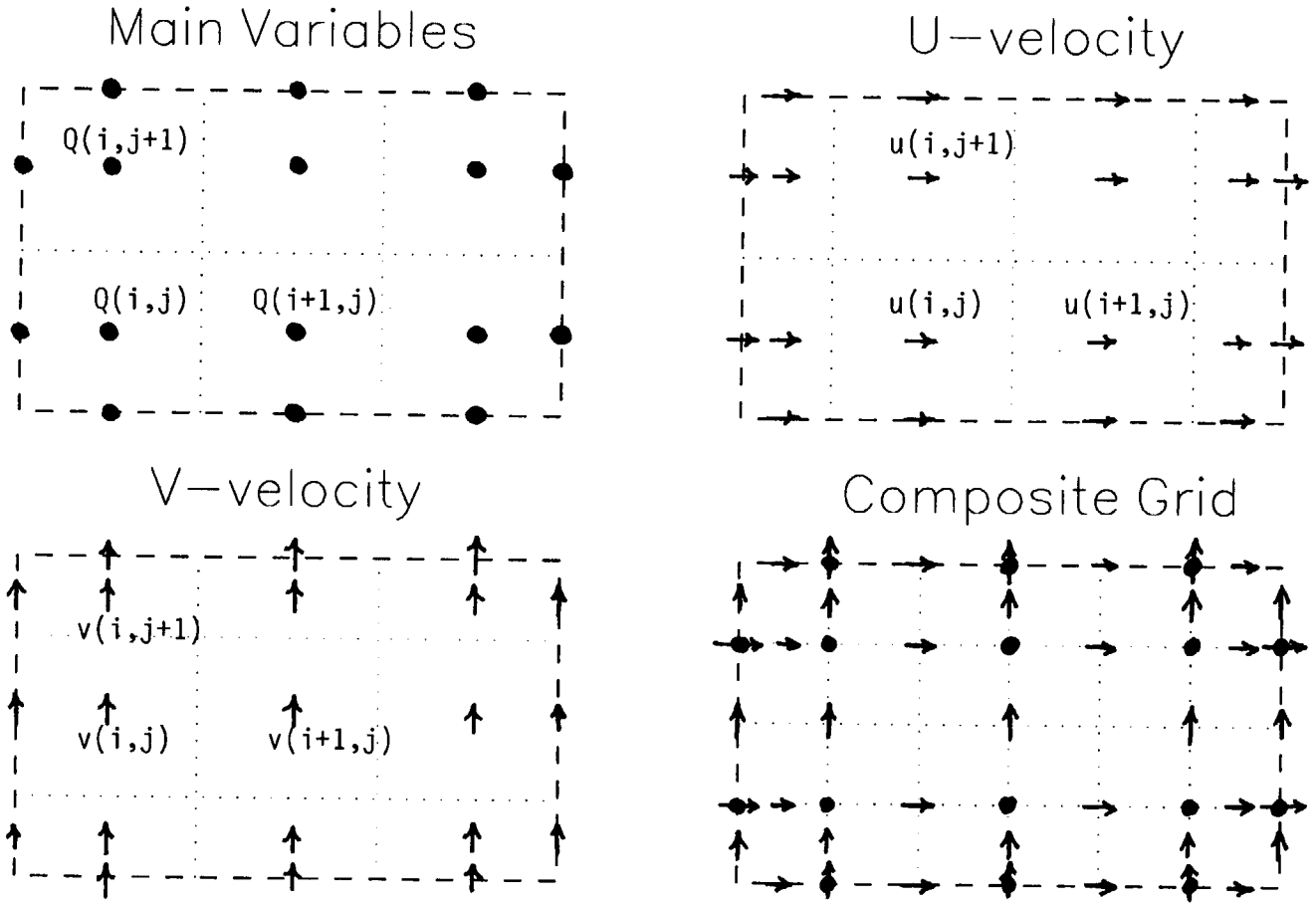

Figure 5. Grid structure for main variables Q, and u and v−velocities.

chopping up the overall domain into smaller control volumes. The grid location for each dependent variable (including pressure) is taken to be the center of the control volume. Then, u-velocity is positioned at each vertical face, and v-velocity at each horizontal control volume face. Thus the composite grid is comprised of three different grid structures.

The advantage of doing this is that in evaluating the pressure force on a velocity control volume, the pressure at adjacent grid points is used. If all variables (including velocity) were evaluated at the same grid points, the pressure force would be calculated by using every other grid point. This would be the result of a simple discretization of the first derivative pressure gradient terms. Unless treated specially, this kind of a formulation permits highly unrealistic solutions.

3.4. The SIMPLER Algorithm

To obtain a solution, the initial variable field is taken from a converged case. Then, the velocity or oxygen percentage is changed by modifying the boundary conditions.

The first step of the algorithm is to start with the non-converged velocity field, which is supplied initially, or taken from the previous iteration. Then, the momentum equations are used to obtain an expression for the velocity (x and y-direction) of the fluid in a control volume.

These finite difference expressions will of course include pressure. By substituting the expressions for velocity into the finite difference form of the continuity equation, an equation for pressure results. Pressure (call it P*) is calculated*. Using this updated pressure field, the momentum equations are solved to obtain new estimates of velocity.

During iteration, these velocity estimates will not satisfy the continuity equation. To speed convergence, a superposed pressure field, called P′, is assumed. Thus, P=P*+P′, and after convergence is reached, P′=0 everywhere. Using the momentum equations, simplified relations for velocity involving P′ are obtained. These are substituted into the continuity equation to obtain a P′ equation. After computing P′, it is used to correct the velocity components.

At this point, all additional conservation equations are solved (in this case, conservation of energy and species). Finally, the entire procedure is repeated until convergence is reached.

---

*In the SIMPLER algorithm, the equations are discretized such that a tri-diagonal matrix results for a given line of grid points. The tri-diagonal matrix is easily inverted. Thus, in two dimensions, each row of grid points is solved by matrix inversion, followed by each column of grid points. This procedure pulls the boundary information into the domain very quickly.

3.5. Domain Structure

The grid structure should be fine enough to adequately capture the changes in the parameters of interest. For example, in a flame spread problem, temperature varies dramatically across the flame. Thus many grid points are required. However, if a uniform distribution of grid points is used throughout the domain, most of the grid points are unnecessary in regions where the temperature does not change as dramatically as in the flame. Therefore it is more efficient to use a variable grid spacing, i.e., in regions where the quantity varies sharply, a higher concentration of grid points is used.*

For the flame stabilized at the leading edge of a fuel plate, the grid points should be concentrated at the leading edge both to capture the high temperature, narrow flame stabilization region as well as the rapid flow field changes due to the sudden appearance of the plate. The variable grid structure used in this problem is shown in fig. 6. Evident in fig. 6 is the concentration of points both immediately upstream and downstream of the leading edge to capture the flame stabilization zone and the abrupt pressure and velocity changes. Additionally, the concen-

---

*An adaptive grid method or multigrid method would be well-suited for this problem, but are not used at this time.

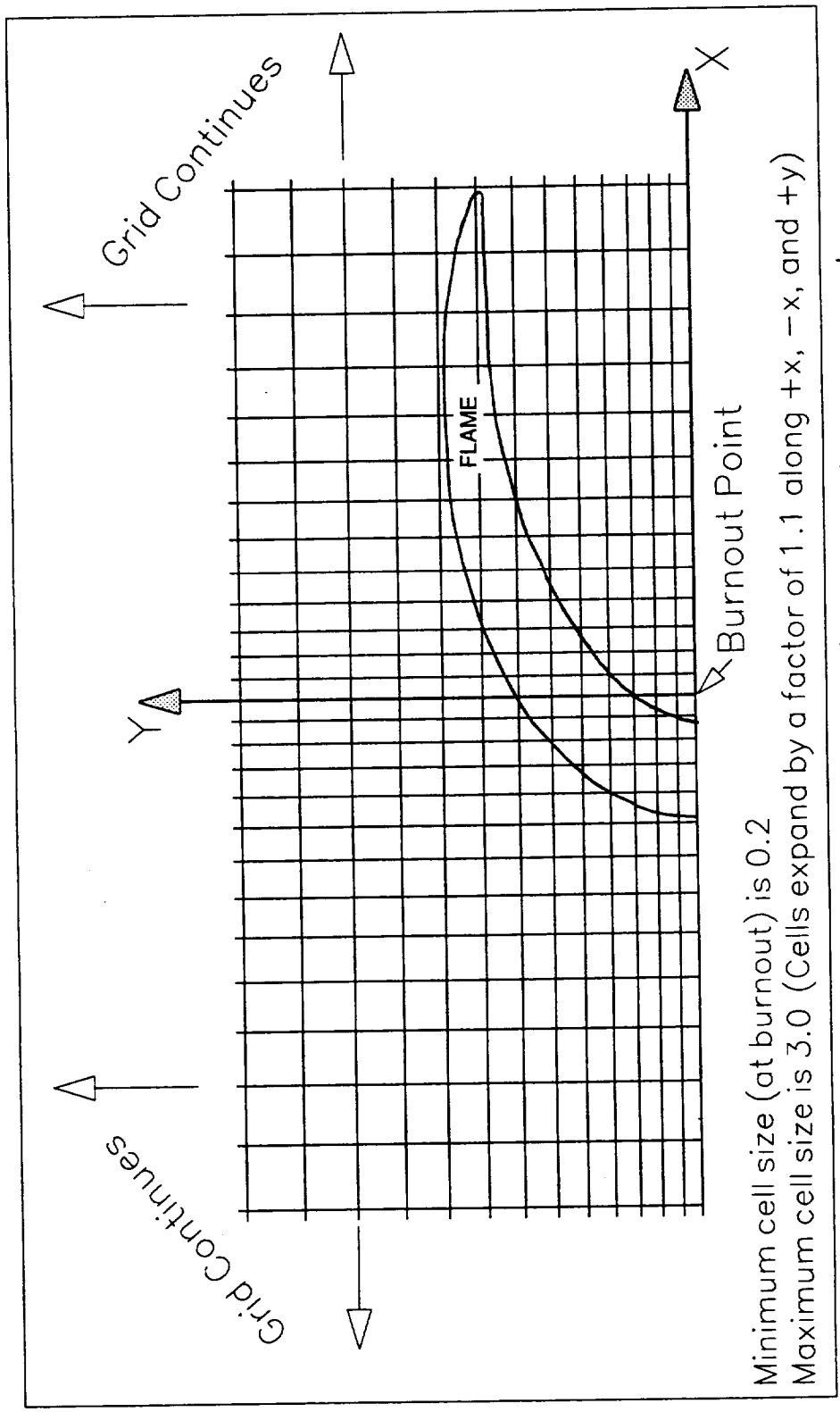

Figure 6. Variable grid structure used in this problem.

tration of points near the fuel plate capture the steep gradients near the plate. The location of a typical flame is shown superimposed on the grid structure. The particular grid spacing used in this problem was found to be more than adequate in an earlier work.[14]

In the elliptic region, x varies from about -20 to 70 and y varies from 0 to 90. The number of grid points in the x-direction is 70 and the number of grid points in the y-direction is 50.

The Reynolds number*, Re_x, as a function of x, for any case is simply calculated as x/Pr, where Pr is the Prandtl number (Pr=0.7). For all cases in this effort, the elliptic/ parabolic boundary occurred at Re_x=100. A test case was run where the elliptic/parabolic boundary was extended to Re_x=200. The thermal structure and spread rate of the flame changed by less than 2%, so the smaller elliptic domain was deemed adequate.

3.6. Parabolic Region

The finite difference scheme in the parabolic region is based on a marching technique.[29] At the outflow of the elliptic domain (Re_x=100 or x=70), parabolic equations take over. The results obtained from the elliptic region provide the initial condition for the parabolic equations.

---

*Re_x is based on the relative velocity, distance from the leading edge, and properties evaluated at T^*.

A single sweep into the far downstream region (Re_x=2200 or x=1570) is utilized.

The same, variable grid structure in the y-direction as used in the elliptic region is utilized. Also, additional points are added to the top of the domain (at $y>y_{max}$ in fig. 2) to give the boundary layer room to grow. Thus, in the parabolic region, x varies from 70 to 1570 and y varies from 0 to 150. The grid spacing in the x-direction gradually increases, since derivatives with respect to x in the far downstream region become smaller and smaller, making a coarser grid adequate. There are 65 grid points in the x-direction and 90 grid points in the y-direction.

An implicit formulation is employed, that is, at any station $x=x_i$, the resulting equations depend only on the values of the variables at $x=x_{i-1}$ (which are known) and at $x=x_i$. To get the solution at $x=x_i$, a tri-diagonal system of equations is solved.

3.7. Computer Usage

To compute a new case, a nearby, converged flame is used as the initial guess. One global iteration step takes about 7 sec. of CRAY X-MP CPU time. It consists of first calculating the elliptic region using line-by-line sweeps (4 horizontal sweeps, 4 vertical sweeps) for each of the conservation equations in series. This is repeated 10 times. Then, the parabolic region is calculated using the

marching technique described above. Finally, the conduction of the gas phase to the solid is used to solve the solid phase equations and get new values of spread rate, temperature, and blowing velocity. Using these values, the boundary conditions are updated, and the global iteration step is concluded. Typically, convergence requires about 1 hr. of CPU time.

3.8. Property Values

The property values used are presented in the nomenclature list. They are based on the choice of cellulose as fuel. Some of the derived parameters require description.

Consider cellulose and air stoichiometric combustion:

$$C_6H_{10}O_5 + 6(O_2 + 3.76N_2) \rightarrow 6CO_2 + 5H_2O + 22.56N_2 \qquad (80)$$

Assuming one mole reacts:

$$(162\,g)_{C_6H_{10}O_5} + (192\,g)_{O_2} + (632\,g)_{N_2} \rightarrow (264\,g)_{CO_2} + (90\,g)_{H_2O} + (632\,g)_{N_2} \qquad (81)$$

In order to calculate $\overline{\rho}^*$, the mixture specific ideal gas constant used is the average value of that for air and for the products (nitrogen is included in the products):

$$\overline{R} = (\overline{R}_{Air} + \overline{R}_{Prod})/2 = (0.287 + 0.302)/2 = 0.295\ J/g/K \qquad (82)$$

Based on the assumed adiabatic flame temperature of 2200 K, the gas-phase specific heat is calculated from the simple energy balance as follows:

$$(\overline{Q} + \overline{L})\,\overline{m}_{Fuel} = \overline{m}_{Prod}\,\overline{C}_P\,(\overline{T}_f - \overline{T}_\infty) \qquad (83)$$

and since $\overline{m}_{Prod}/\overline{m}_{Fuel} = 6.084$, we get $\overline{C}_P = 0.30$ cal/g/K.

Chapter 4. Results

Concurrent flow flame spread over a thin fuel in a zero gravity* environment has been modelled. Steady computations have been carried out over a range of forced flow velocities and ambient oxygen concentrations at one atmosphere pressure. The molar† oxygen percentage was varied from 13.5 to 21, and the flow velocity was varied from 16 cm/s down to 0.8 cm/s‡. As will be described later, the lower range of both parameters was determined by an extinction boundary. The upper ranges were chosen arbitrarily, but were high enough to adequately present the desired trends. The property values, which are given in the nomenclature list, correspond to a thin cellulosic sheet, which has been used extensively in recent microgravity experiments.[20,30,31]

While the computation was carried out in nondimensional coordinates, some results will be presented in dimensional form. As a reminder, the space coordinates ($\overline{x}$ and $\overline{y}$) were non-dimensionalized by the thermal length. The

---

*Low-speed forced flow at strictly zero gravity is modelled. The effect of microgravity is not considered at this time.

†Unless otherwise noted, the oxygen content will always be expressed on a molar basis.

‡The magnitude of all of the forced flow velocities considered were well below those encountered in normal gravity flame spread.

elliptic domain extended from x=-20 to 70 and y=0 to 90. The parabolic domain extended from x=70 to 1570 and y=0 to 150. Over the range of velocities in this study, the thermal length varied from 2.6 to 0.15 cm.

A total of 40 cases have been found. The computational test matrix is shown in fig. 7. Each circle on this plot represents a converged, steady flame. The two parameters varied were flow velocity and oxygen percentage.

4.1. Detailed Flame Characteristics For One Case

Before proceeding with any comparisons, one case will first be presented in detail which shows all of the features that the computational model is capable of. For this flame, the oxygen content was 15% and the free stream velocity 5 cm/s. The thermal length for this case was 0.46 cm. This typical case was roughly in the center of the parameter space.

4.1.1 Gas Phase Profiles; 5 cm/s, 15% O_2

Fig. 8 shows isotherms in the nondimensional space. The temperature field is able to be probed extensively. In part (a), a long view is shown to demonstrate the extent of the flame and thermal plume. This view in fact covers a portion of the elliptic and parabolic domain. More will be said later, but it is evident that the isotherms smoothly span the interface (x=72) between the two domains. The maximum temperature in the gas phase occurs very near the

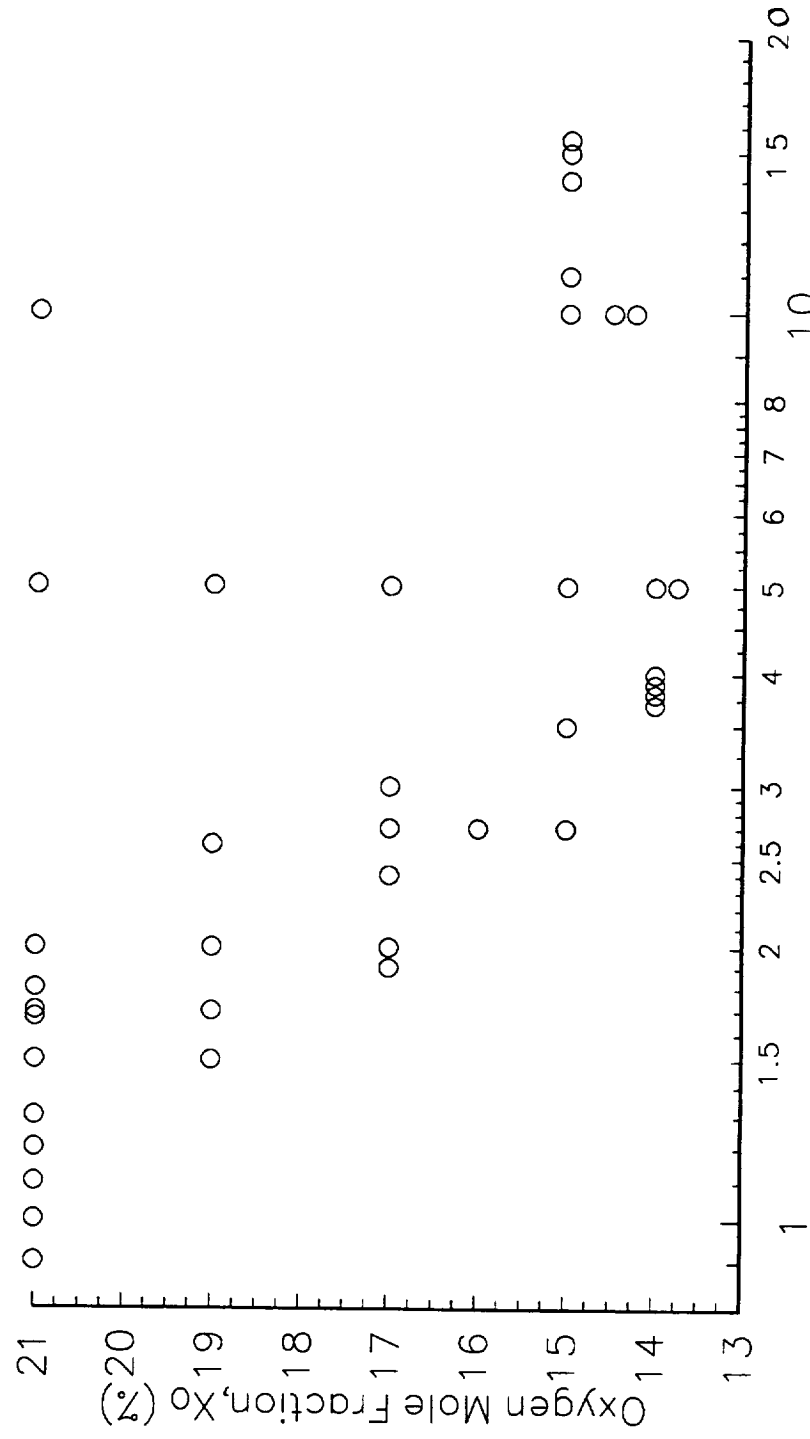

Figure 7. Computational test matrix.

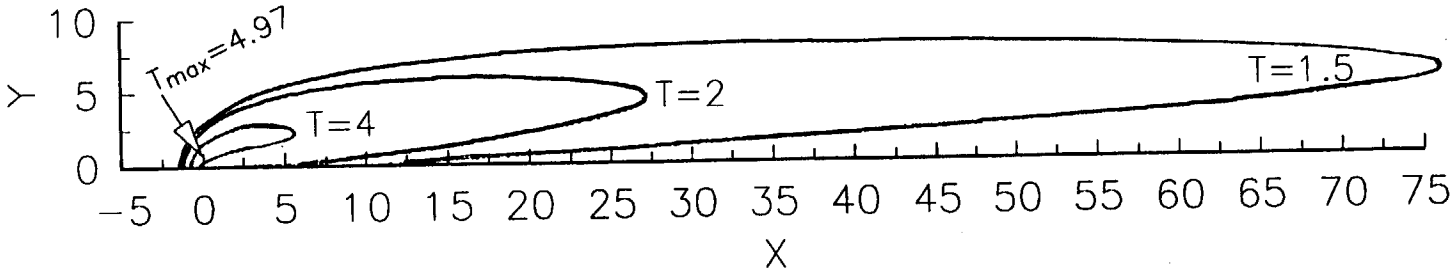

(a) View showing overall isotherm structure

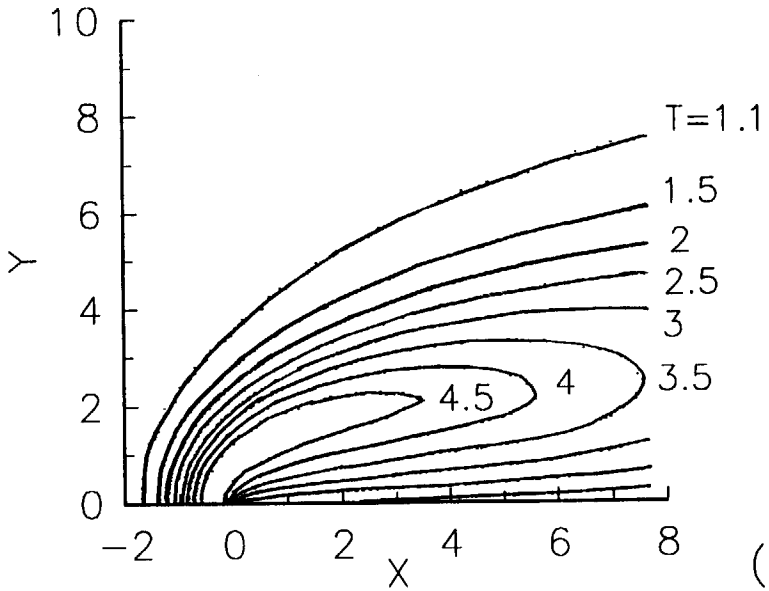

(b) Blow−up of leading edge

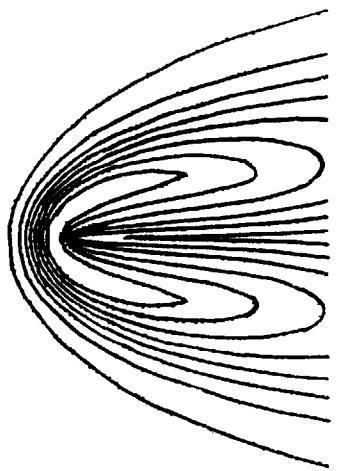

(c) Thermal structure (using symmetry)
Isotherm values are the same as in (b)

Figure 8. Nondimensional Isotherms. $\bar{U}_\infty$=5 cm/s, X_0=15%

burnout location (x=0), as indicated. This is true for most of the cases examined. Only as the flame approaches blowoff does the maximum temperature get shifted downstream. In part (b), the flame structure at the leading edge is enlarged to show the detail of the heat transfer in this region. Clearly, the diffusion is two-dimensional since significant heat and mass transfer upstream of the fuel has occurred. This is one of the justifications for using an elliptic treatment to capture the flame stabilization region. Notice that the temperature changes from the ambient value to the maximum value in the span of about one or two units. This verifies the choice of thermal length as the important length scale. In part (c), the solution is reflected about the y=0 plane to show what the thermal structure for the entire flame leading edge looks like. The temperature tends to fan out somewhat as it cools. This is a characteristic of the small, short flames predicted in this work. In contrast, a flame burning in a normal gravity buoyant environment tends to stay closer to the fuel in the downstream region. This flame shape effect is demonstrated in the small, low-velocity flames of refs. 20, 30, and 31.

In fig. 9, the mass transfer aspects of this diffusion flame are presented. In part (a), the fuel and oxygen mass fraction contours are shown in the leading edge region.

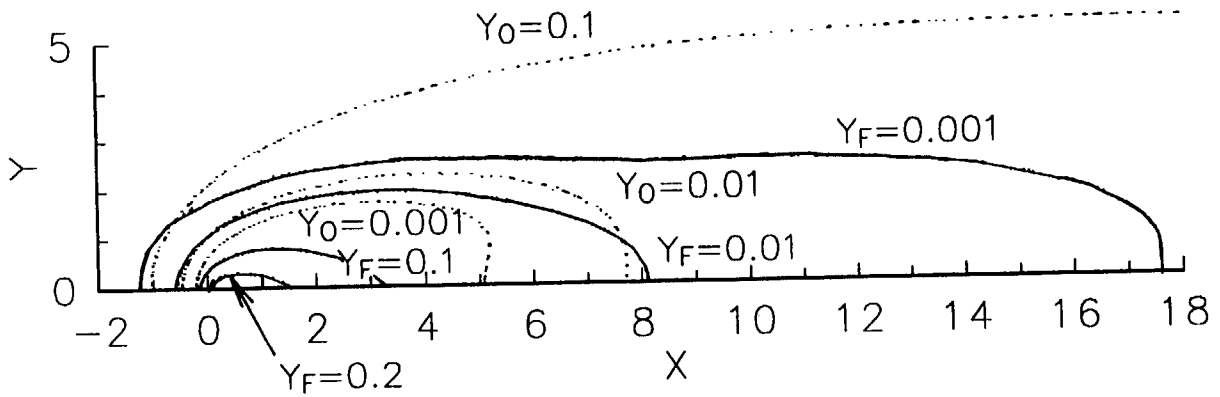

(a) Fuel and oxygen mass fraction contours showing overlap

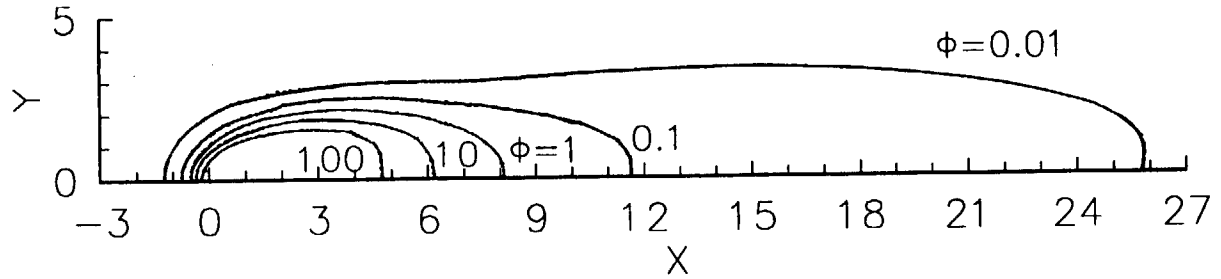

(b) Local equivalence ratio contours

Figure 9. Concentration profiles. $\bar{U}_\infty$=5 cm/s, X_O=15%

The contours overlap most near the burnout point. Notice how slowly the fuel is consumed in the downstream region, based on the large separation of contours there. In part (b), the local equivalence ratio* contours are shown. Again, the contours are drawn out downstream. In some earlier works, the flame length is defined as equalling the length of the ϕ=1 contour.[15] This definition is an artifact of the flame sheet models which defined the flame as existing at the location of stoichiometric equivalence ratio.

In examining the expression for reaction rate, it is seen that the three requirements needed for a robust reaction are: 1) presence of fuel, 2) presence of oxygen, and 3) an elevated temperature. This common sense description suggests that the maximum reaction rate for this case should also be confined to the near-burnout region since this is where the temperature is highest and significant oxygen and fuel overlap occurs. Indeed, in fig. 10, part (a), the reaction rate contours are clustered near x=0. The highly non-linear Arrhenius expression for the reaction rate is unmistakable in the very sharp gradients (the contours are separated by a factor of ten).

---

*The local equivalence ratio is defined as the ratio of fuel to oxygen, divided by the stoichiometric fuel to oxygen ratio.

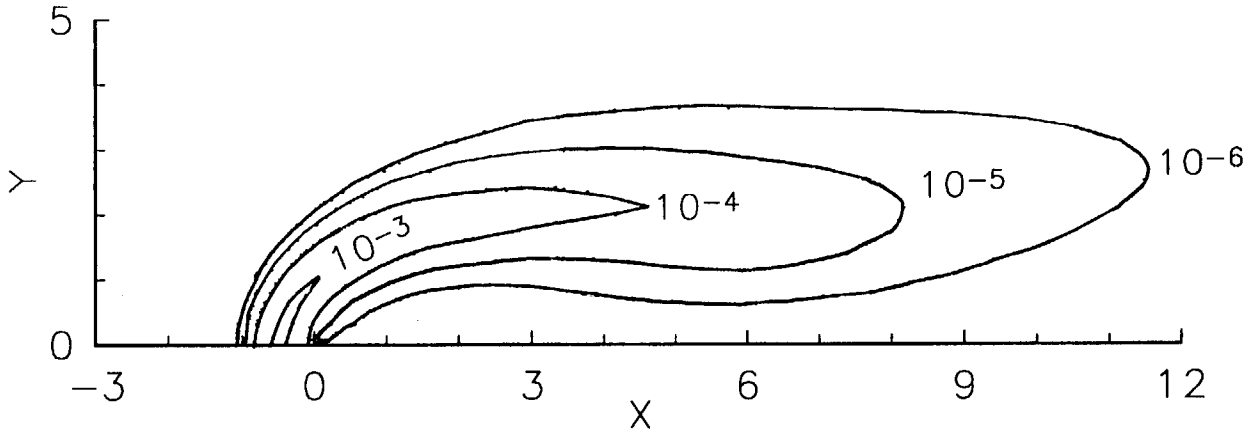

(a) Fuel Reactivity contours; units given in g/cm^3/s

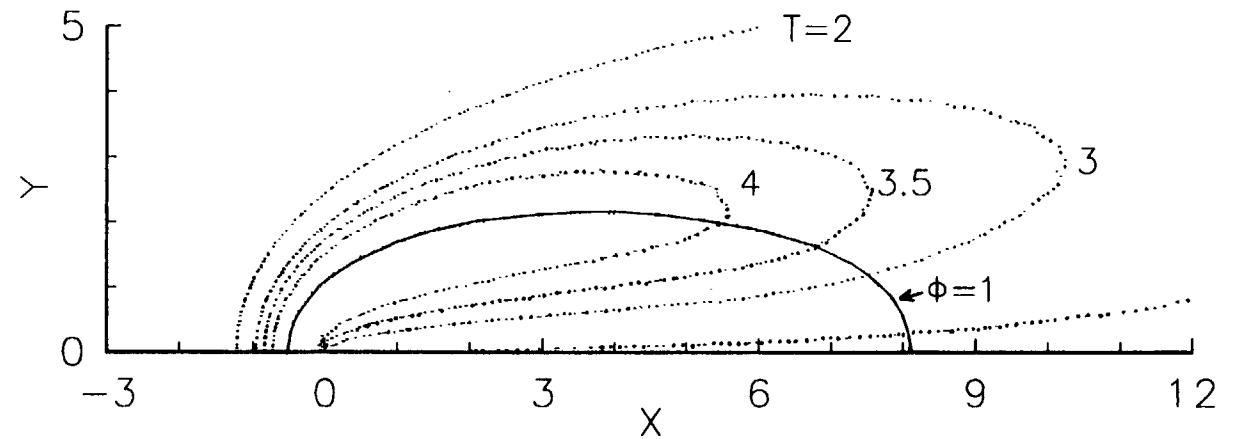

(b) Isotherms and stoichiometric equivalence ratio line

Figure 10. Various flame length depictions. $\overline{U}_\infty$=5 cm/s, X_O=15%

One way of defining the visible flame is to choose a reactivity contour. This is perhaps the best way in that the reactivity level should roughly scale with the number of photons emitted in the reaction such that our eyes can register something there. In this work, the reactivity contour equal to 10^{-4} g/cm^3/s is arbitrarily defined as the boundary of the visible flame (as seen later, this gives a flame shape very similar to that found in experiment). In a numerical study such as this, it is important mainly to use a consistent definition of the visible flame. For comparison, part (b) gives the isotherms and ϕ=1 contour on the same scale.

A benefit of solving the Navier-Stokes equations is that we can probe the velocity field in detail. In fig. 11, velocity vectors are plotted in the flame leading edge region*. There are several features which should be pointed out. As the flow approaches the fuel plate (x=0), it decelerates and is deflected up. Initially, the flow decelerates due to the plate and the hot flame (the visible flame, as defined above, is shown). The flow is deflected both merely by the presence of the plate and due to the influence of the blowing of pyrolysis products from the

*The velocity vectors in fig. 11 were nondimensionalized by the relative velocity, which for this case was 4.62 cm/s.

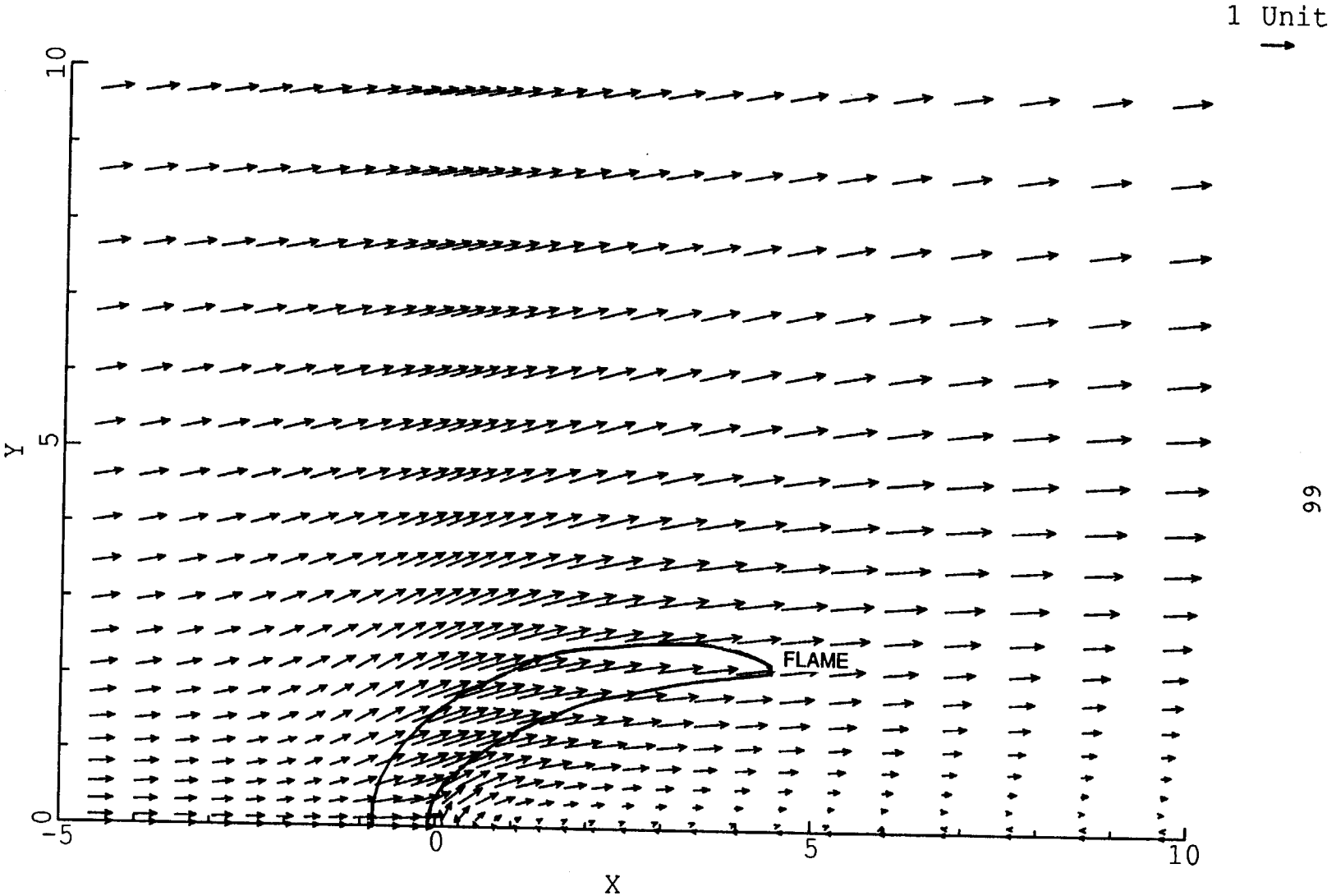

Figure 11. Velocity vector plot. $\bar{U}_\infty$=5 cm/s, X_O=15%

fuel. Since there is gas expansion due to the heat release, the flow accelerates in the flame zone. As we move downstream, the velocity profile flattens out due to viscous effects and the cooling of the gas stream. As described earlier, the equations have been solved in flame fixed coordinates. The fuel feeds in from the right at the flame spread rate. In fig. 11, the velocity on and near the fuel plate is indeed to the left. If the transformation is made back to the laboratory reference frame, the velocity vectors in fig. 12 result. Here, the flow characteristics near the plate are quite conventional. The fuel issues from the surface in the y-direction and is blown downstream.

In fig. 13, streamlines in both flame and laboratory fixed coordinate systems are shown. The stagnation streamline is chosen as $\Psi=0$. It shows the influence of the fuel blowing, as it is lifted off the surface. The streamlines given by $\Psi<0$ are a result of pyrolysis gases being blown off the fuel surface. The streamlines given by $\Psi>0$ represent the imposed forced flow.

In the velocity and streamline plots for this case, the difference between flame and laboratory fixed coordinate systems is small because the spread rate is a small percentage of the relative velocity. The spread rate is at most 18% of the relative velocity in all cases studied.

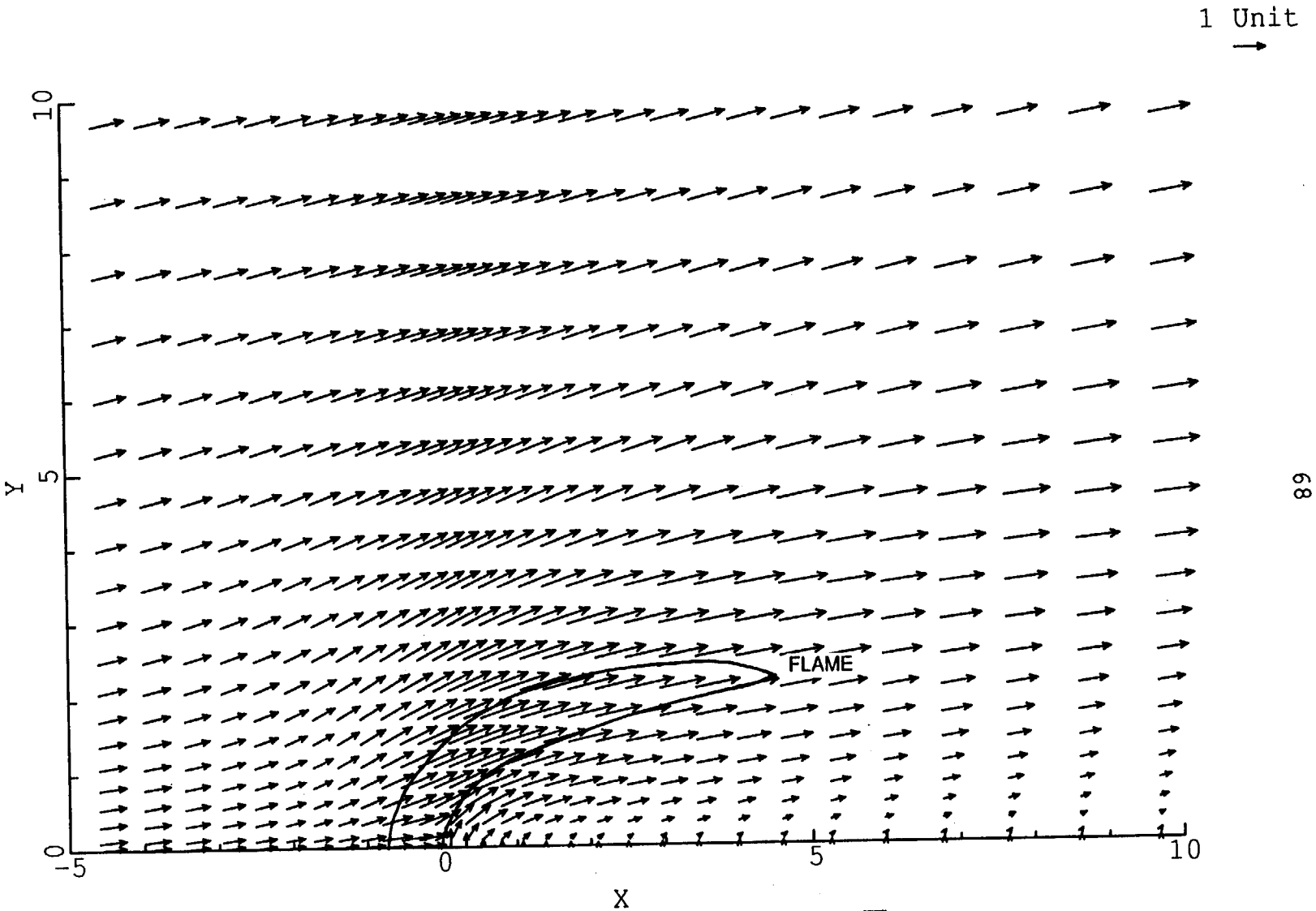

Figure 12. Velocity vector plot (lab. coordinates). $\bar{U}_\infty$=5 cm/s, X_0=15%

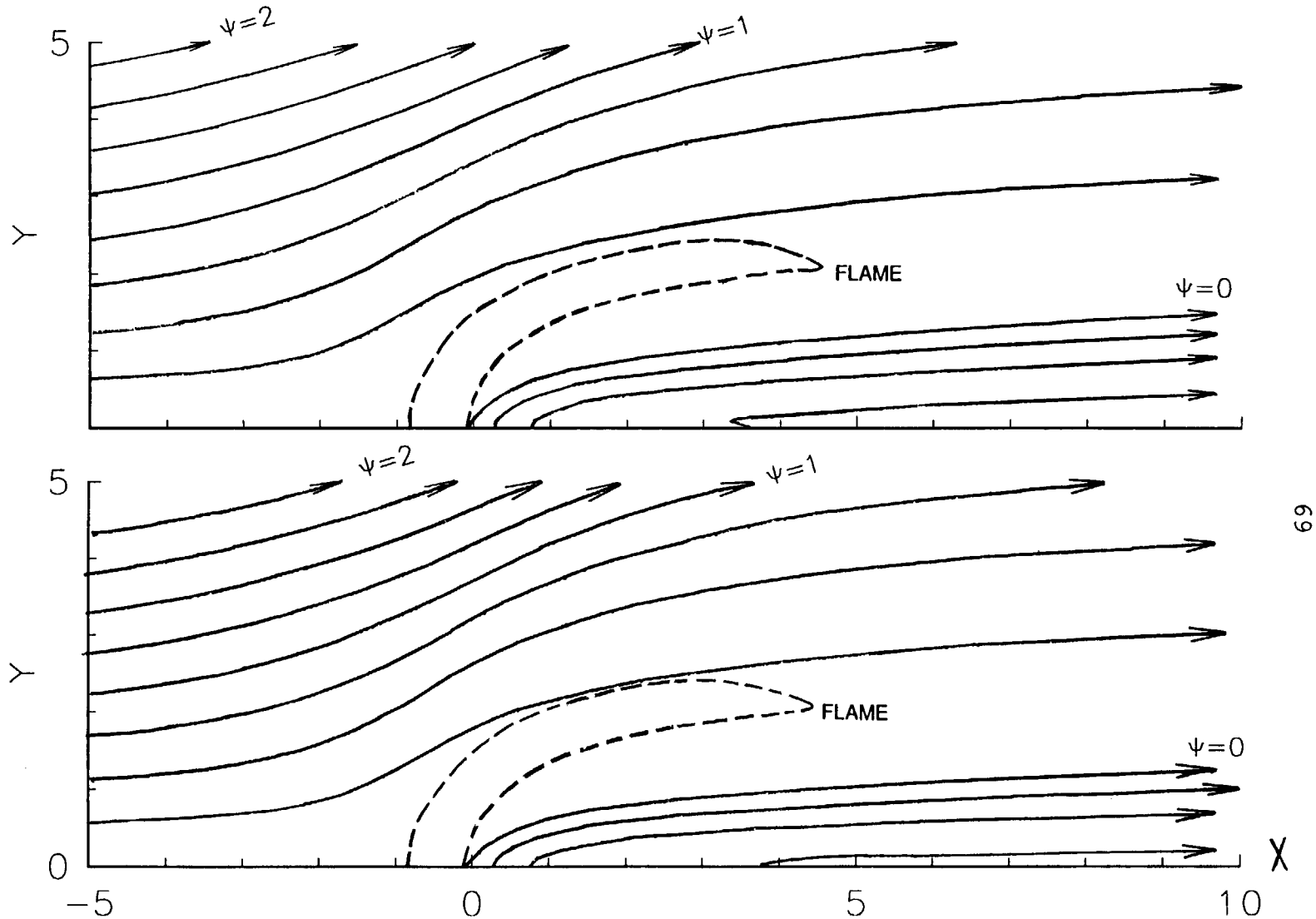

Figure 13. Streamlines in flame (top) and lab. (bot.) coordinates.
$\overline{U}_\infty$=5 cm/s, X_0=15%

The pressure field in the flame leading edge region is depicted in fig. 14. Remember that nondimensional pressure is used, referenced to ambient pressure, $P = (\overline{P} - \overline{P}_\infty) / \overline{\rho}^* / \overline{U}_R^2$. The magnitude of the pressure changes in dimensional terms is tiny, because of the very low speed flows considered. Two pressure rises, the first due to the presence of the hot flame and the second due to the plate are shown. Downstream, the pressure slowly returns to the ambient value as the gas flows from the influence of the leading edge and flame.

4.1.2 Solid Phase; 5 cm/s; 15% O_2

The solid phase will now be presented. In fig. 15, the heat flux incident on the solid, the solid temperature, thickness*, and blowing velocity are all shown over the whole domain. All variables are in nondimensional terms. The heat flux curve is quite spiked at the burn out point. This is because the flame gets closest to the fuel there. The surface temperature is relatively level in the pyrolysis zone. At about x=8, there is an inflection point in both the solid temperature and heat flux curves. This indicates the end of the pyrolysis region. At this point, the solid thickness is at 99.9% of its unburned value. This criterion for solid thickness is used to find the

*Here, thickness is nondimensionalized by its initial value.

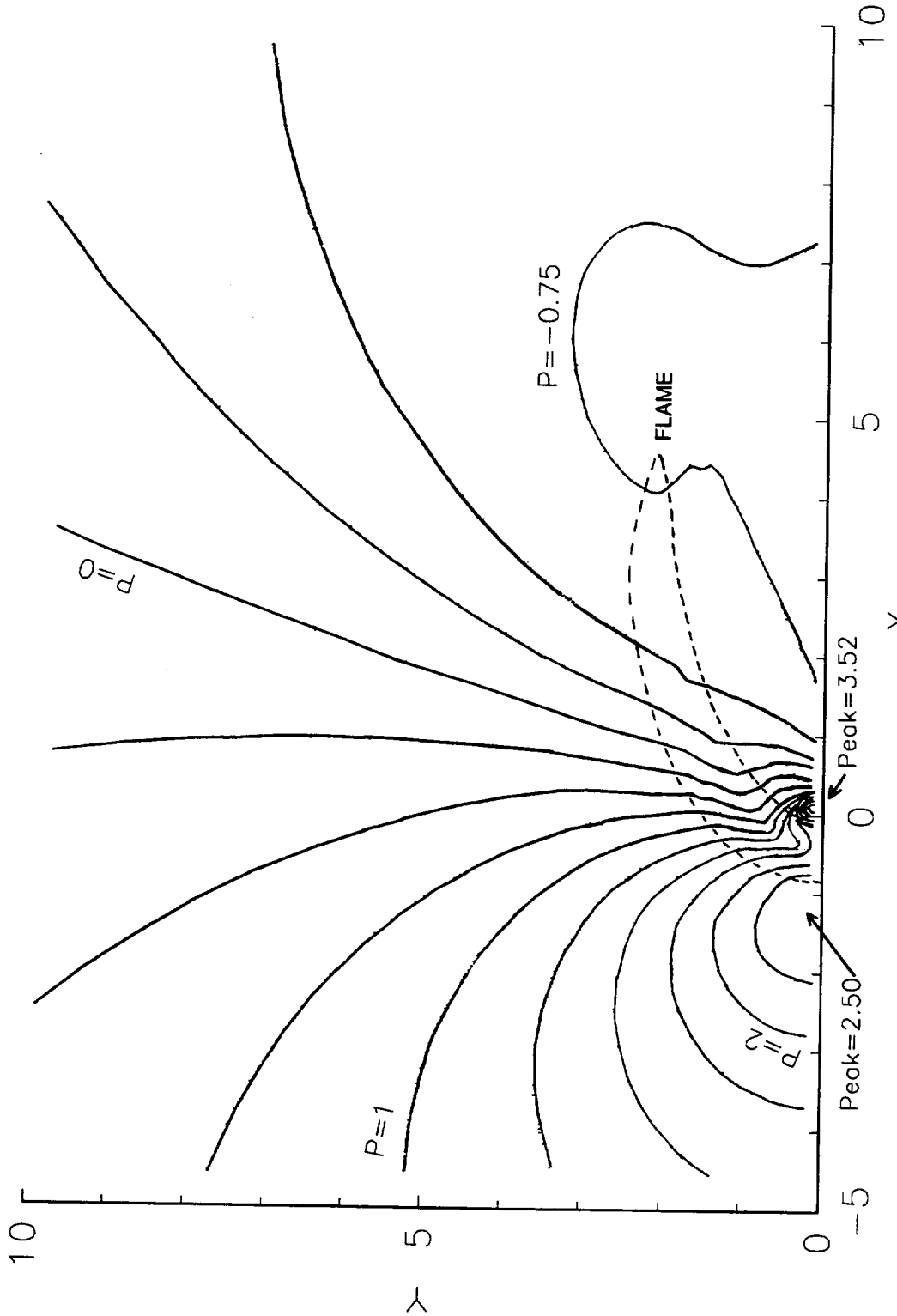

Figure 14. Isobars. $\bar{U}_\infty$=5 cm/s, X_O=15%

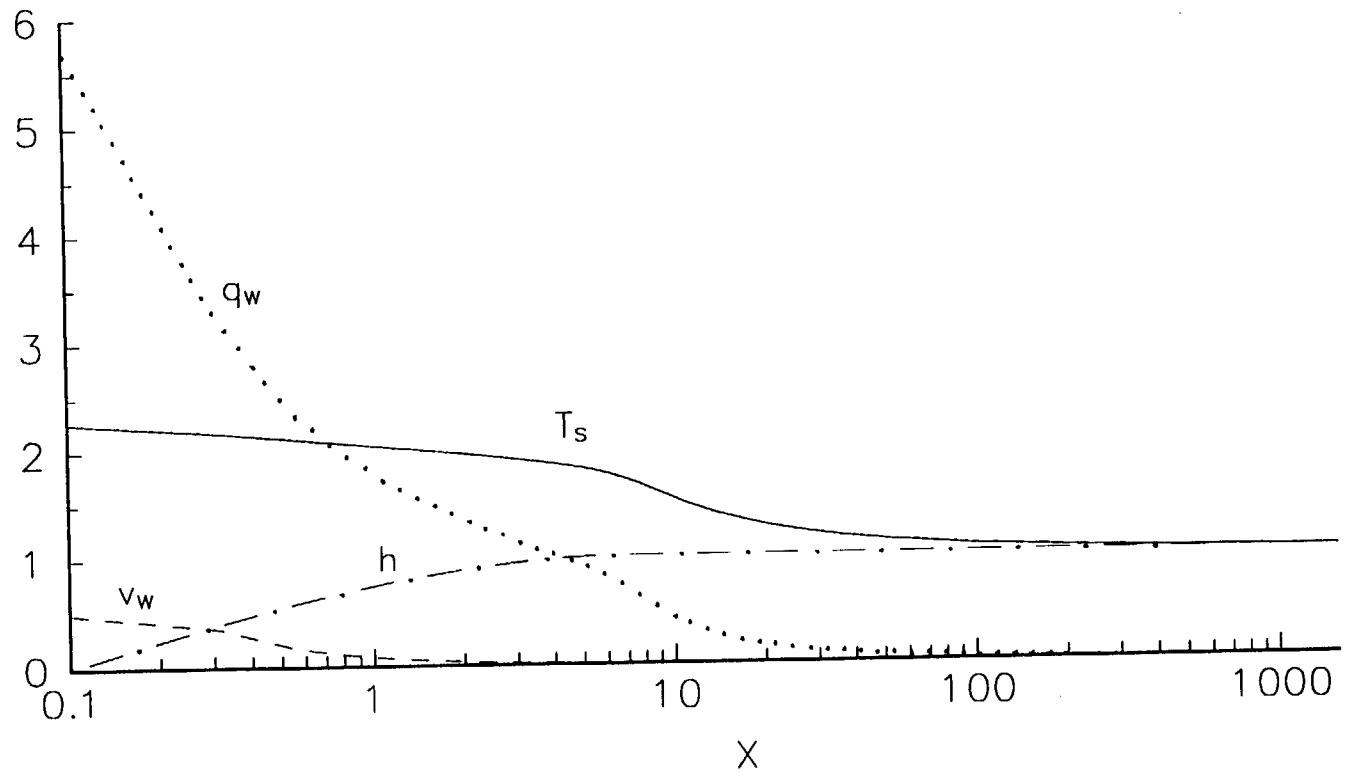

Figure 15. Solid phase profiles: incident heat flux, surface temperature, fuel thickness, and blowing velocity. $\overline{U}_\infty$=5 cm/s, X_0=15%

pyrolysis length in all cases (used later in §4.3), and corresponds very nearly to the inflection points evident in the T_s and q_w curves. Most of the fuel blowing into the gas phase is confined to a small region on the x-axis.

4.2. Comparison With Experiment

In ref. 30, a number of experiments were performed in the 5.18 sec. Zero Gravity Facility at NASA Lewis Research Center in Cleveland. The effort focused on concurrent flow flame spread over a thin fuel (tissue paper, Kimwipes*) in very slow speeds. The forced flow was generated by moving the entire fuel plate into a quiescent oxidizer.

While the fuel sheet was not perfectly flat or uniform in appearance, care was taken to get as good a sample as possible. The detailed modelling of the macrostructure and pyrolysis of the fuel was outside the scope of this effort. We use a simplified model to capture the important trends.

For most of the cases, 5.18 seconds was not enough for the flames to reach steady state. However, some of the flames seemed to be close to steady. One such case will be used for comparison. The experiment was performed at 15% O_2 and 4.84 cm/s. The theoretical comparison is done at 15% O_2 and 5 cm/s. The experiment recorded only the visible flame using motion picture photography. Therefore,

---

*Trademark of Kimberly-Clark Corporation, Roswell, GA

only a comparison of the overall flame dimensions and spread rate is possible. In fig. 16, the computed fuel reactivity contours are compared to the reported experimental flame shape (this is how the flame looks just prior to the end of the 5.18 sec. drop). The flame shape is predicted quite well if the proper reactivity level is chosen to define the threshold of visible emission. For this case, that level is around 10^{-4} g/cm^3/s. In the experiment, it was not possible to resolve where the flame was relative to the burnout point, so the location of the flame in fig. 16b is a guess. The predicted spread rate of 0.38 cm/s was below the experimental value of 0.55 cm/s*.

Although the experimental data is not existent, various solid phase dimensional profiles from the computation are presented in fig. 17.

Finally, spread rate data at a free stream velocity of approximately 5 cm/s and at different oxygen concentrations are shown in fig. 18. The model is compared to the experiment. In the experiment, the velocity of both the flame base and the flame tip is reported, as shown in fig. 18, just before the end of the drop. Thus, the flames were

---

*The experimental spread rate actually is the mean of the flame tip and flame base spread rates. They were close (0.53 and 0.57 cm/s, respectively) but the flame was still shrinking slightly as it approached steady state. The shrinking flame suggests the spread rate would slow down, given more time.

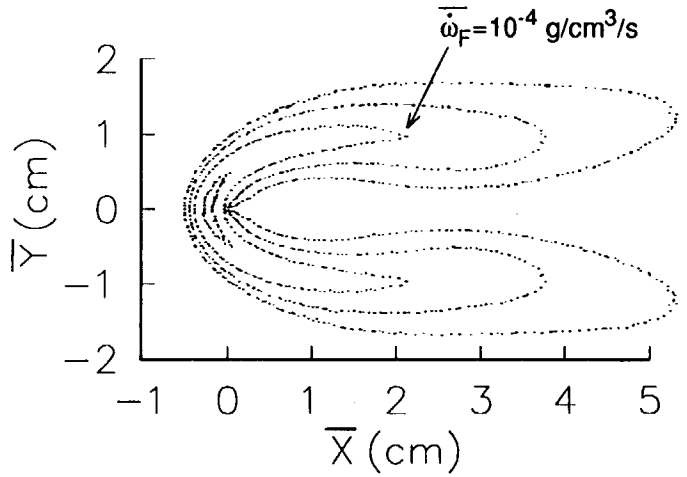

(a) Contour levels are same as in fig. 7a

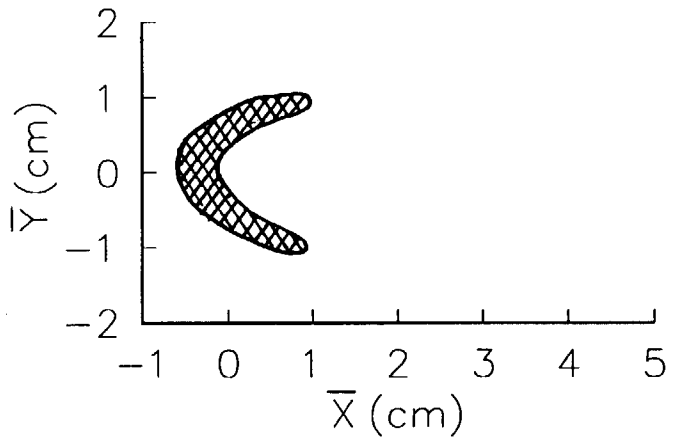

(b) Burnout point is not exactly known

Figure 16. Comparison of calculated fuel reactivity levels (a) with experimental flame shape (b). $\bar{U}_\infty \approx 5$ cm/s, $X_O=15\%$

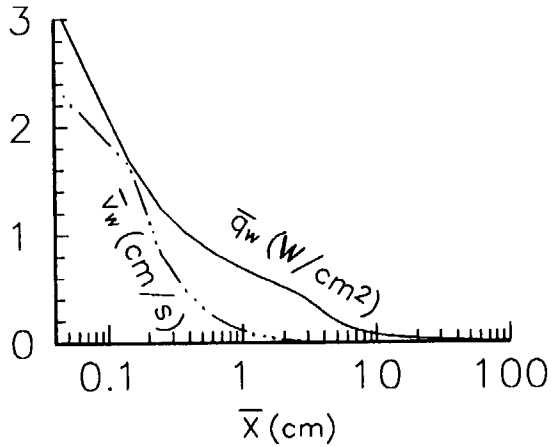

(a) Heat flux and Blowing velocity

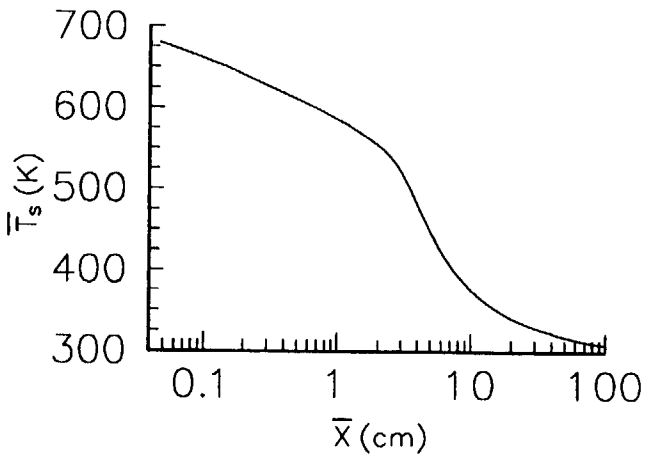

(b) Surface temperature

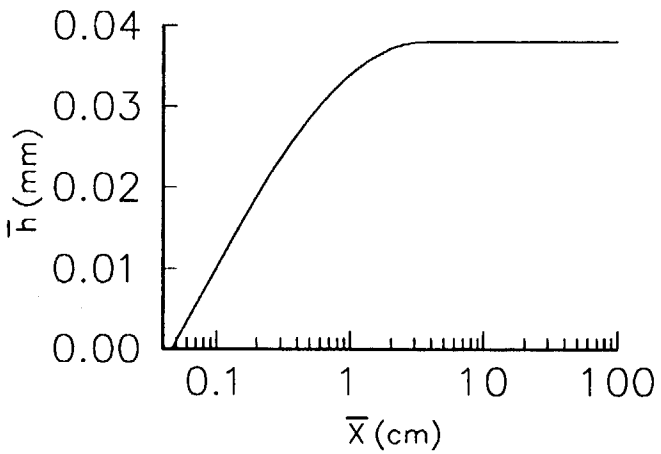

(c) Solid thickness

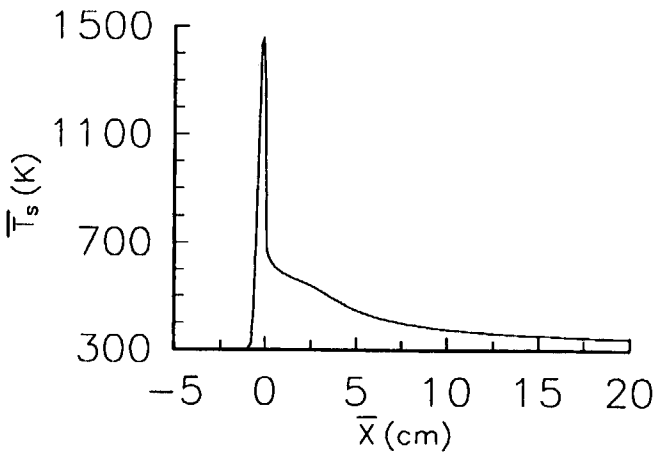

(d) Temperature along symmetry line (y=0)

Figure 17. Dimensional profiles. $\overline{U_\infty}$= 5 cm/s, X_0=15%

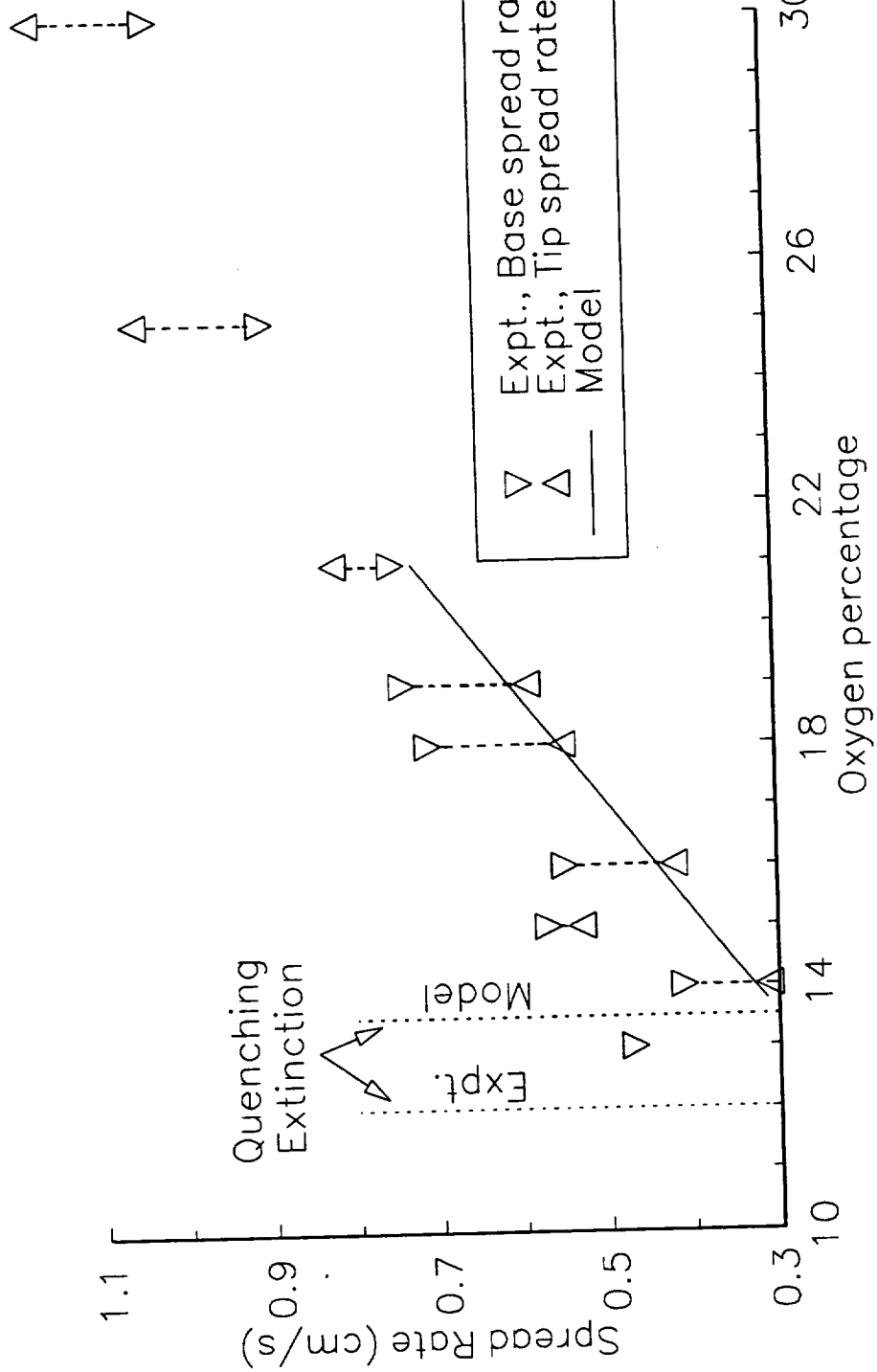

Figure 18. Comparison of model and experiment at a free stream velocity of approximately 5 cm/s.

reported as either getting shorter or longer at the end of the drop. Reasonably good agreement is obtained, assuming the flames will eventually reach steady state. One reason for the difference in the quench limits may be due to the short drop time, as a flame may need more time to go out.

An extensive comparison of all of the experimental data at this time is not practical since, as mentioned, many of the tests were still transient. The above data are presented to show that the model produces qualitatively the correct flame shape and spread rate trends, even though gas phase radiation, detailed flame chemistry, and a complicated pyrolysis model were not considered.

4.3. Parametric Comparison of Theoretical Results

The two parameters varied in this work are free stream velocity and oxygen concentration. Several comparisons will be presented.

4.3.1. Global Results: Spread Rates and Maximum Temperature

In fig. 19, the computed spread rates and maximum gas phase temperatures are presented for all of the computed cases. The data are plotted against the reference velocity, which is the relative gas velocity with respect to the solid burnout point (or flame) and is the quantity used in nondimensionalizing the equations. The spread rate increases approximately linearly with either flow velocity or oxygen percentage. Linear regression is used to get the

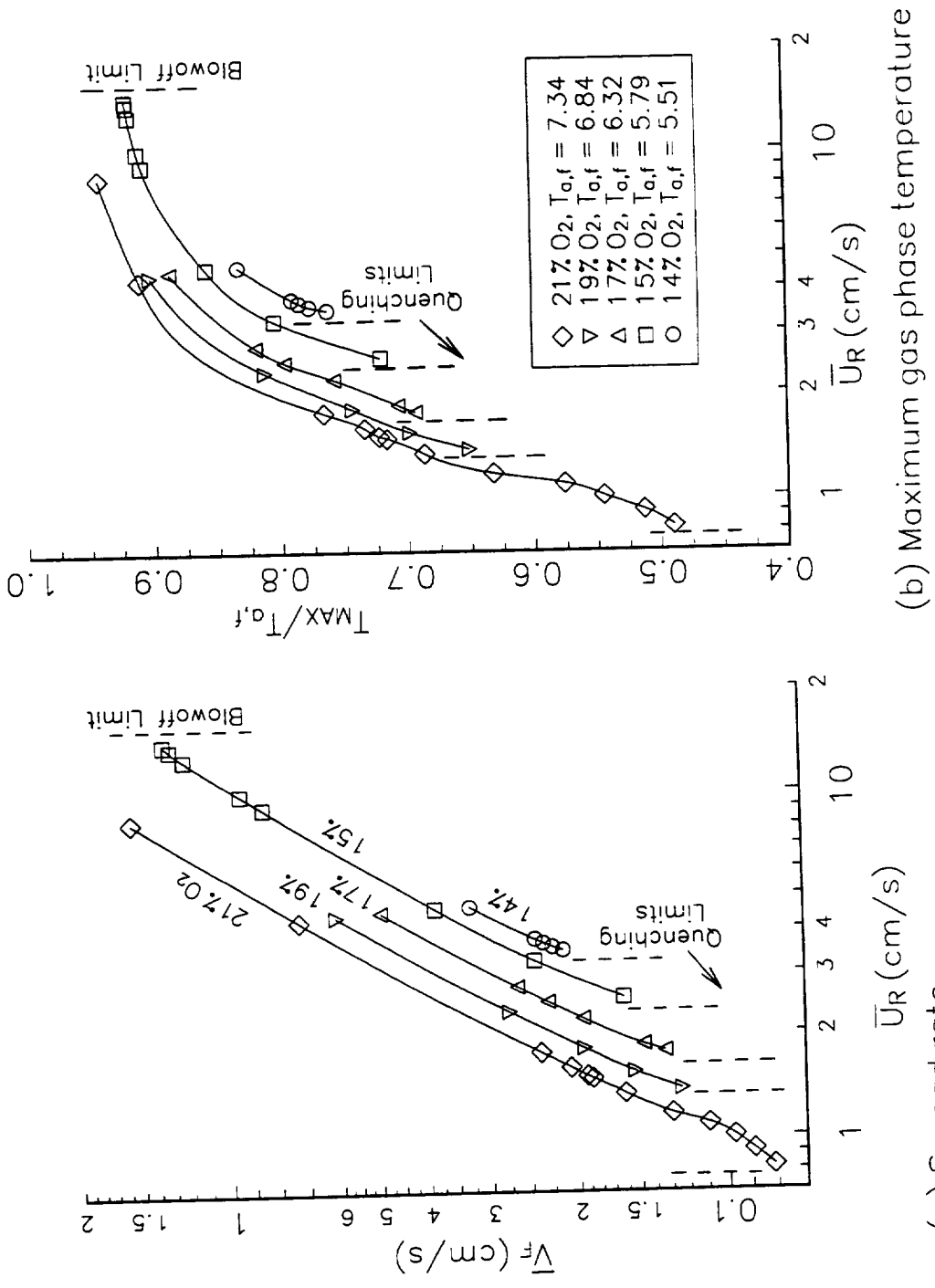

(a) Spread rate

(b) Maximum gas phase temperature

Figure 19. Spread rate and T_{max} as a function of relative velocity.

following relation, specific for the fuel used in this work:

$$\overline{V}_F = 1.12 X_{O_2} \overline{U}_\infty - 0.073 \overline{U}_\infty + 0.194 X_{O_2} - 0.121 \qquad (84)$$

In eq. (84), $\overline{U}_\infty$ and $\overline{V}_F$ are expressed in cm/s. In fig. 19, the dotted lines are flammability limits beyond which a solution does not exist. (The flammability limits will be discussed in a §4.4.) The spread rate trends and magnitudes are qualitatively similar to those obtained in the experiment.[30] Another study[32] examined concurrent flow flame spread over a thin fuel in a normal gravity horizontal wind tunnel at higher speed (>35 cm/s). After ignition, the flames would grow and eventually reach a steady state. Consistent with the theoretical results shown in fig. 19a, in ref. 32, the flame spread rate increased monotonically with forced velocity, in the velocity range less than 1 m/s. At high velocity (>1 m/s), however, the spread rate became constant as the flow velocity was increased.

In fig. 19b, the maximum flame temperature, normalized by adiabatic flame temperature, is plotted. Near the quench limit (at low velocities) the maximum temperature drops off dramatically. This is a result of the increased relative importance of heat loss for these small flames. The rate of heat loss becomes a significant percentage of

the combustion heat release rate. The resulting drop in flame temperature corresponds to the decrease in spread rate, as the heat flux to the fuel is reduced.

4.3.2. Parametric Comparison of Flame Structure

In order to demonstrate the effect of oxygen and flow velocity on flame structure, two sets of cases will be presented, one at constant oxygen level and the other at constant velocity.

In fig. 20, reactivity contours are shown in non-dimensional coordinates. The oxygen concentration is held at 15% and the flow velocity is varied from 2.7 to 15.5 cm/s. The flame becomes longer as velocity increases. The flame strength also increases. This is evident in the larger size of the highest reactivity zone. Also, at higher velocity, the reactivity contours tend to bend back toward the fuel downstream, indicating increased flame strength.*

The visible flame can be defined as the region enclosed by a reactivity contour (10^{-4} g/cm^3/s is assumed in this work). For the simple reaction scheme in this model, the rate of fuel reaction is the best measure of how the flame appears. Based on these contours, then, the

---

*The flame strength can be quantified as the area of the reactivity contours. This is a measure of the total heat release.

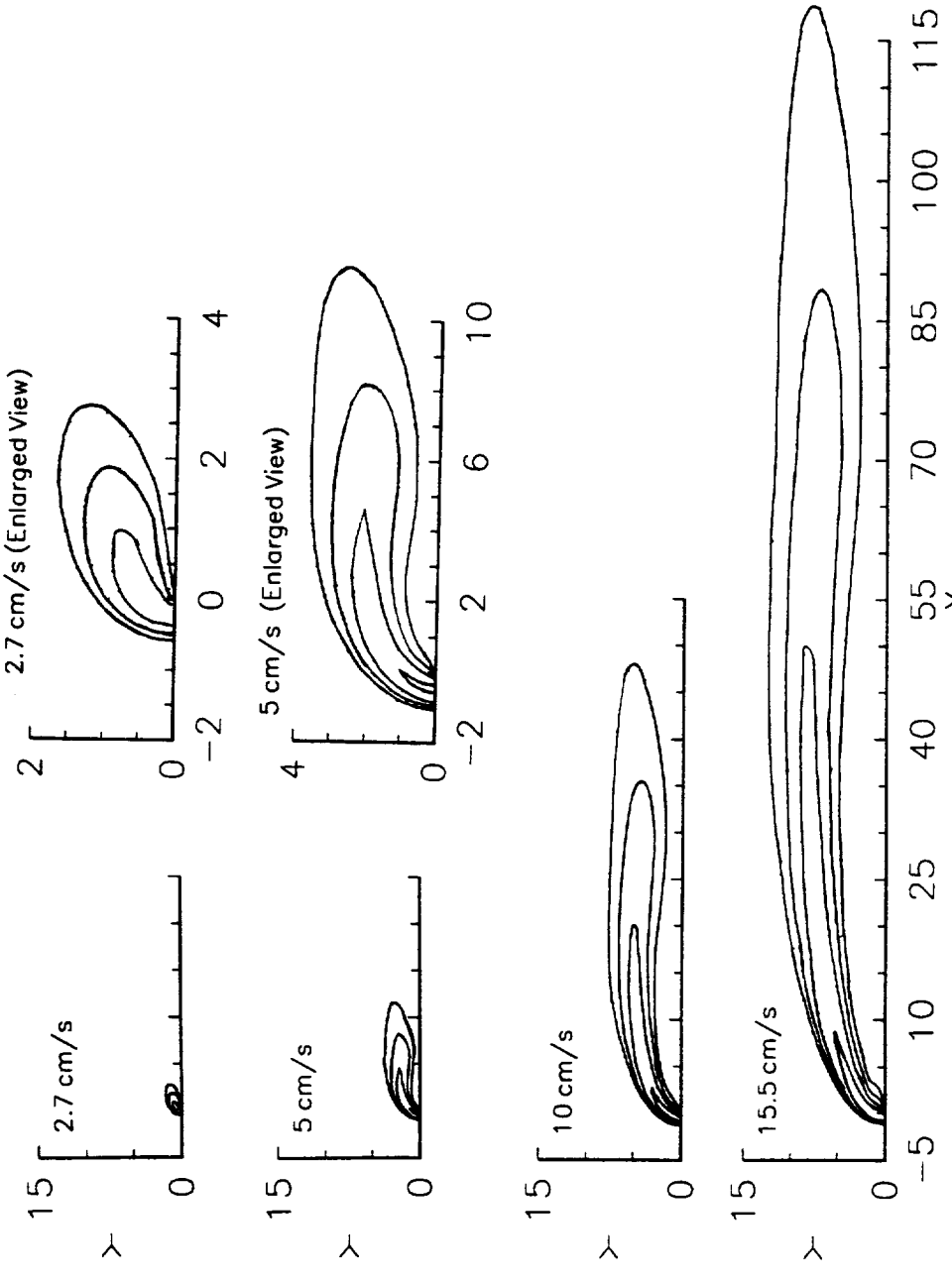

Figure 20. Fuel reactivity contours at 15% O_2. Weakest (outermost) contour is 10^{-6} g/cm^3/s. A factor of 10 separates contours.

flame aspect ratio (i.e., the length to width ratio) changes dramatically with velocity. Additionally, the maximum reactivity is always located very near the burnout point, which is the most upstream part of the flame and sees the oxygen first.

In fig. 21, the same flames are presented in dimensional coordinates. This plot demonstrates that flame length is greatly affected by velocity. In ref. 32, the flame length is reported to decrease with an increase in flow velocity (when $\overline{U}_\infty$ is between 0.35 and 1 m/s) before leveling off at high velocity (greater than 1 m/s). While contrary to the predicted results, this may be an effect evident only at higher velocities.

The effect of different oxygen concentrations at a fixed free stream velocity is shown in fig. 22. The flame length decreases slightly with oxygen. Again, the flames at higher oxygen are stronger based on the fact that they are bigger and tend to curve back toward the fuel downstream. In fig. 23, the flames are shown in dimensional coordinates. The difference between fig. 22 and fig. 23 is small because the relative velocity does not change to much for the different cases. Hence, the thermal lengths are approximately equal.

4.3.3. Flame Stand-off Distance and Thickness

When the flame thickness and stand-off distance are

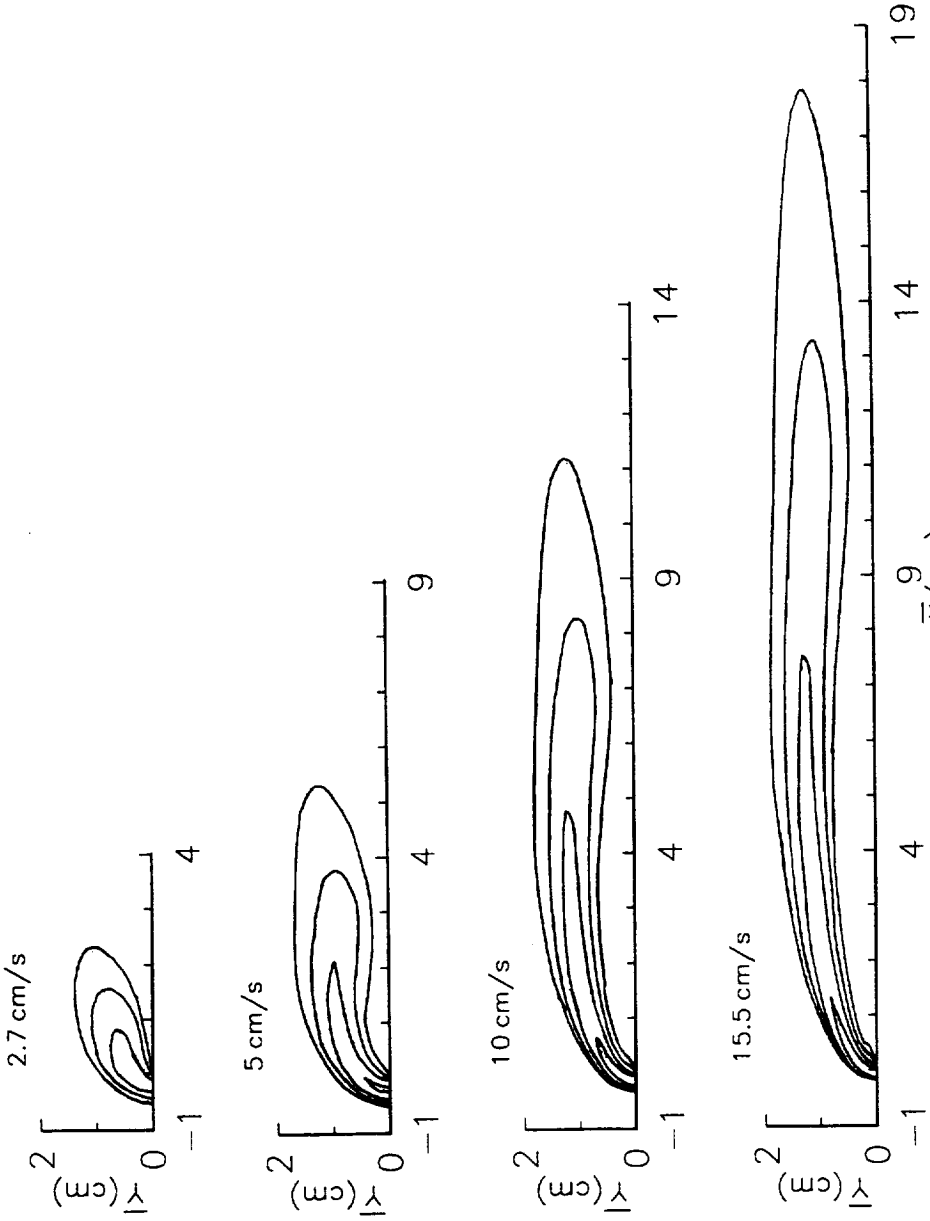

Figure 21. Dimensional fuel reactivity contours at 15% O_2. Weakest (outermost) contour is 10^{-6} g/cm^3/s. A factor of 10 separates contours.

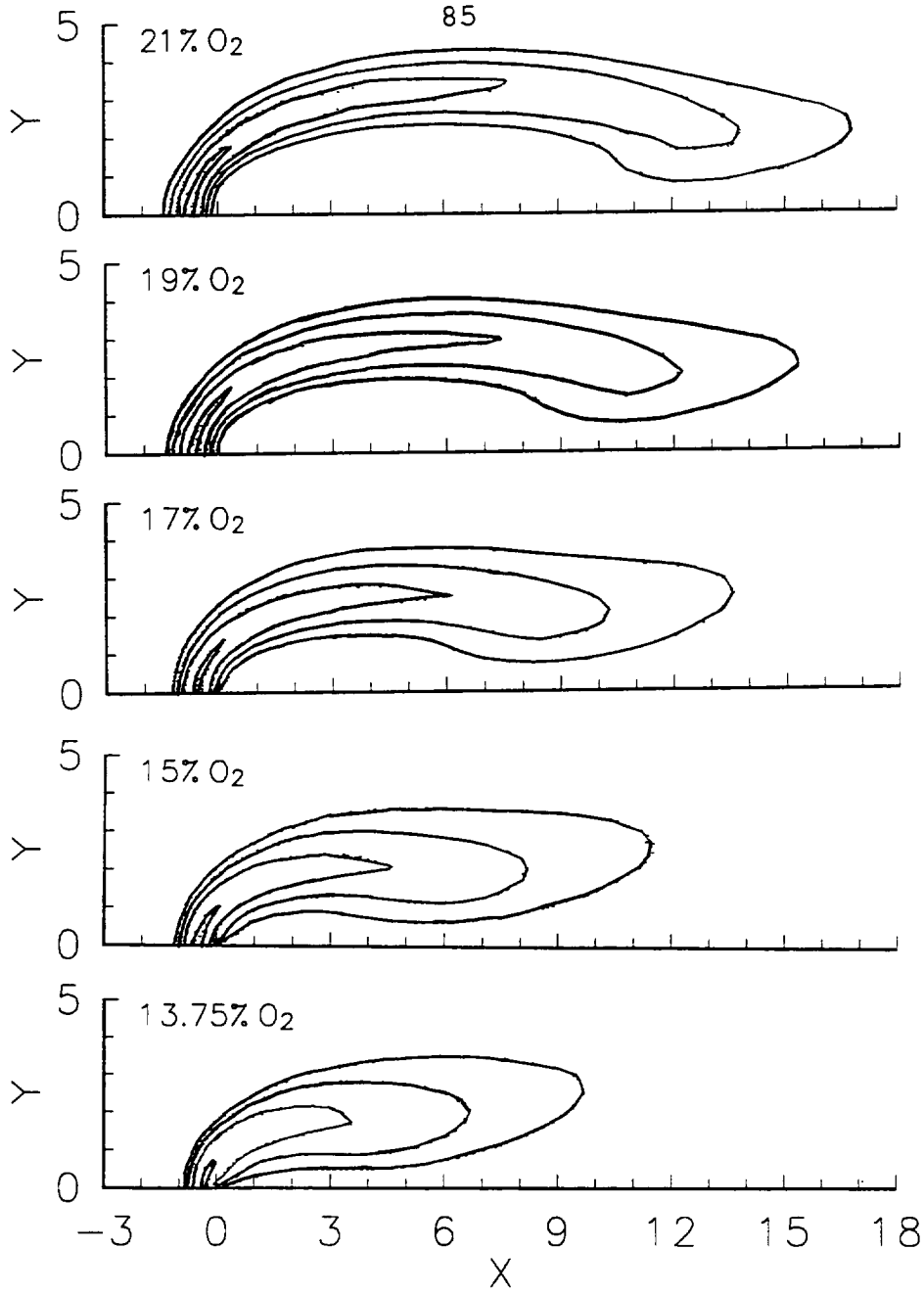

Figure 22. Fuel reactivity contours at 5 cm/s. Weakest (outermost) contour is 10^{-6} g/cm^3/s. A factor of 10 separates contours.

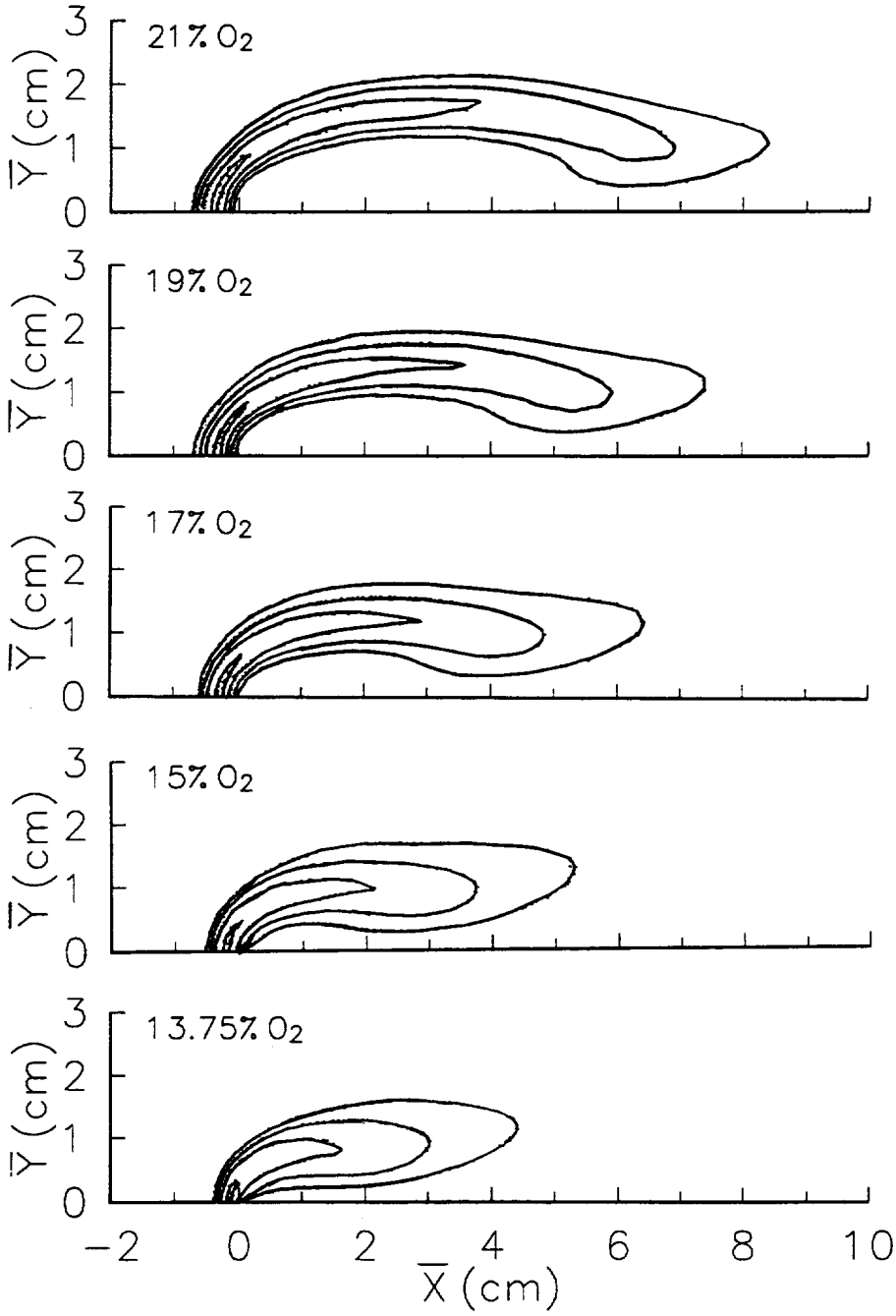

Figure 23. Dimensional fuel reactivity contours at 5 cm/s. Weakest (outermost) contour is 10^{-6} g/cm^3/s. A factor of 10 separates contours.

defined as shown in fig. 24, a comparison can be made. Fig. 24 presents both dimensional and nondimensional results. Looking at part (a) first, the dimensional flame stand-off distance and thickness increase with decreasing flow velocity except very near the quenching extinction limit. This is explained as follows. Initially, as the flow velocity is reduced, the flame moves away from the fuel and thickens, as it tries to move closer to the region of fresh oxidizer. As the flame moves away, the heat flux to the solid diminishes, leading to a decrease in the rate of pyrolysis. This makes the flame shorter and increases the relative importance of heat loss, hence cooling the flame. When the flame dimensions become the same order as the thermal length, two-dimensional heat conduction loss becomes important, further decreasing the flame temperature.* When this heat conduction loss becomes important, the flame forsakes the search for more oxygen and actually moves back toward the fuel in an attempt to maximize the ratio of heat flux to the solid to heat loss to the environment.

In fig. 24b, the dimensional flame stand-off distance increases monotonically with oxygen percentage. This is due to the increase in flame temperature with oxygen

*In a three-dimensional problem, the conductive loss in all three dimensions would become important.

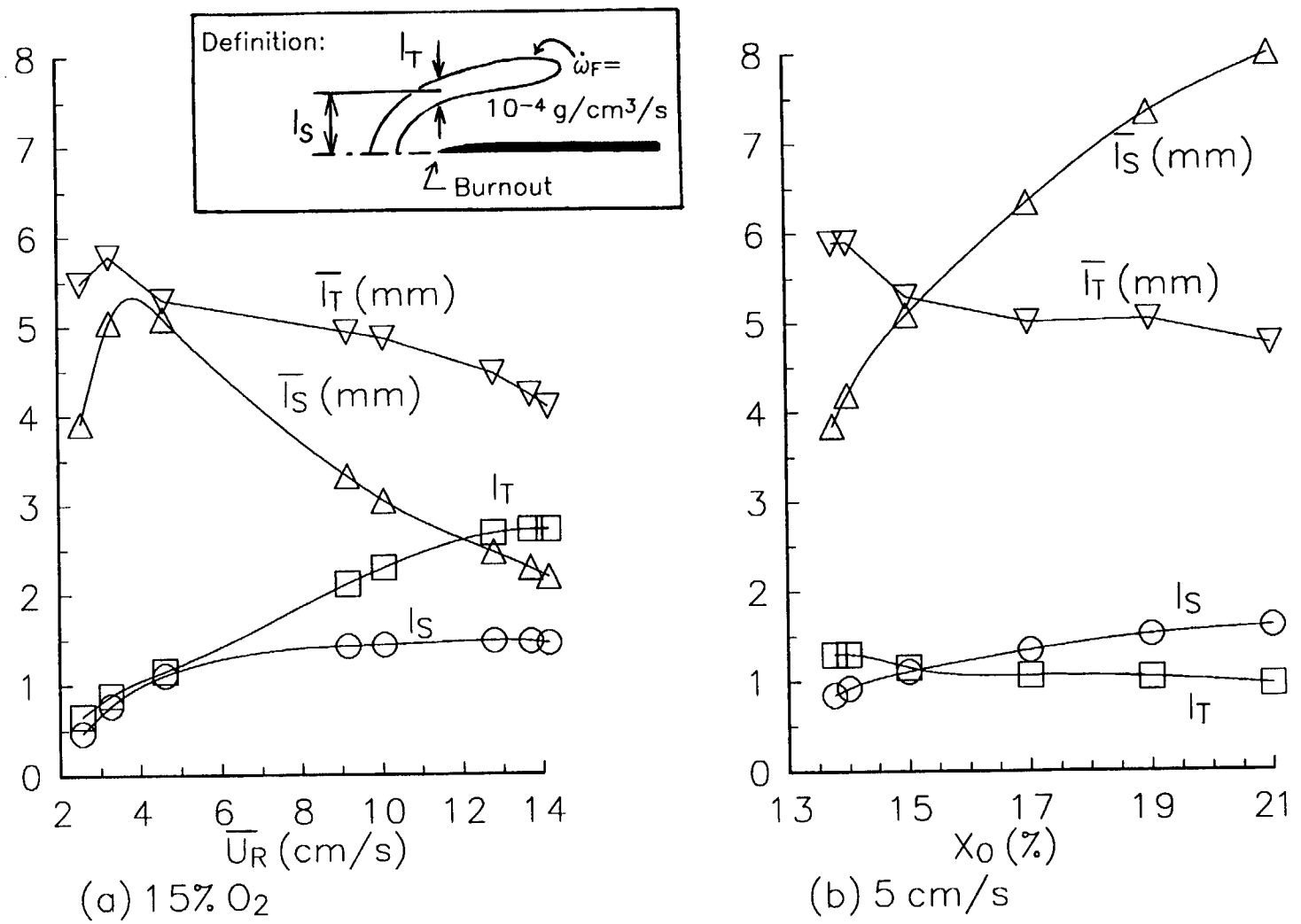

Figure 24. Stand–off distance, l_S, and flame thickness, l_T.

percentage. At higher oxygen, the flame simply does not have to get as close to the fuel because it is hotter. The burning rate is also higher, pushing the flame farther from the fuel. The flame is thinner at higher oxygen percentage because the mass diffusion driving potential is higher. Ultimately, the flame goes out as the oxygen percentage is reduced through the finite-rate chemical reaction term. The extinction mechanisms will be described in §4.4.

4.3.4. Solid Phase Parametric Results

The characteristics of the solid fuel are compared in fig. 25 which shows the effect of varying forced flow velocity on solid temperature and incident heat flux. In part (a), the surface temperature plots indicate that the maximum always occurs at the burnout point, as expected. Furthermore, the maximum increases as the flow velocity increases. This is due to the fact that the flame is pressed closer to the fuel at high velocities, increasing the heat flux and thus increasing the temperature. The heat flux profiles are shown in part (b). The increase in maximum heat flux due to increasing flow velocity is shown. Note the sharp bend in the curves. The point where the bend occurs indicates the end of the pyrolysis region. In general, as flow velocity is decreased, the heat flux, solid temperature, and pyrolysis length decrease. For the lowest-energy flames in this work (i.e. low fuel consump-

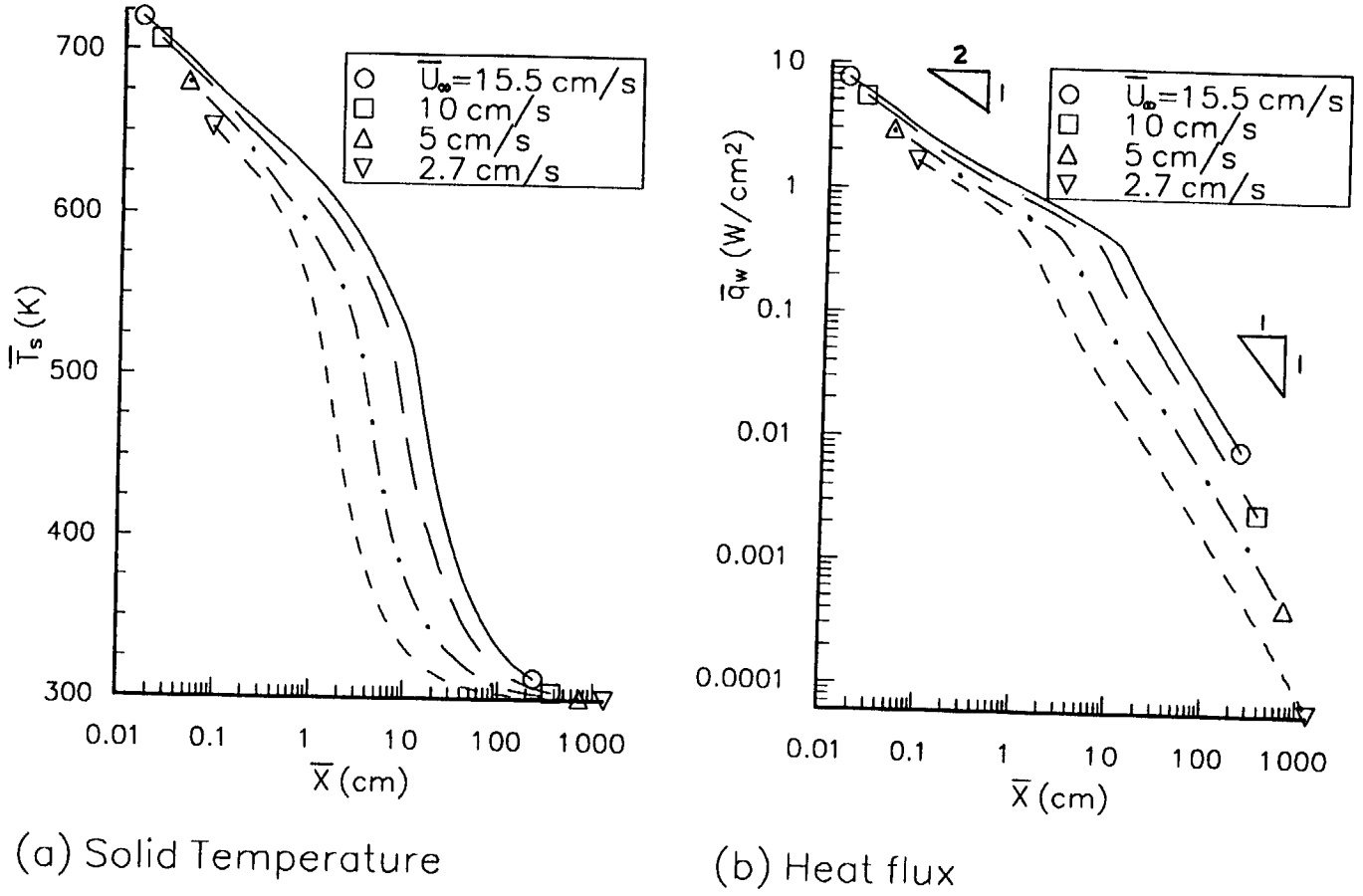

Figure 25. Solid temperature and heat flux profiles at 15% O_2.

tion rate or spread rate), the pyrolysis region begins to approach point source behavior, as quenching extinction is neared (described in §4.4).

The heat flux in all cases varies approximately as $\bar{x}^n$, where $n \approx -1/2$ in the pyrolysis region, and $n \approx -1$ in the preheat region.* Considering a non-reacting boundary layer with heat transfer, for an isothermal plate, $\bar{q}_w \sim \bar{x}^{-1/2}$. This is approximately given in the pyrolysis region. In general, if the appropriate temperature difference in the boundary layer is specified as $(\bar{T}_g - \bar{T}_w) \sim \bar{x}^m$, then $\bar{q}_w \sim \bar{x}^{m-1/2}$. Thus, if $m=-1/2$, the heat flux to the solid in the preheat region for this problem is reasonable.

In fig. 26, similar results are plotted to demonstrate the effect of varying oxygen percentage at fixed free stream velocity. Again, the pyrolysis length is clearly shown by the bend in the heat flux curves. The solid temperature, heat flux, and pyrolysis length, decrease with decreasing oxygen percentage. (In fig. 26b, the curve at 21% O_2 has a small kink right at the elliptic/parabolic interface, $\bar{x}$=40 cm. This is a manifestation of the difference between the equations in the two domains.)

4.3.5. Definition of Various Length Scales

The definition of pyrolysis length is somewhat

---

*The actual exponents are closer to n=-0.43 in the pyrolysis region and n=-1.1 in the preheat region.

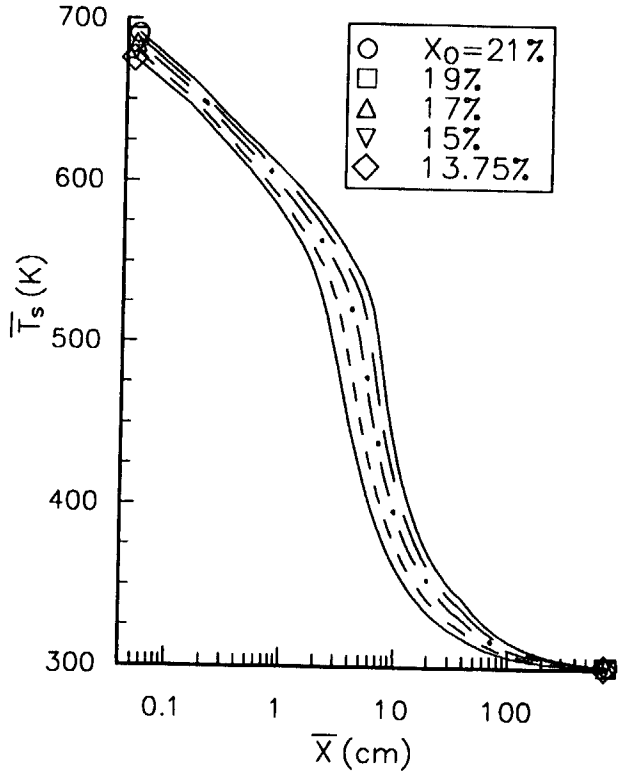

(a) Solid Temperature

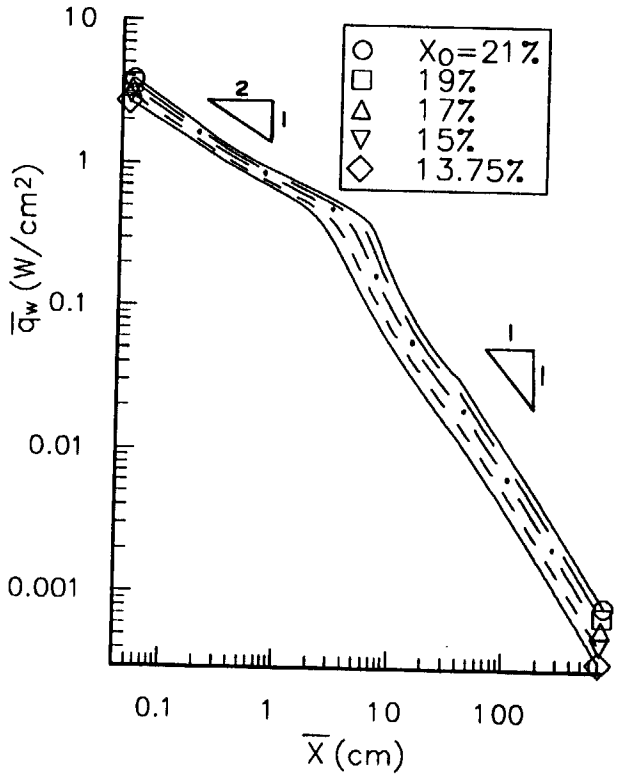

(b) Heat flux

Figure 26. Solid temperature and heat flux profiles at 5 cm/s.

arbitrary. In an experiment, the pyrolysis front may be determined as the point where blackening of the paper first occurs.[32] In a theoretical model, the pyrolysis front is often described as the point where a certain percentage of fuel remains. In this work, the pyrolysis front was chosen as the point where 99.9% of the fuel remains. It turns out that for all cases, this specification corresponds very closely to the bend in the heat flux curves (seen in fig. 26, for example).

Another length scale of interest in the solid phase is the preheat length, which is the distance required for the fuel to heat up to the temperature at which pyrolysis first occurs. In this work, the definition of preheat length is based on the heat flux to the solid, as follows. The heat flux at the end of pyrolysis is found. The preheat length is defined as the point from the end of pyrolysis to the point where the heat flux has dropped by a factor of ten.

Finally, the flame length is defined as the length of the visible flame, which was defined earlier as the region bounded by the fuel reactivity contour of 10^{-4} g/cm^3/s.

The results are summarized in fig. 27. The pyrolysis, flame and preheat lengths all vary linearly with flow velocity and oxygen concentration.

4.4. Extinction Boundary

One of the main goals of this work was to determine

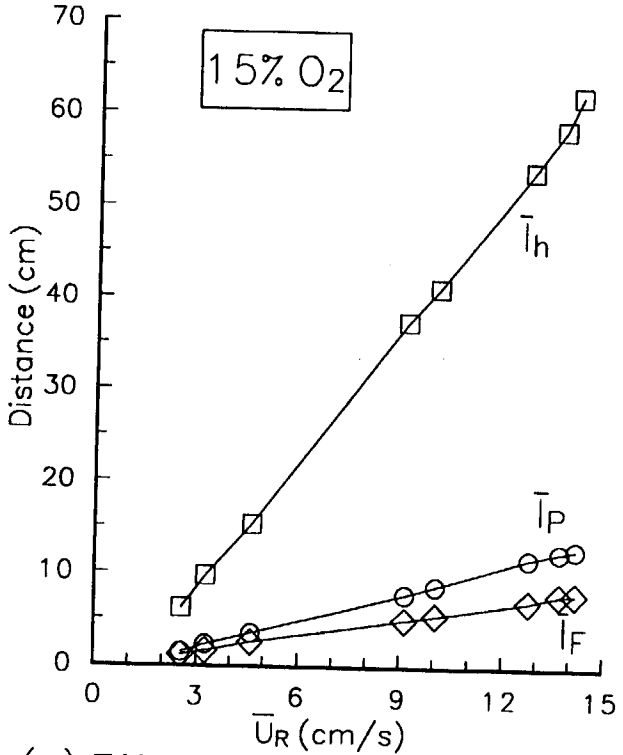

(a) Effect of Flow velocity

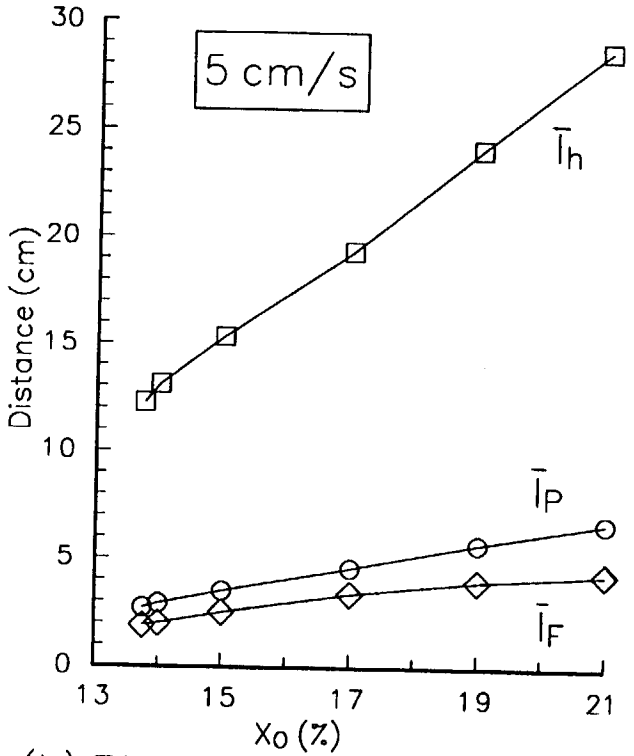

(b) Effect of oxygen concentration

Figure 27. Flame ($\bar{l}_F$), pyrolysis ($\bar{l}_P$), and preheat ($\bar{l}_h$) lengths.

the extinction characteristics of this flame spread problem. Work done in the past has demonstrated that flames in very low speed flows will eventually go out since they become weakened due to heat loss (see ref. 20, for example). This mode of extinction is called quenching. Another more familiar mode of extinction, called blowoff, occurs when the flow velocity becomes too high. The chemical reactions are too slow compared to the rate of incoming oxidizer, so the flame cannot be stabilized and is blown off.

At normal gravity, there is a limit to how small the velocity of oxidizer into the flame zone can be. This is due to buoyancy, which sets up flow velocities on the order of several tens of centimeters per second. At first, our experience with blowoff in normal gravity suggests that if we first removed buoyancy, then reduced the flow velocities to arbitrarily small values, the flame would always exist. This is because the chemical reactions have relatively more and more time to proceed at the lower flow speeds. What actually happens is that the reduced flow of oxidizer diminishes the overall power of the flame in that heat losses (due to radiative loss, for example) drop the flame temperature below the point that the reaction can be sustained. This is the quenching extinction mechanism.

In fig. 28, the extinction boundary is presented. The

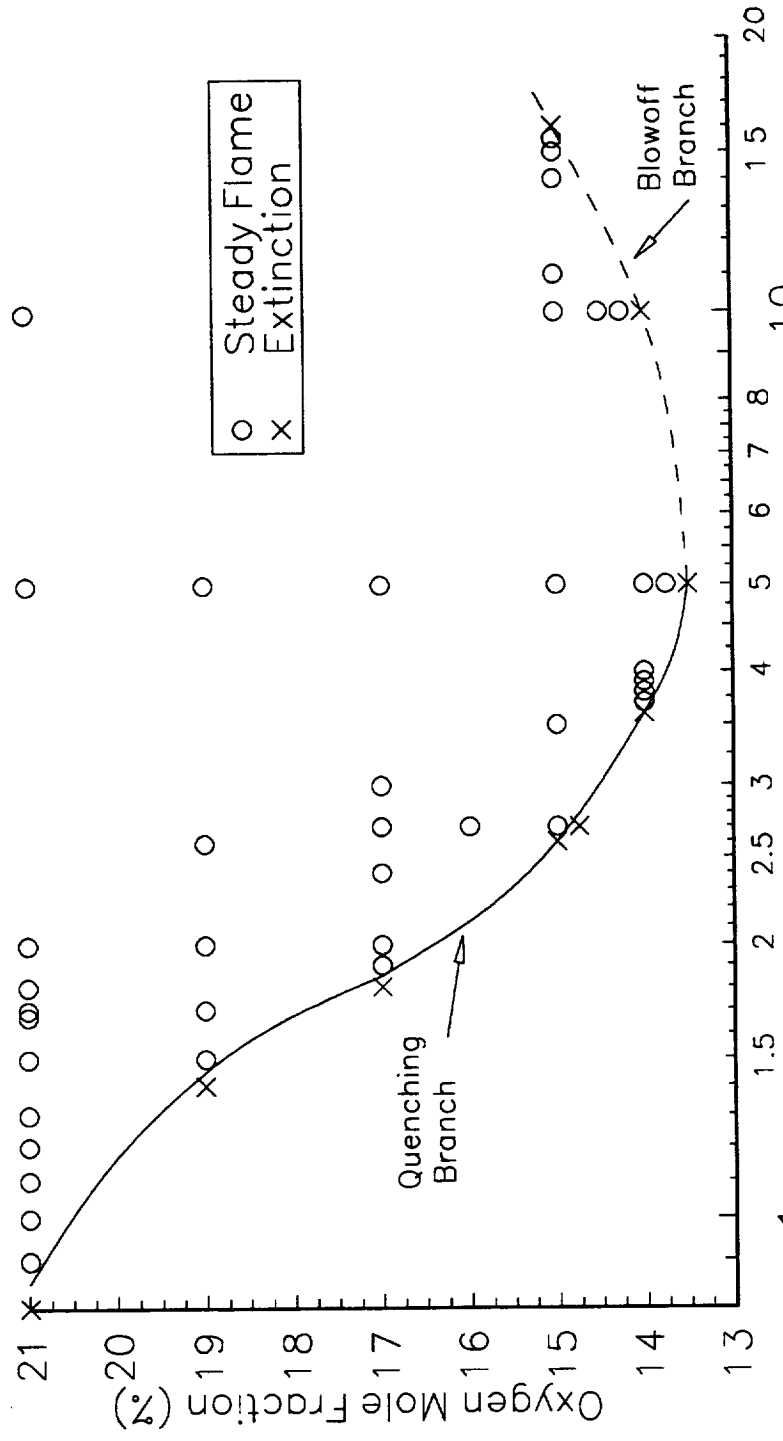

Figure 28. Extinction boundary.

40 circles represent flame solutions, and the 9 X's show the extinction points. The two extinction branches, quenching and blowoff, are shown. In obtaining the extinction points, care was taken to make small changes in velocity or mole fraction. In a steady model such as this, there is always a possibility that the extinction point is actually a non-convergence point. By making small changes in the parameters, however, it is possible to get arbitrarily close to the actual extinction boundary.

In fig. 28, a logarithmic scale is used to plot free stream velocity so that detail at low velocity is evident. A plot using a regular scale is given in fig. 29. The quenching and blowoff branches have dramatically different slopes on this scale.

4.4.1. Differences Between Blowoff and Quenching

The blowoff and quenching branches have different characteristics. While the equations used are steady, some indication of an unsteady time response is obtained by looking at the results during iteration.* The blowoff phenomenon is indicated in fig. 30. The qualitative, temporal response is correct. Here, the top view shows reactivity contours for a converged flame near the blowoff boundary. As the blowoff boundary is crossed (by increas-

*Underrelaxation is employed, so the iteration number is not exactly proportional to time.

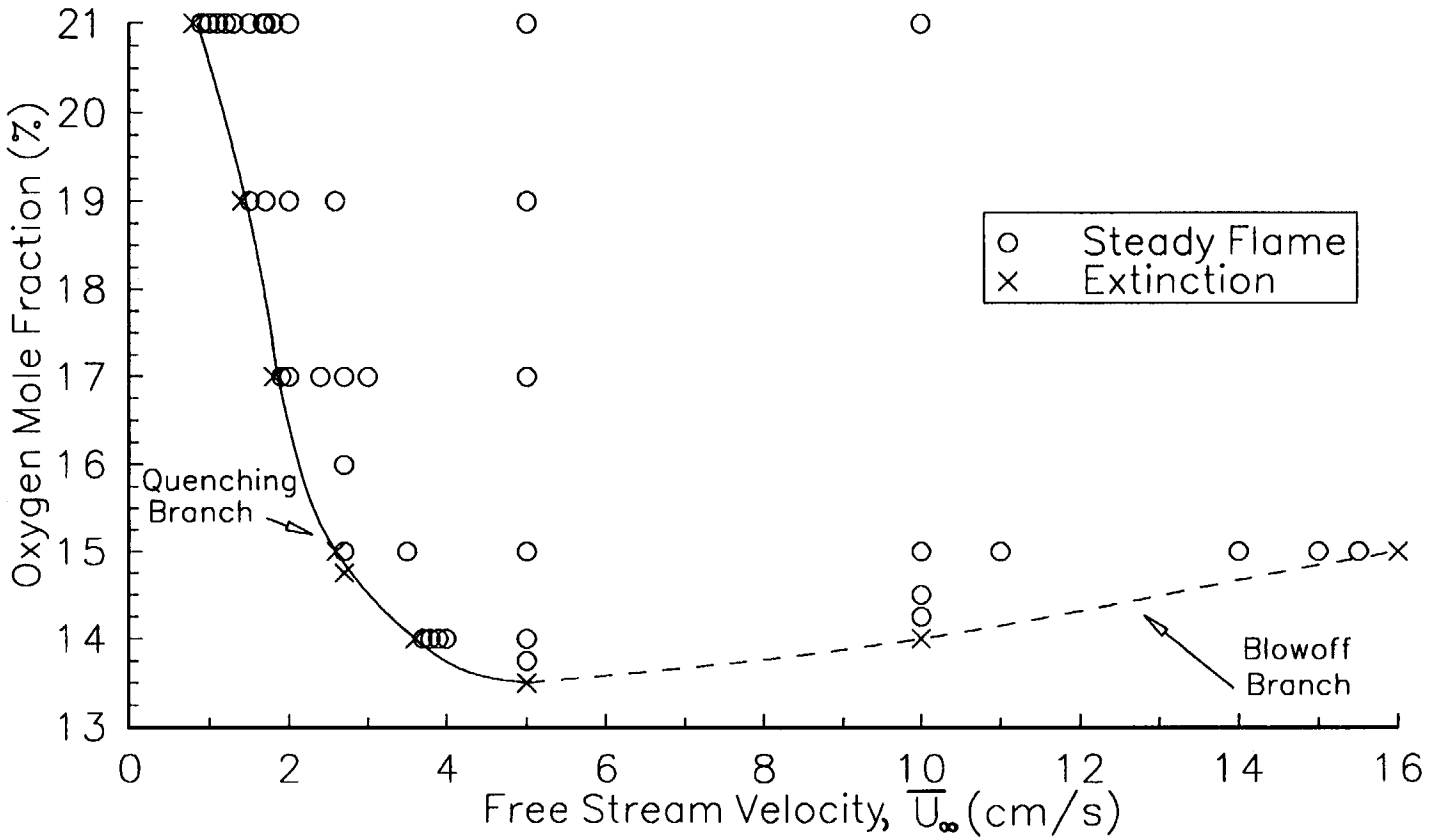

Figure 29. Extinction boundary plotted in regular coordinates.

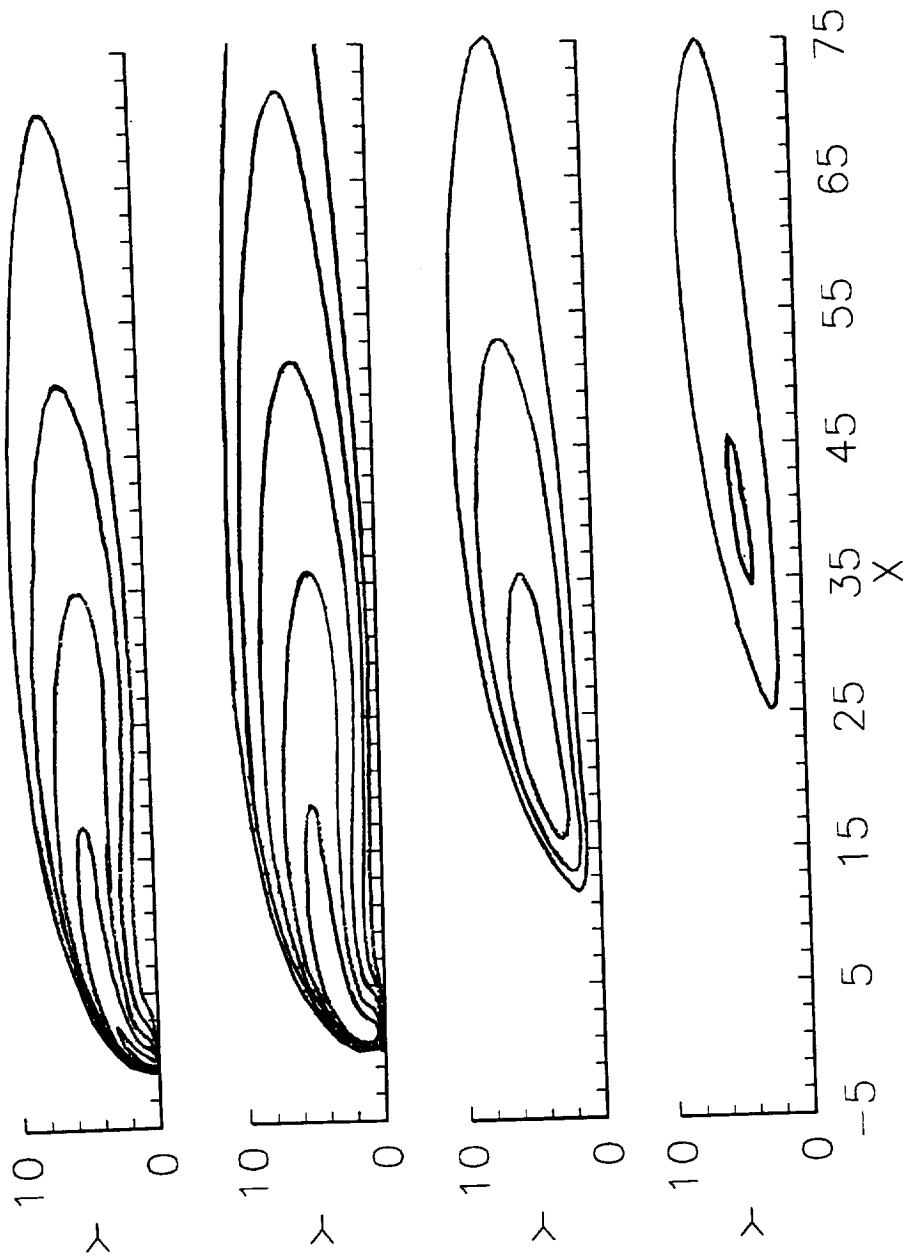

Figure 30. Blowoff extinction sequence. Fuel reactivity contours are shown. The outermost (smallest) contour is 10^{-7} g/cm^3/s. A factor of ten separates contours.

ing velocity or decreasing oxygen concentration) the sequence of plots show that the flame is unable to stabilize and is blown downstream. In the second view, the flame starts to lift off at x=0. This flame is actually stronger (based on increased area of reactivity contours) than the one above it, due to the penetration of oxygen beneath the flame. The remaining views show the flame getting weaker and moving farther downstream. Eventually, the flame is blown out.

In contrast, quenching extinction is observed to be very different. If the quenching boundary is crossed (by decreasing velocity or oxygen concentration) the flame always remains firmly anchored to the burnout point (x=0) but merely gets weaker and smaller until it disappears entirely.

There are other clues indicating the different nature of the two extinction modes. Comparing a near quenching and near blowoff flame, fig. 31 depicts the isotherm structure and maximum temperature. At 2.7 cm/s, the flame has its maximum temperature slightly upstream of the burnout point. At 15.5 cm/s, the maximum temperature is blown downstream somewhat. The effect is even more dramatic in nondimensional coordinates: the maximum occurs

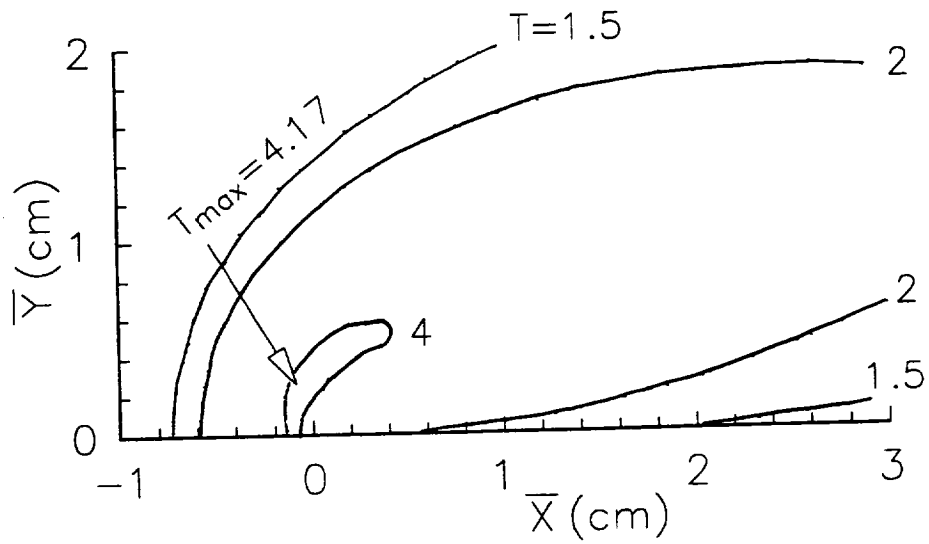

(a) X_O=15%, $\overline{U}_\infty$=2.7 cm/s

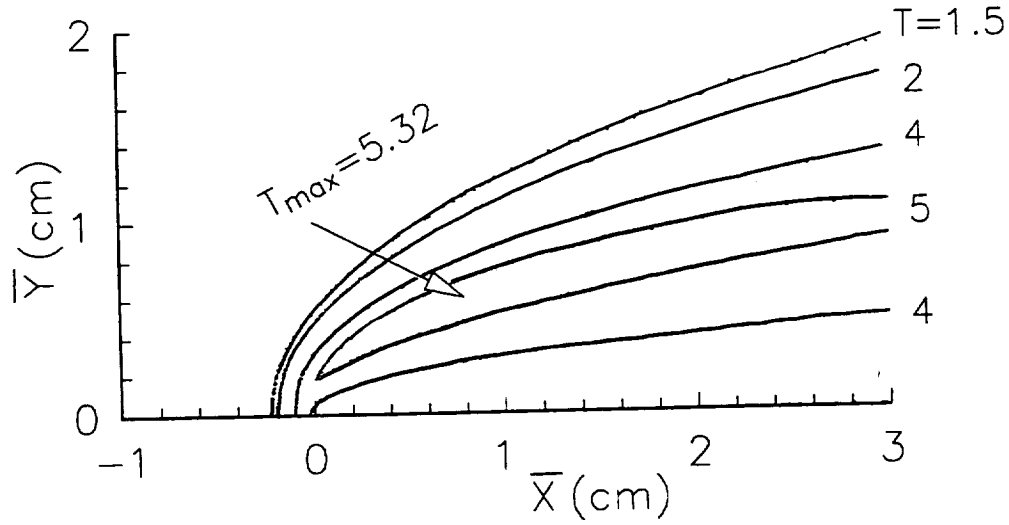

(b) X_O=15%, $\overline{U}_\infty$=15.5 cm/s

Figure 31. Isotherms for a near quench point (a) and near blowoff point (b) at 15% O_2.

over five thermal lengths downstream of the burnout point.*

To get a better understanding of the overall flammability boundary, fig. 32 presents maximum temperature and spread rate for points on the boundary. The inset shows the boundary and the points used. The maximum temperatures on the quenching branch are quite low. Furthermore, it appears that a near-limit flame will tolerate a larger reduction in temperature at higher oxygen concentrations. At blowoff, the maximum temperature is a healthy percentage of the adiabatic flame temperature. Quenching extinction, on the other hand, is ultimately due to weakened chemical kinetics through flame temperature reduction.†

In both blowoff and quenching extinction, the flame eventually goes out due to weakened chemical kinetics. In the nondimensional expression for reaction rate, given by eq. (33), the Damkohler number, Da, appears. As described earlier, Da is the ratio of the characteristic flow time to the characteristic chemical reaction time, in one thermal length. At blowoff, the reaction does not have time to proceed because of the high flow velocity. In this case,

---

*However, in all cases, the maximum reactivity occurs very near the burnout point.

†Since chemical kinetics play an important role in quenching extinction, predicting the boundary more accurately requires a better reaction scheme. However, we are confident that the simplified chemistry used here is adequate to capture the essential features of the problem.

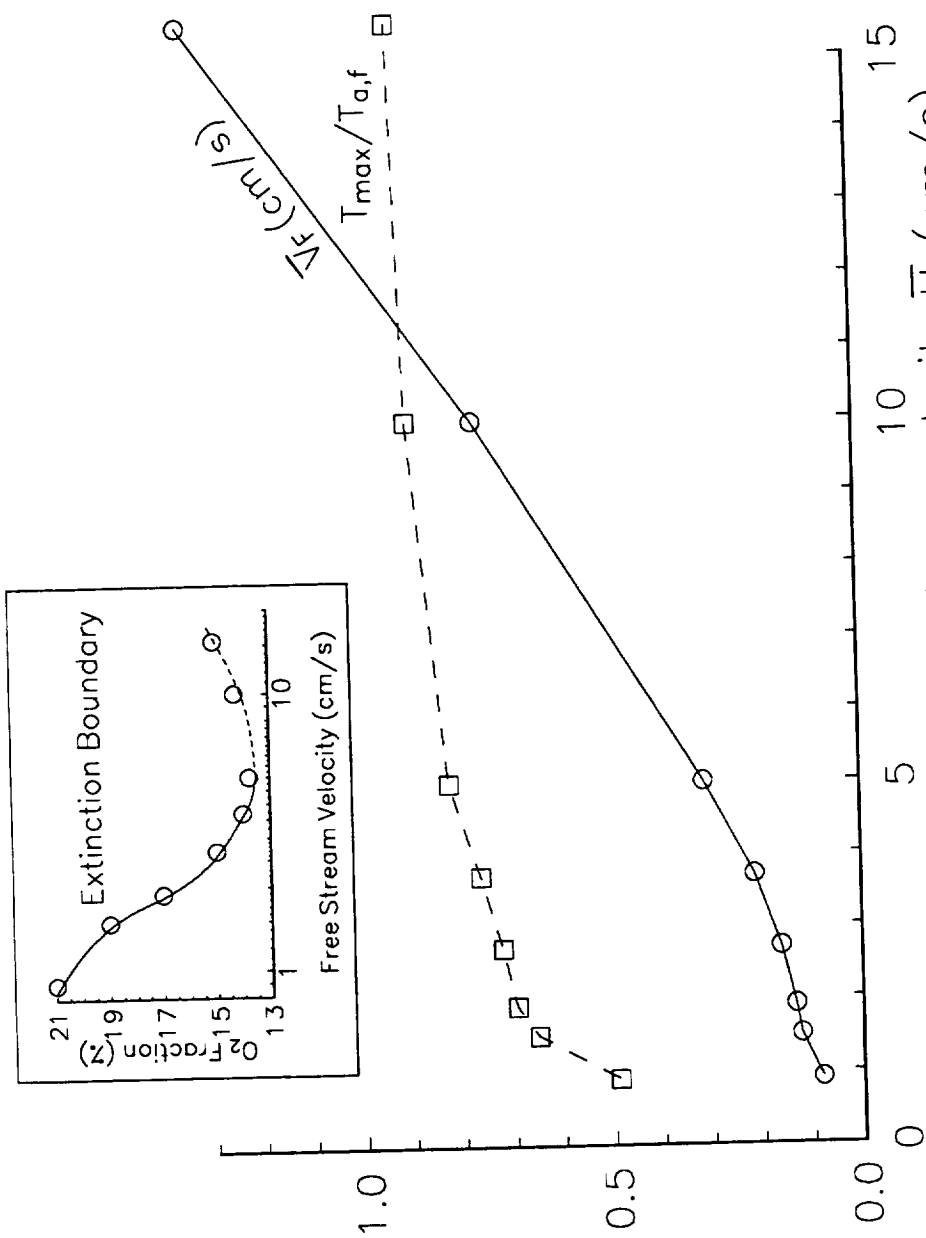

Figure 32. Variation of flame spread rate and maximum temperature along the extinction boundary.

Da becomes too small. At quenching, Da is large, but the reduced flame temperature due to heat loss slows the reaction rate. Thus, while the mechanisms are quite different, the flame goes out in either case as a result of the finite-rate reaction.

There are other characteristics of the near blowoff (high velocity) flames. In fig. 33, two effects are shown. First, look at the reactivity contours near the fuel in the region from x=0 to x=3. These contours are distorted due to the large flux of pyrolysis products. The concentration is so large that the reaction rate is noticeably enhanced. Second, follow the Y_F=0.001 contour from small to large x-values. At first, the line indicates that some fuel has escaped the reaction zone since it lies outside the indicated reactivity contours. Eventually, the fuel is blown back into the flame where it is consumed. This effect is also seen to a lesser extent in the Y_F=0.01 contour.

4.4.2. Incomplete Combustion

Another interesting aspect relates to the flux of fuel in the x-direction as a function of x. In fig. 34, fuel flux (normalized by the total burning rate) is plotted for all cases at 15% O_2. Looking at an individual profile, the flux of fuel is incremented by the flow of pyrolysis gases from the solid. At the same time, the flame consumes the

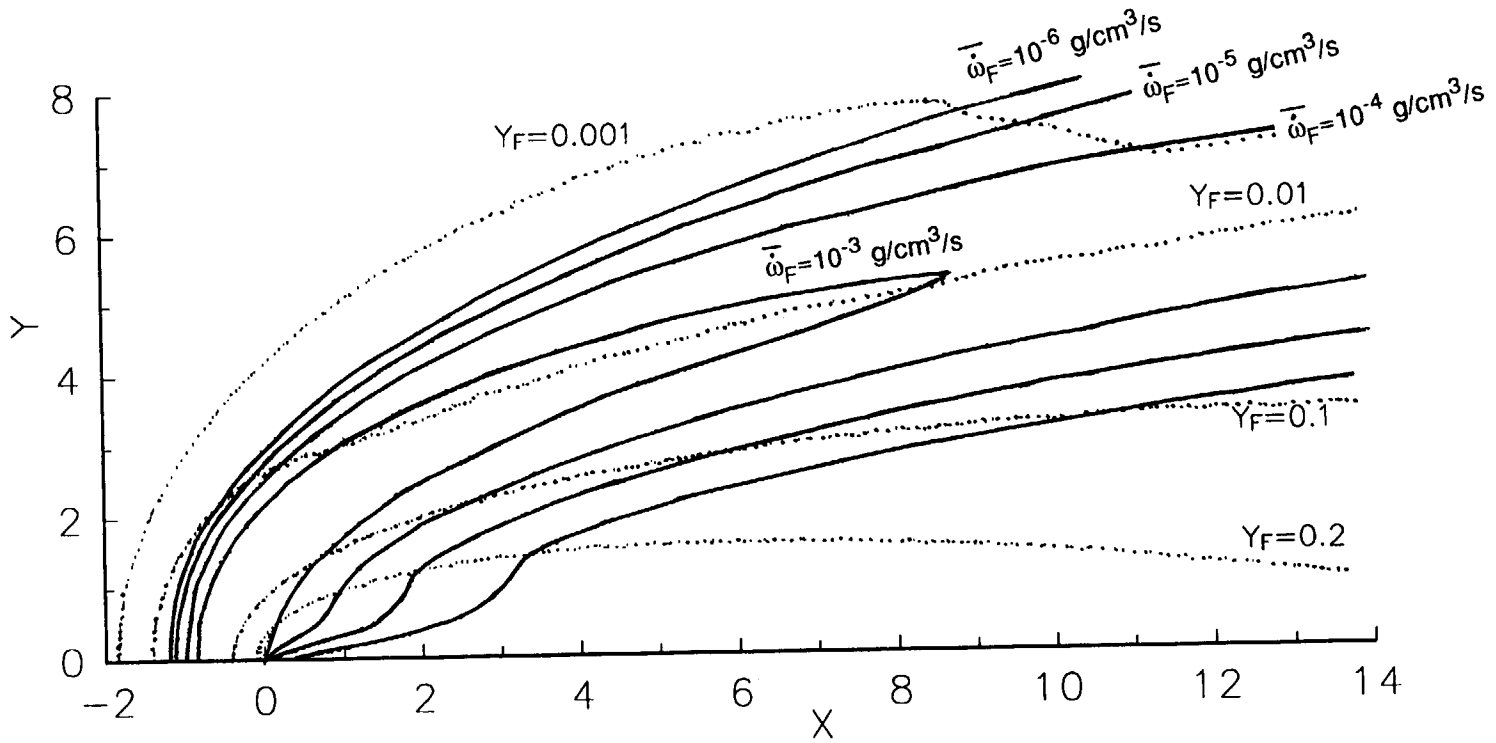

Figure 33. Flame structure effects near blowoff. Dotted lines are fuel mass fraction. Solid lines are fuel reactivity contours.

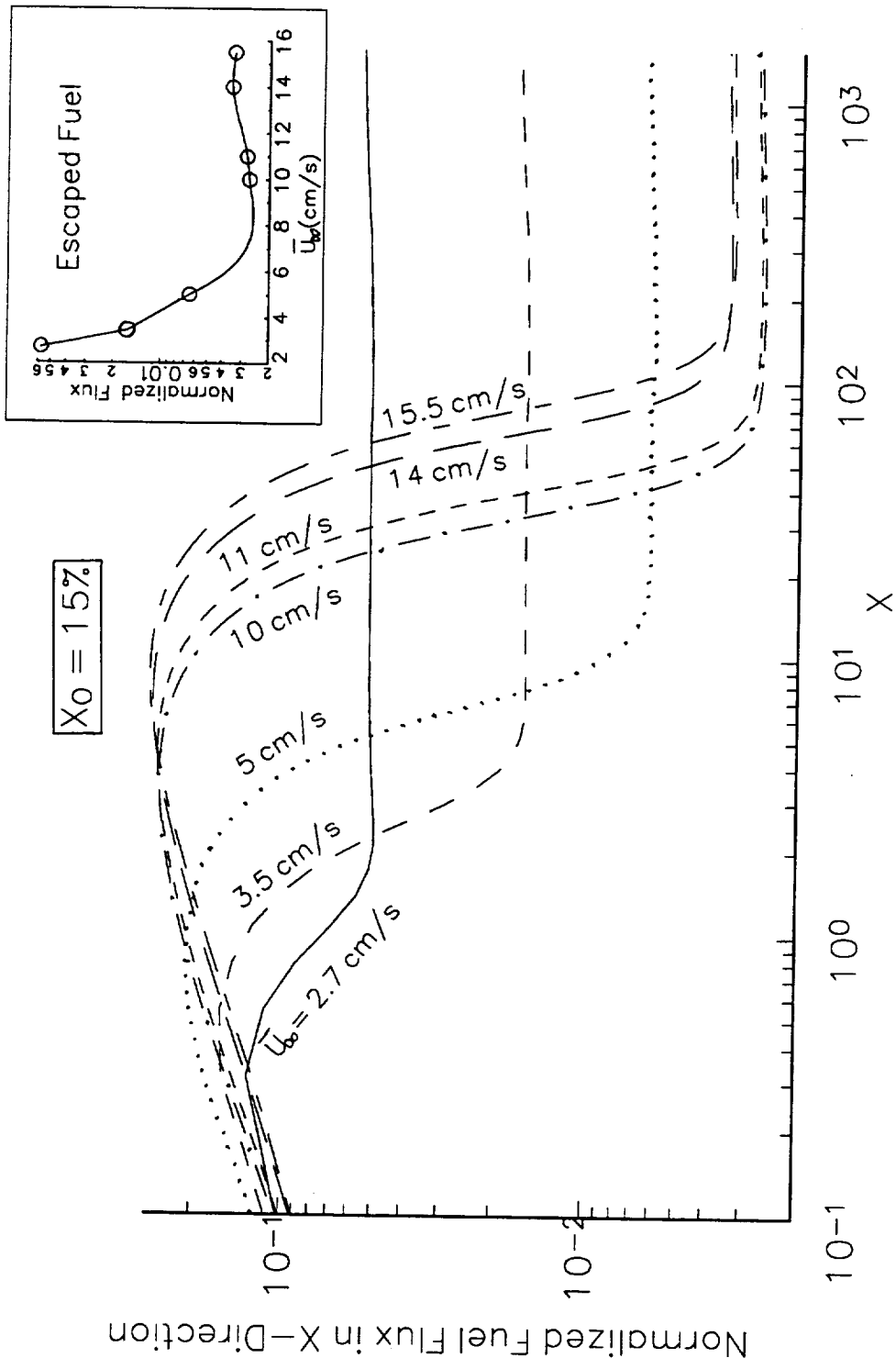

Figure 34. Fuel Flux in x−direction at different free stream velocities.

fuel and eventually leads to a drop in fuel flux. Finally, the reaction ceases and an amount of fuel escapes from the flame unreacted. This "escaped fuel" or (incomplete combustion) is plotted in the inset. As quenching is approached, the amount of escaped fuel increases dramatically. There are three reasons the escaped fuel increases near quenching. First, the relatively cool fuel plate quenches the gas phase reaction near the plate. Second, the radiative heat loss from the solid fuel leads to reduced gas phase temperature. Third, the short flames simply permit an increased amount of fuel to escape. This is based on simple geometric considerations, namely, the flame length shrinks to about the same order as the flame stand-off distance.

As a final word, blowoff at higher oxygen levels was not searched for in this work. There are three reasons. First, this work was mainly interested in low speed quenching effects. Second, flames at high velocity eventually become turbulent, making this laminar model inadequate. Third, in some cases, a near-blowoff flame can become side stabilized. The flame retreats downstream of the burnout point, where the velocity is lower. After burning through the fuel at this location, it retreats again, and repeats the cycle. Clearly, this steady model is insufficient in this case.

Conclusions

A numerical model of concurrent flow flame spread over a thin fuel has been formulated. The effect of oxygen concentration and forced flow velocity on flame structure and extinction limits in a zero gravity environment has been found.

The governing equations included the steady, laminar, two-dimensional, fully elliptic conservation equations for momentum, energy, and species. To capture the long flame and preheat zone without using an elliptic formulation everywhere, parabolic equations were solved at a point sufficiently downstream from the leading edge region. The parabolic solution provided the boundary condition for the elliptic equations, minimizing the effect of the transition between the two sets of equations.

To get a steady solution, the coordinate system was chosen to move with the flame. Thus, the flame was stationary and the fuel fed in at the rate of flame spread.

The flame structure has been presented in detail. Contours of temperature, fuel reactivity rate, and equivalence ratio have been compared. The solution of the Navier-Stokes equations allowed the velocity and pressure fields to be visualized. Streamlines showed the deflection of the flow due to the presence of the flame and fuel, as well as the flow of fuel vapor emanating from the solid due

to pyrolysis. Solution of the solid phase equations gave the pyrolysis length, the incident heat flux distribution, and of course the solid temperature.

A comparison was made with experiment, which reported visible flame shape and spread rate. Since the experimental data was in many cases still approaching steady state, only one nearly steady flame was compared. Using a contour of constant fuel reactivity to represent the visible flame, the flame shape was predicted quite accurately. The spread rate was under-predicted by about 20% for the case examined. No attempt was made to adjust the parameter values in the model to more closely match the experiment, but results agreed qualitatively.

An extinction boundary, with flow velocity and oxygen concentration as coordinates, was presented. It consisted of two branches, a blowoff branch and a quenching branch. This type of extinction boundary has been observed experimentally in opposed flow flame spread tests.

The flame went out in different ways depending on which branch of the extinction boundary was crossed. In blowoff, the chemical reaction did not have time to proceed because of the high rate of flow, and the flame was subsequently blown downstream. The flame temperature was high enough to allow the chemical reaction to proceed, however, it was found that the maximum temperature zone in the flame

was pushed downstream of the burnout point and higher off the fuel surface as the blowoff branch was approached. Therefore, the delayed chemical reaction effectively reduced the heat flux back to the fuel in the burnout region. Thus, the required amount of fuel vapors needed to stabilize the flame could not be generated, and the flame was eventually blown downstream.

As the quenching branch was approached, on the other hand, the flame was always firmly stabilized at the burnout point. Furthermore, the maximum temperature in the flame always occurred very near the burnout point. Thus, the chemistry had plenty of time to proceed. However, the maximum flame temperature decreased steadily as the quenching branch was neared. This was due to the increased importance of heat loss (radiation from the solid fuel) as the visible flame size and power output (equivalently, spread rate) were reduced. The flame was quenched when the temperature became too low to sustain combustion. Additionally, flames near the quench limit permitted an increased percentage of fuel vapors to escape unreacted, an indication of the relatively low flame temperatures and short flames.

By looking at cases which go to extinction during iteration, an indication of the unsteady time response of the flame could be obtained, even though the model was for

steady solution. These results showed that blowoff was characterized by the flame being de-stabilized and pushed downstream, while quenching was due to the gas phase flame becoming cooler and cooler.

The theoretical results are compared. At constant oxygen concentration, the effect of flow velocity from quenching to blowoff was presented. At constant free stream velocity, the effect of different oxygen levels, from 21% (air) all the way down to the extinction limit, was shown. Flame length, pyrolysis length, preheat length, and spread rate increased approximately linearly with both free stream velocity and oxygen concentration. The maximum temperature in the gas phase decreased as flow velocity was reduced, and dropped off steeply as the quenching branch was approached.

From one case to another, the solid temperature and incident heat flux profiles had similar shapes. Pyrolysis and preheat regions were identifiable. The biggest difference was that the maximum temperature and incident heat flux (which always occurred right at the burnout point) increased with flow velocity and oxygen percentage.

This model provides a powerful tool in examining flame spread and extinction characteristics. It is a solid base upon which further modifications can be made. Eventually, it will be generalized to consider unsteady flame spread

over more common (thicker) fuels.

Other issues worth considering include the following. Gas phase radiation should be included to get a better gauge of its effect on flame spread, structure, and extinction (as a heat loss mechanism). An improved gas phase chemical reaction formulation is needed to model the low temperatures near quenching, where intermediate species could be important. The presence of soot will have an influence on both the gas phase chemistry and radiation. Finally, the solid fuel model should be improved to more realistically predict the rate and type of pyrolysis products being generated.

References

1. Williams, F. A., "Combustion Phenomena in Relationship to Microgravity Research," Microgravity Science and Technology, vol 3, pp. 154-161 (1990)

2. Microgravity Combustion Science: Progress, Plans, and Opportunities, The Microgravity Combustion Group, NASA TM 105410, NASA LeRC, Cleveland, Ohio (1992)

3. Friedman, R., "Fire Safety Practices in the Shuttle and the Space Station Freedom," Proceedings of the Second International Combustion Workshop, NASA LeRC, Cleveland, Ohio (1992)

4. T'ien, J. S., "Diffusion Flame Extinction at Small Stretch Rates: The Mechanism of Radiative Loss," Combustion and Flame, vol. 65, pp. 31-34 (1986)

5. Dietenberger, M. A., "Piloted Ignition and Flame Spread on Composite Solid Fuels in Extreme Environments," Ph.D. Dissertation, University of Dayton, Dayton OH (1991)

6. Fernandez-Pello, A. C. and Hirano, T., "Controlling Mechanisms of Flame Spread," Combustion Science and Technology, vol. 32, pp. 1-31 (1983)

7. Fernandez-Pello, A. C., "Flame Spread Modeling," Combustion Science and Technology, vol. 39, pp. 119-134 (1984)

8. Di Blasi, C., "Ignition and Flame Spread Across Solid Fuels," in Numerical Approaches to Combustion Modelling (ed. E. S. Oran and J. P. Boris), Progress in Astronautics and Aeronautics, Vol. 135, Ch. 21, AIAA (1991)

9. Ahmad, T. and Faeth, G. M., "An Investigation of the Laminar Overfire Region Along Upright Surfaces," ASME Journal of Heat Transfer, vol. 100, pp. 112-119 (1978)

10. Fernandez-Pello, A. C. and Mao, C.-P., "A Unified Analysis of Concurrent Modes of Flame Spread," Combustion Science and Technology, vol. 26, pp. 147-155 (1981)

11. Frey A. E., Jr. and T'ien, J. S., "A Theory of Flame Spread over a Solid Fuel Including Finite-Rate Chemical Kinetics," Combustion and Flame, vol. 36, pp. 263-289 (1979)

12. Chen, C. H. and T'ien, J. S., "Fire Plume Along Vertical Surfaces: Effect of Finite-Rate Chemical Reactions," Journal of Heat Transfer, vol. 106, pp. 713-720 (1984)

13. Mao, C.-P., Kodama, H., and Fernandez-Pello, A. C., "Convective Structure of a Diffusion Flame over a Flat Combustible Surface," Combustion and Flame, vol. 57, pp. 209-236 (1984)

14. Chen, C. S. and T'ien, J. S., "Diffusion Flame Stabilization at the Leading Edge of a Fuel Plate," NBS-GCR-86-509, National Institute of Standards and Technology, Gaithersburg, Maryland (1986)

15. Di Blasi, C., Crescitelli, S., Russo, G., and Fernandez-Pello, A. C., "Model of the Flow Assisted Spread of Flames over a Thin Charring Combustible," 22nd Symposium (International) on Combustion, The Combustion Institute, Pittsburgh, Pennsylvania, pp. 1205-1212 (1988)

16. Chen, C. H., "Diffusion Flame Extinction in Slow Convective Flow Under Microgravity Environment," NASA TM 88799, NASA LeRC, Cleveland, Ohio (1986)

17. T'ien, J. S., "The Flame Front Problem: Combustion in Low-Reynolds-Number Flow," 86-WA/HT-49, ASME, New York, New York (1986)

18. Olson, S. L., "The Effect of Microgravity on Flame Spread Over a Thin Fuel," NASA TM 100195, NASA LeRC, Cleveland, Ohio (1987)

19. Ferkul, P. V., "An Experimental Study of Opposed Flow Diffusion Flame Extinction Over a Thin Fuel in Microgravity," NASA CR-182185, NASA LeRC, Cleveland, Ohio (1989)

20. Olson, S. L., Ferkul, P. V., and T'ien, J. S., "Near-Limit Flame Spread Over a Thin Solid Fuel in Microgravity," 22nd Symposium (International) on

Combustion, The Combustion Institute, Pittsburgh, Pennsylvania, pp. 1213-1222 (1988)

21. Olson, S. L., "Mechanisms of Microgravity Flame Spread Over a Thin Solid Fuel: Oxygen and Opposed Flow Effects," Combustion Science and Technology vol. 76, pp. 233-249 (1991)

22. Bhattacharjee, S. and Altenkirch, R. A., "Radiation-Controlled Opposed-Flow Flame Spread in a Microgravity Environment," 23rd Symposium (International) on Combustion, The Combustion Institute (1990)

23. Altenkirch, R. A., Bhattacharjee, S., Olson, S. L., and Sacksteder, K., "Opposed-Flow Flame Spreading in Reduced Gravity," Proceedings of the Second International Microgravity Combustion Workshop, NASA LeRC, Cleveland, Ohio (1992)

24. Nakabe, K., Baum, H. R., and Kashiwagi, T., "Ignition and Subsequent Flame Spread Over a Thin Cellulosic Material," Proceedings of the Second International Microgravity Combustion Workshop, NASA LeRC, Cleveland, Ohio (1992)

25. Kimzey, J. H., "Skylab Experiment M-479 Zero Gravity Flammability," JSC 22293, NASA JSC, Houston, Texas (1986)

26. Stocker, D., Greenberg, P. and Ross, H., "Small-Scale Combustion Experiments on the USML-1 Shuttle Mission," Presented at the 1992 Spring Technical Meeting of the Central States Section of the Combustion Institute (1992)

27. Potter, M. C. and Foss, J. F., "Fluid Mechanics," Great Lakes Press, Inc., Okemos, Michigan, p. 186 (1982)

28. Patankar, S. V., Numerical Heat Transfer and Fluid Flow, Hemisphere Publishing Corporation, New York (1980)

29. Hornbeck, R. W., "Numerical Marching Techniques for Fluid Flows with Heat Transfer," NASA SP-297, NASA LeRC, Cleveland, Ohio, pp. 21-28 (1973)

30. Grayson, G. D., "An Experimental Study of Low Speed Concurrent Flow Flame Spread Over a Thin Fuel," M. S. Thesis, Case Western Reserve University, Cleveland, Ohio (1991)

31. Sacksteder, K. R., and T'ien, J. S., "Downward Diffusion Flame Spread and Extinction in Variable Gravitational Field: Lunar and Martian Simulation," to be presented at the AIAA 31st Aerospace Sciences Meeting, Reno, Nevada (1993)

32. Loh, H. T. and Fernandez-Pello, A. C., "Flow Assisted Flame Spread Over Thermally Thin Fuels," Proceedings of the First International Symposium on Fire Safety Science, pp. 65-74 (1986)

Appendix

The FORTRAN computer program used to generate these results follows. In addition, the important parameter values (read in unit 10 in the program) are listed below:

```
  1   1   1   1   1   1   1   1
  4   4   4   4   4   0   1
  1   0   3   4   0
 69  49  26   1.1000   1.1000   0.2000   0.2000   3.0000   3.0000
150   1   1  -0.0001  -0.0002  -0.0001  -0.0001  -1.0000  -0.0012
 7.00000E-01  9.00000E-01  6.50000E-01  6.50000E-01
 6.50000E-01  6.50000E-01  6.50000E-01  3.80000E+07  5.03000E+01
 1.00000E+00  4.16667E+00  9.25485E+08  4.04000E+01  4.53000E+01
 1.18500E+00  2.10000E-01  2.00000E+00  2.38254E-01  1.00000E+00
 2.75000E-04  2.63000E-01  3.00000E-01  3.30000E-01  1.35600E-12
 3.00000E+02  3.00000E+02 -1.80000E+02  3.80000E-03  2.13000E+00
 9.09000E-01  1.00000E+00  3.00000E+01  1.00000E+00  0.00000E+00
 70  20  65   1.1000   3.0000  30.0000
  0   1  65   0.0000   2.0000
 30   5   1
```

```
      PROGRAM FLAME
      COMMON/L1/DX(0:93),DY(0:50),NX,NY,NLE
      COMMON/L2/U(0:93,0:50),V(0:93,0:50),T(0:93,0:50,1:3),
     -          R(0:93,0:50),P(0:93,0:50),PPR(0:93,0:50)
      COMMON/L3/UHAT(0:93,0:50),DU(0:93,0:50),USTAR(0:93,0:50),
     -          UAP(93,50),UAE(93,50),UAW(93,50),
     -          UAN(93,50),UAS(93,50),UB(93,50),GRASH,RINFNON
      COMMON/L4/VHAT(0:93,0:50),DV(0:93,0:50),VSTAR(0:93,0:50),
     -          VAP(93,50),VAE(93,50),VAW(93,50),
     -          VAN(93,50),VAS(93,50),VB(93,50)
      COMMON/L5/AP(93,50),AE(93,50),AW(93,50),AN(93,50),
     -          AS(93,50),SC(93,50),SP(93,50),B(93,50)
      COMMON/L6/AA(0:93),BB(0:93),CC(0:93),DD(0:93),XX(0:93)
      COMMON/L7/RSTAR,RS,CS,CP,SIG,T0,TL,XL,ES,TAU,ASTAR,TSTAR
      COMMON/L8/DXP(0:500),DYP(0:100),UPAR(2,0:100),VPAR(2,0:100),
     -          TPAR(2,0:100,3),TS(0:570,2),USPAR(0:570),VSPAR(0:570)
      COMMON/L9/IBC,UBC(0:50),VBC(0:50),TBC(0:50,3)
      REAL RX,RY,DXMIN,DYMIN,DXMAX,DYMAX,TAMB,DA,Q,E,PR,FO,YOAMB,
     -ERM,ERP,ERU,ERV,ERPP,ERF,PDAM,UDAM,VDAM,FDAM(3),VEL,TOVI(0:570),
     -POLD(0:93,0:50),PH(2),MAINPDIF,THICK(0:570),DAD,VE0,VF,EPS,
     -ASW,VFINI,QO,QN,QOL,QNL,GLEVEL,GRASH,RINFNON,UBUOY
C----------------------GET GENERAL DATA--------------------------------
      READ(10,910) IPC,IUC,IVC,IPPC,ITC,IYFC,IYOC,IOUV
      READ(10,910) IBP,IBU,IBV,IBPP,IBF,IUSTVST,IDA
      READ(10,910) ITSSMOO,ISBC,JSK,KSOL,ISKPP
      READ(10,900) NX,NY,NLE,RX,RY,DXMIN,DYMIN,DXMAX,DYMAX
      READ(10,900) NALL,IREADOLD,NSCH,ERM,ERP,ERU,ERV,ERPP,ERF
      READ(10,905) PR,PDAM,UDAM,VDAM
      READ(10,905) FDAM(1),FDAM(2),FDAM(3),ASW,ES
      READ(10,905) TAMB,TSTAR,DAD,Q,E
      READ(10,905) FO,XOAMB,VE0,VF,EPS
      READ(10,905) RSTAR,RS,CS,CP,SIG
      READ(10,905) T0,TL,XL,TAU,ASTAR
      READ(10,905) QO,QN,QOL,QNL,GLEVEL
      READ(10,900) IBEG,JTOP,IRIGHT,RDXP,DXPMIN,DXPMAX
      READ(10,900) ISKIP,ISR,IPARN,VFL1,VFU1
      READ(10,900) MMAX,KPAR,IBC
      YOAMB=1./(1.+(1./XOAMB-1.)*0.8754513)
C----------------------GENERATE GRID-----------------------------------
      CALL GRID(RX,RY,DXMIN,DYMIN,DXMAX,DYMAX)
C----------------------GENERATE INITIAL FIELD--------------------------
      CALL READIN(TAMB,YOAMB,TSTAR,IREADOLD,IUSTVST,ISR,IBEG,IRIGHT)
C--------------------TAILOR INITIAL SURFACE TEMPERATURE DATA-----------
      IF (ISR.EQ.1) THEN
        IF (IRIGHT.GT.IPARN) IRIGHT=IPARN
        IF (IRIGHT.LT.IPARN) THEN
          DO 3 I=IBEG+IRIGHT+1,IBEG+IPARN
            TS(I,1)=TS(IBEG+IRIGHT,1)
    3       TS(I,2)=TS(IBEG+IRIGHT,2)
            IRIGHT=IPARN
        ENDIF
        DO 4 J=NLE+1,IBEG+IRIGHT
C*****************************************************************
C**     NOTE!!! THE FOLLOWING LINE ASSUMES EQU. OF STATE      **
C*********************  RHO=TSTAR/T  *********************
    4   VSPAR(J)=EXP(-ES/TS(J,1))*ASW*RS/TSTAR*TS(J,1)/RSTAR/
     -          (VE0+UBUOY-VF)
      ENDIF
```

```
C----NOTE: IT IS IMPORTANT THAT IBEG+IRIGHT>=NX+1--------------------
C---------------------MAIN ROUTINE-----------------------------------
      NF=0
      NG=0
      IPAR=0
      IOKO=0
      VFRI=VF
      QORI=QO
      UBUOY=(ASTAR*981.*GLEVEL)**(1./3.)
C***************** THE FOLLOWING LINE ASSUMES AN EQUATION OF STATE ***
      RINFNON=TSTAR/TAMB
      VEL=VE0+UBUOY-VF
      DA=DAD/VEL/VEL
      GRASH=(UBUOY/VEL)**3.
      CHERPP=0.04
      IF (ERPP.EQ.-1.) CHERPP=0.
      CHQO=0.
      IF (QN.EQ.1.) CHQO=1.
      DO 200 I=1,NALL
      VEL=VE0+UBUOY-VF
      DA=DAD/VEL/VEL
      GRASH=(UBUOY/VEL)**3.
      IF (IOUV.EQ.0) GO TO 5
      CALL OLDS(POLD,P,NX,NY)
C-----------------CALCULATE UHATS AND VHATS---------------------------
      CALL UHATS(PR,TSTAR)
      CALL VHATS(PR,TSTAR)
C----------------SOLVE FOR THE PRESSURE FIELD-------------------------
    5   DO 10 K=1,IPC
   10 CALL PRESSURE(ERP,PDAM,IBP)
C-----------------CALCULATE USTAR AND VSTAR---------------------------
        DO 20 K=1,IUC
   20 CALL USTARS(ERU,UDAM,IBU,PR,TSTAR)
        DO 30 K=1,IVC
   30 CALL VSTARS(ERV,VDAM,IBV,PR,TSTAR)
C--------------------SOLVE THE P' EQUATION-----------------------------
        DO 40 K=1,IPPC
      CALL PPRIME(ERPP,IBPP,ISKPP)
C--------------------CORRECT VELOCITY-----------------------------------
   40 CALL CORVEL(PR,TSTAR)
C-----------------COMPUTE OXYGEN CONCENTRATION FIELD-------------------
        DO 50 K=1,IYOC
   50 CALL PHI(TAMB,DA,Q,E,FO,ERF,FDAM,3,TSTAR,IBF)
C----------------COMPUTE FUEL CONCENTRATION FIELD----------------------
        DO 60 K=1,IYFC
   60 CALL PHI(TAMB,DA,Q,E,FO,ERF,FDAM,2,TSTAR,IBF)
C-----------------COMPUTE TEMPERATURE, DENSITY-------------------------
        DO 70 K=1,ITC
      CALL PHI(TAMB,DA,Q,E,FO,ERF,FDAM,1,TSTAR,IBF)
   70 CALL DENS(TSTAR)
C-----------------------SET UP GRID AND INITIAL PARABOLIC VALUES-------
      IF ((IOKO.NE.I/KPAR).OR.I.EQ.1) THEN
      IF (IBEG.GT.NX+1.OR.IRIGHT.LE.0) THEN
       DO 80 I4=NLE+1,NX+1
       TS(I4,1)=T(I4,0,1)
   80  TS(I4,2)=T(I4,1,1)
      ELSE
       CALL PARGRID(NF,IBEG,JTOP,IRIGHT,RDXP,DXPMIN,DXPMAX)
```

```
      IF (NG.EQ.1) GO TO 83
      NG=1
      CALL SETSUR(IBEG,JTOP,IRIGHT,ES,ASW,RS,TSTAR,RSTAR,VF,VEL,ISR)
   83 IF (I.EQ.NALL) IPAR=1
     ENDIF
     ENDIF
     IF ((IOKO.NE.I/KPAR).OR.I.EQ.1) THEN
C-----------------COMPUTE SOLID TEMPERATURE AND THICKNESS-----------
     IF (NSCH.EQ.1) THEN
       DO 87 IK=NLE+1,IBEG
   87  TS(IK,2)=T(IK,1,1)
       DO 90 IK=NLE+1,IBEG+IRIGHT
   90  TOVI(IK)=TS(IK,1)
        VFINI=VF
        ZZZ=0.
        VFL=VFL1
        VFU=VFU1
       CALL SOLID(EPS,VFL,VFU,VF,VE0,UBUOY,
     -            THICK,ZZZ,TX,QO,QN,ASW,IBEG,IRIGHT,MMAX,KSOL)
       DO 100 J=NLE+1,IBEG+IRIGHT
  100  TS(J,1)=(QNL*TS(J,1)+QOL*TOVI(J))/(QNL+QOL)
       IF (ITSSMOO.NE.0) THEN
         DO 102 J=NLE+2,IBEG+IRIGHT
  102      IF (TS(J,1).GT.TS(J-1,1)) TS(J,1)=TS(J-1,1)
       ENDIF
C) ) ) ) ) ) ) )  COMPUTE SPREAD RATE BY INTEGRATING MASS FLUX ( ( ( (
       XINTVF=0.
       DO 103 L=NLE+1,IBEG+IRIGHT-1
       IF (L.LT.IBEG) DDX=DX(L)
       IF (L.EQ.(NLE+1)) DDX=DX(L)/2.
       IF (L.GE.IBEG) DDX=DXP(L-IBEG+1)
C--- NOTE: THE INTEGRAL BELOW ASSUMES SQRT(1+(DH/DX)**2) = 1 ---------
  103  XINTVF=XINTVF+DDX*EXP(-ES/TS(L,1))
       XINTVF=ASW/TAU*ASTAR/(VE0+UBUOY-VF)*XINTVF
       QO=QO*XINTVF/VF*CHQO+QO*(1.-CHQO)
       WRITE(56,104) VF,XINTVF
       VF=(QNL*VF+QOL*VFINI)/(QNL+QOL)
  104  FORMAT(1P,2E12.5)
C------------CALCULATE BLOWING VELOCITY-------------------------------
       DO 105 J=NLE+1,IBEG+IRIGHT
C*************************************************************
C********  NOTE!!! THE FOLLOWING LINE ASSUMES EQU. OF STATE  **
C************************  RHO=TSTAR/T  ***********************
  105  VSPAR(J)=EXP(-ES/TS(J,1))*ASW*RS/TSTAR*TS(J,1)/RSTAR/
     -         (VE0+UBUOY-VF)
       VSPAR(NLE+1)=VSPAR(NLE+1)/2.
C--------------------SET B.C. FOR SOLID FUEL--------------------------
       IF (ISBC.EQ.0) THEN
         TS(IBEG+IRIGHT,1)=TS(IBEG+IRIGHT-1,1)
        ELSE
         TS(IBEG+IRIGHT,1)=1.
        ENDIF
        IF (ZZZ.EQ.1.) GOTO 210
     ENDIF
     IF (JSK.EQ.0) GO TO 185
C-------------------SOLVE PARABOLIC REGION---------------------------
     IF (IBEG.LE.NX+1.AND.IRIGHT.GT.0)
    - CALL PARCA(IBEG,JTOP,IRIGHT,PR,TSTAR,GR,RINFNON,DA,Q,E,FO,
```

```
     -            IPAR,IDA,VEL,RSTAR,ASTAR)
C-----------------CORRECT BOUNDARY CONDITIONS FOR U-VELOCITY---------
      DO 110 II=NLE+1,IBEG-1
      VMEAN=(VSPAR(II)*DX(II)+VSPAR(II+1)*DX(II+1))/(DX(II)+DX(II+1))
      DHDX=(THICK(II+1)-THICK(II))/(DX(II+1)+DX(II))*2.
      DHQ=DHDX/SQRT(1.+DHDX*DHDX)
  110 USPAR(II)=-VF/(VE0+UBUOY-VF)-DHQ*VMEAN
      DO 120 II=IBEG,IBEG+IRIGHT-1
      VMEAN=VSPAR(II)
      IF ((II.EQ.IBEG).AND.(IBEG.EQ.NX+1)) THEN
        DXL=DX(NX)/2.
        DXU=DXP(1)
        GOTO 112
       ENDIF
      IF (II.EQ.IBEG) THEN
       DXL=DX(IBEG)/2.
       DXU=DXP(1)
      ELSE
       DXL=DXP(II-IBEG)
       DXU=DXP(II-IBEG+1)
      ENDIF
  112 RREP=DXL/(DXL+DXU)
      DHDX=(THICK(II+1)-THICK(II))/DXU*RREP+
     -     (THICK(II)-THICK(II-1))/DXL*(1.-RREP)
      DHQ=DHDX/SQRT(1.+DHDX*DHDX)
  120 USPAR(II)=-VF/(VE0+UBUOY-VF)-DHQ*VMEAN
      USPAR(IBEG+IRIGHT)=USPAR(IBEG+IRIGHT-1)
      II=NLE
      VMEAN=VSPAR(II+1)
      DHDX=(THICK(II+2)-THICK(II+1))/(DX(II+2)+DX(II+1))*2.
      DHQ=DHDX/SQRT(1.+DHDX*DHDX)
      USPAR(II)=-VF/(VE0+UBUOY-VF)-DHQ*VMEAN
C---------------------UPDATE ELLIPTIC SURFACE VARIABLES--------------
      IF (NSCH.NE.1) GO TO 155
      DO 130 II=NLE+1,NX+1
      T(II,0,1)=TS(II,1)
  130 V(II,0)=VSPAR(II)
      DO 140 II=NLE+1,IBEG-1
  140 U(II,0)=USPAR(II)
      U(NLE,0)=USPAR(NLE)
      DO 150 II=IBEG,NX
      RR1=DX(II+1)/(DX(II)+DX(II+1))
  150 U(II,0)=USPAR(II)*RR1+USPAR(II+1)*(1.-RR1)
  155 CONTINUE
      ENDIF
      IOKO=I/KPAR
C---------------UPDATE LEFT AND TOP VELOCITIES-----------------------
      DO 170 II=0,NX
  170 U(II,NY+1)=(VE0-VF)/(VE0+UBUOY-VF)
      DO 180 JJ=0,NY+1
  180 U(0,JJ)=(VE0-VF)/(VE0+UBUOY-VF)
C
  185 IF (ISKIP.NE.0) GO TO 200
      CALL FINDDIF(P,POLD,NX,NY,MAINPDIF,'P,MAIN IT.',IDP,JDP)
        PH(1)=PH(2)
        PH(2)=ABS(MAINPDIF)
      IF(PH(2).GT.PH(1)) THEN
        ICOUNT=ICOUNT+1
```

```
        ELSE
          ICOUNT=0
        ENDIF
        IF ((ICOUNT.GE.10).AND.(PH(1).GT.0.1)) GO TO 210
C-----------------FIND LARGEST, SMALLEST P PRIME----------------------
        PPMAX=-100000.
        PPMIN=+100000.
        DO 190 I2=1,NX
         DO 190 J2=1,NY
          IF (PPR(I2,J2).GT.PPMAX) THEN
            PPMAX=PPR(I2,J2)
            IDMA=I2
            JDMA=J2
           ENDIF
          IF (PPR(I2,J2).LT.PPMIN) THEN
            PPMIN=PPR(I2,J2)
            IDMI=I2
            JDMI=J2
           ENDIF
  190   CONTINUE
        WRITE (22,915) PPMAX,IDMA,JDMA,PPMIN,IDMI,JDMI,(PPMAX-PPMIN)
        IF ((PPMAX-PPMIN).LT.CHERPP) GO TO 210
  200   IF (ABS(MAINPDIF).LT.ERM) GO TO 210
C-------------------------WRITE DATA--------------------------------
  210   CONTINUE
        CALL WRITE3(T,0,NX+1,0,NY+1,2)
        CALL WRITE2(U,0,NX,0,NY+1,2)
        CALL WRITE2(V,0,NX+1,0,NY,2)
        CALL WRITE2(P,1,NX,1,NY,2)
        CALL WRITE2(PPR,1,NX,1,NY,2)
        CALL WRITE2(USTAR,0,NX,0,NY+1,2)
        CALL WRITE2(VSTAR,0,NX+1,0,NY,2)
        CALL WRITE4(TS,NLE+1,IBEG+IRIGHT,1,2,2)
        WRITE(13,905)  (UBC(J),J=1,NY)
        WRITE(13,905)  (VBC(J),J=1,NY)
        WRITE(13,905)  (TBC(J,1),J=1,NY)
        WRITE(13,905)  (TBC(J,2),J=1,NY)
        WRITE(13,905)  (TBC(J,3),J=1,NY)
        CALL WRITE1(THICK,TX,NLE+1,IBEG+IRIGHT,2)
        IF (IDA.EQ.1)  THEN
C----------------------TO SAVE SPACE, DA DATA WRITTEN TO PPR----------
         PREF=DA*VEL*VEL*RSTAR/ASTAR
        DO 220 I=0,NX+1
        DO 220 J=0,NY+1
        PPR(I,J)=PREF*R(I,J)*R(I,J)*T(I,J,2)*T(I,J,3)*EXP(-E/T(I,J,1))
        IF (PPR(I,J).LT.1.E-78) PPR(I,J)=0.
  220   CONTINUE
        DO 230 I=0,NX+1
  230   WRITE(26,905)  (PPR(I,J),J=0,NY+1)
      ENDIF
C
      CLOSE (UNIT=10)
      OPEN (UNIT=10)
      IF (ZZZ.EQ.1.) VF=VFRI
      IF (ZZZ.EQ.1.) QO=QORI
C-----------------REWRITE GENERAL DATA--------------------------------
      WRITE(10,910)  IPC,IUC,IVC,IPPC,ITC,IYFC,IYOC,IOUV
      WRITE(10,910)  IBP,IBU,IBV,IBPP,IBF,IUSTVST,IDA
```

```
      WRITE(10,910) ITSSMOO,ISBC,JSK,KSOL,ISKPP
      WRITE(10,900) NX,NY,NLE,RX,RY,DXMIN,DYMIN,DXMAX,DYMAX
      WRITE(10,900) NALL,IREADOLD,NSCH,ERM,ERP,ERU,ERV,ERPP,ERF
      WRITE(10,905) PR,PDAM,UDAM,VDAM
      WRITE(10,905) FDAM(1),FDAM(2),FDAM(3),ASW,ES
      WRITE(10,905) TAMB,TSTAR,DAD,Q,E
      WRITE(10,905) FO,XOAMB,VE0,VF,EPS
      WRITE(10,905) RSTAR,RS,CS,CP,SIG
      WRITE(10,905) T0,TL,XL,TAU,ASTAR
      WRITE(10,905) QO,QN,QOL,QNL,GLEVEL
      WRITE(10,900) IBEG,JTOP,IRIGHT,RDXP,DXPMIN,DXPMAX
      WRITE(10,900) ISKIP,ISR,IPARN,VFL1,VFU1
      WRITE(10,900) MMAX,KPAR,IBC
C
C-----------------CHECK OUT OVERALL MASS BALANCE IN ELLIPTIC REGION
C
      FLXBOT=0.
      FLXTOP=0.
      FLXRGT=0.
      FLXLFT=0.
      RINFASTAR=RSTAR*TSTAR*ASTAR
      DO 240,I=1,NX
      FLXBOT=FLXBOT+V(I,0)*DX(I)/T(I,0,1)*RINFASTAR
  240 FLXTOP=FLXTOP+V(I,NY)*DX(I)/T(I,NY,1)*RINFASTAR
      DO 250 J=1,NY
      FLXLFT=FLXLFT+U(0,J)*DY(J)/T(0,J,1)*RINFASTAR
  250 FLXRGT=FLXRGT+U(NX,J)*DY(J)/T(NX,J,1)*RINFASTAR
      FLXNET=FLXBOT+FLXLFT-FLXTOP-FLXRGT
      WRITE(72,*) 'MASS FLUX'
      WRITE(72,920)
      WRITE(72,905) FLXBOT,FLXTOP,FLXRGT,FLXLFT,FLXNET
C
  900 FORMAT(3(1X,I3),6(1X,F8.4))
  905 FORMAT(1P,5(1X,E12.5))
  910 FORMAT(10(1X,I3))
  915 FORMAT(3(1X,F10.5,1X,I3,1X,I3))
  920 FORMAT(4X,'BOTTOM',8X,'TOP',9X,'RIGHT',9X,'LEFT',9X,'NET')
      STOP
      END
      SUBROUTINE GRID(RX,RY,DXMIN,DYMIN,DXMAX,DYMAX)
      COMMON/L1/DX(0:93),DY(0:50),NX,NY,NLE
      REAL RX,RY,DXMIN,DYMIN,DXMAX,DYMAX
      DY(1)=DYMIN
      DX(NLE)=DXMIN
      DX(NLE+1)=DXMIN
      DO 10 J=2,NY
        DY(J)=DY(J-1)*RY
   10   DY(J)=CVMGT(DY(J),DYMAX,DY(J).LT.DYMAX)
      DO 20 IB=1,NLE-1
        I=NLE-IB
        DX(I)=DX(I+1)*RX
   20   DX(I)=CVMGT(DX(I),DXMAX,DX(I).LT.DXMAX)
      DO 30 I=NLE+2,NX
        DX(I)=DX(I-1)*RX
   30   DX(I)=CVMGT(DX(I),DXMAX,DX(I).LT.DXMAX)
      DX(0)=0.
      DY(0)=0.
      DX(NX+1)=0.
```

```
      DY(NY+1)=0.
      RETURN
      END
      SUBROUTINE READIN(TAMB,YOAMB,TSTAR,IREADOLD,IUSTVST,ISR,
     -                  IBEG,IRIGHT)
      COMMON/L1/DX(0:93),DY(0:50),NX,NY,NLE
      COMMON/L2/U(0:93,0:50),V(0:93,0:50),T(0:93,0:50,1:3),
     -          R(0:93,0:50),P(0:93,0:50),PPR(0:93,0:50)
      COMMON/L3/UHAT(0:93,0:50),DU(0:93,0:50),USTAR(0:93,0:50),
     -          UAP(93,50),UAE(93,50),UAW(93,50),
     -          UAN(93,50),UAS(93,50),UB(93,50),GRASH,RINFNON
      COMMON/L4/VHAT(0:93,0:50),DV(0:93,0:50),VSTAR(0:93,0:50),
     -          VAP(93,50),VAE(93,50),VAW(93,50),
     -          VAN(93,50),VAS(93,50),VB(93,50)
      COMMON/L8/DXP(0:500),DYP(0:100),UPAR(2,0:100),VPAR(2,0:100),
     -          TPAR(2,0:100,3),TS(0:570,2),USPAR(0:570),VSPAR(0:570)
      COMMON/L9/IBC,UBC(0:50),VBC(0:50),TBC(0:50,3)
      REAL TAMB,YOAMB,TSTAR
        DO 10 M=1,3
        DO 10 I=0,NX+1
10        READ(11,905) (T(I,J,M),J=0,NY+1)
        DO 20 I=0,NX
20        READ(11,905) (U(I,J),J=0,NY+1)
        DO 30 I=0,NX+1
30        READ(11,905) (V(I,J),J=0,NY)
        DO 40 I=1,NX
40        READ(11,905) (P(I,J),J=1,NY)
        DO 50 I=1,NX
50        READ(11,905) (PPR(I,J),J=1,NY)
        DO 52 I=0,NX
52        READ(11,905) (USTAR(I,J),J=0,NY+1)
        DO 54 I=0,NX+1
54        READ(11,905) (VSTAR(I,J),J=0,NY)
      IF (ISR.EQ.1) THEN
        DO 56 I=NLE+1,IBEG+IRIGHT
56        READ(11,905) (TS(I,J),J=1,2)
      ENDIF
      IF (IBC.EQ.1) THEN
        READ(11,905) (UBC(J),J=1,NY)
        READ(11,905) (VBC(J),J=1,NY)
        READ(11,905) (TBC(J,1),J=1,NY)
        READ(11,905) (TBC(J,2),J=1,NY)
        READ(11,905) (TBC(J,3),J=1,NY)
       ELSE
        DO 58 J=1,NY
        UBC(J)=0.
        VBC(J)=0.
        TBC(J,1)=0.
        TBC(J,2)=0.
58      TBC(J,3)=0.
      ENDIF
      IF (IUSTVST.EQ.1) THEN
      DO 60 I=0,NX+1
        DO 60 J=0,NY+1
          USTAR(I,J)=U(I,J)
          VSTAR(I,J)=V(I,J)
60  CONTINUE
       ENDIF
```

```
      CALL DENS(TSTAR)
C---------------------SET B.C.'S FOR YO-----------------------------
      DO 110 J=0,NY+1
  110 T(0,J,3)=YOAMB
      DO 120 I=0,NX+1
  120 T(I,NY+1,3)=YOAMB
C
  905 FORMAT(1P,5(1X,E12.5))
      RETURN
      END
      SUBROUTINE UHATS(PR,TSTAR)
      COMMON/L1/DX(0:93),DY(0:50),NX,NY,NLE
      COMMON/L2/U(0:93,0:50),V(0:93,0:50),T(0:93,0:50,1:3),
     -          R(0:93,0:50),P(0:93,0:50),PPR(0:93,0:50)
      COMMON/L3/UHAT(0:93,0:50),DU(0:93,0:50),USTAR(0:93,0:50),
     -          AP(93,50),AE(93,50),AW(93,50),
     -          AN(93,50),AS(93,50),B(93,50),GRASH,RINFNON
      REAL PR,TSTAR,FE,FW,FN,FS,TP,TE,TW,TN,TS,GP,GE,GW,GN,GS,
     -     DE,DW,DN,DS,GVE,GVW,GVN,GVS,SPDXDY,
     -     TNORTH,TSOUTH,VOLUME
C-------EVALUATE COEFFICIENTS FOR INTERIOR U-CONTROL VOLUMES---------
      DO 10 I=1,NX-1
        DO 10 J=1,NY
          FE= R(I+1,J) * ( U(I,J)+U(I+1,J) )/2. * DY(J)
          FW=  R(I,J)  * ( U(I,J)+U(I-1,J) )/2. * DY(J)
          FN=( R(I,J+1)*DY(J) + R(I,J)*DY(J+1) )/(DY(J)+DY(J+1))
     -         * V(I,J) * DX(I)/2.
     -       +( R(I+1,J+1)*DY(J) + R(I+1,J)*DY(J+1) )/(DY(J)+DY(J+1))
     -         * V(I+1,J) * DX(I+1)/2.
          FS=( R(I,J-1)*DY(J) + R(I,J)*DY(J-1) )/(DY(J)+DY(J-1))
     -         * V(I,J-1) * DX(I)/2.
     -       +( R(I+1,J)*DY(J-1) + R(I+1,J-1)*DY(J) )/(DY(J)+DY(J-1))
     -         * V(I+1,J-1) * DX(I+1)/2.
          TP=(T(I,J,1)  *DX(I+1) + T(I+1,J,1)  *DX(I)  )/(DX(I) + DX(I+1))
          TE=(T(I+1,J,1)*DX(I+2) + T(I+2,J,1)  *DX(I+1))/(DX(I+1)+DX(I+2))
          TW=(T(I-1,J,1)*DX(I)   + T(I,J,1)    *DX(I-1))/(DX(I) + DX(I-1))
          TN=(T(I,J+1,1)*DX(I+1) + T(I+1,J+1,1)*DX(I)  )/(DX(I) + DX(I+1))
          TS=(T(I,J-1,1)*DX(I+1) + T(I+1,J-1,1)*DX(I)  )/(DX(I) + DX(I+1))
            GP=GAMMAV(TP,PR,TSTAR)
            GE=GAMMAV(TE,PR,TSTAR)
            GW=GAMMAV(TW,PR,TSTAR)
            GN=GAMMAV(TN,PR,TSTAR)
            GS=GAMMAV(TS,PR,TSTAR)
          DE=2. * GP*GE / (DX(I+1)*GE + DX(I+1)*GP) * DY(J)
          DW=2. * GP*GW / (DX(I)*GW   + DX(I)*GP  ) * DY(J)
          DN=2. * GP*GN / (DY(J)*GN   + DY(J+1)*GP) * (DX(I)+DX(I+1))/2.
          DS=2. * GP*GS / (DY(J)*GS   + DY(J-1)*GP) * (DX(I)+DX(I+1))/2.
            AE(I,J)=DE*A(ABS(FE/DE)) + AMAX1(-FE,0.)
            AW(I,J)=DW*A(ABS(FW/DW)) + AMAX1(FW,0.)
            AN(I,J)=DN*A(ABS(FN/DN)) + AMAX1(-FN,0.)
            AS(I,J)=DS*A(ABS(FS/DS)) + AMAX1(FS,0.)
          TNORTH=( (T(I,J+1,1)+T(I+1,J+1,1))/2. * DY(J)
     -       +(T(I,J,1)  +T(I+1,J,1)  )/2. * DY(J+1) )/(DY(J)+DY(J+1))
          TSOUTH=( (T(I,J-1,1)+T(I+1,J-1,1))/2. * DY(J)
     -       +(T(I,J,1)  +T(I+1,J,1)  )/2. * DY(J-1) )/(DY(J)+DY(J-1))
           GVE=GAMMAV(T(I+1,J,1),PR,TSTAR)
           GVW=GAMMAV(T(I,J,1),PR,TSTAR)
           GVN=GAMMAV(TNORTH,PR,TSTAR)
```

```
          GVS=GAMMAV(TSOUTH,PR,TSTAR)
       B(I,J) = ( GVE/DX(I+1)*U(I+1,J)+GVW/DX(I)*U(I-1,J) )*DY(J)/3.
      -      -2.*( GVE*(V(I+1,J)-V(I+1,J-1))-GVW*(V(I,J)-V(I,J-1)) )/3.
      -         +( GVN*(V(I+1,J)-V(I,J))-GVS*(V(I+1,J-1)-V(I,J-1)) )
      -         +GRASH*( RINFNON*( DX(I)+DX(I+1) )
      -                  -( R(I,J)*DX(I)+R(I+1,J)*DX(I+1) ) )*DY(J)/2.
       SPDXDY = ( -GVE/DX(I+1)-GVW/DX(I) ) * DY(J)/3.
          AP(I,J)=AE(I,J)+AW(I,J)+AN(I,J)+AS(I,J)-SPDXDY
        DU(I,J)=DY(J)/AP(I,J)
       UHAT(I,J)=(AE(I,J)*U(I+1,J)+AW(I,J)*U(I-1,J)+AN(I,J)*U(I,J+1)
      -         + AS(I,J)*U(I,J-1)+B(I,J))/AP(I,J)
   10 CONTINUE
        DO 20 J=1,NY
          DU(0,J)=0.
          DU(NX,J)=0.
        UHAT(0,J)=U(0,J)
   20   UHAT(NX,J)=U(NX,J)
       RETURN
       END
       SUBROUTINE VHATS(PR,TSTAR)
       COMMON/L1/DX(0:93),DY(0:50),NX,NY,NLE
       COMMON/L2/U(0:93,0:50),V(0:93,0:50),T(0:93,0:50,1:3),
      -          R(0:93,0:50),P(0:93,0:50),PPR(0:93,0:50)
       COMMON/L4/VHAT(0:93,0:50),DV(0:93,0:50),VSTAR(0:93,0:50),
      -          AP(93,50),AE(93,50),AW(93,50),
      -          AN(93,50),AS(93,50),B(93,50)
       REAL PR,TSTAR,FN,FS,FE,FW,TP,TN,TS,TE,TW,GP,GN,GS,GE,GW,
      -     DN,DS,DE,DW,GVN,GVS,GVE,GVW,SPDXDY,
      -     TEAST,TWEST,VOLUME
C-------EVALUATE COEFFICIENTS FOR INTERIOR V-CONTROL VOLUMES---------
       DO 10 I=1,NX
         DO 10 J=1,NY-1
           FN= R(I,J+1) * ( V(I,J)+V(I,J+1) )/2. * DX(I)
           FS=  R(I,J)  * ( V(I,J)+V(I,J-1) )/2. * DX(I)
           FE=( R(I+1,J)*DX(I) + R(I,J)*DX(I+1) )/(DX(I)+DX(I+1))
      -        * U(I,J) * DY(J)/2.
      -      +( R(I+1,J+1)*DX(I) + R(I,J+1)*DX(I+1) )/(DX(I)+DX(I+1))
      -        * U(I,J+1) * DY(J+1)/2.
           FW=( R(I-1,J)*DX(I) + R(I,J)*DX(I-1) )/(DX(I)+DX(I-1))
      -        * U(I-1,J) * DY(J)/2.
      -      +( R(I,J+1)*DX(I-1) + R(I-1,J+1)*DX(I) )/(DX(I)+DX(I-1))
      -        * U(I-1,J+1) * DY(J+1)/2.
        TP=(T(I,J,1)  *DY(J+1) + T(I,J+1,1)  *DY(J)  )/(DY(J) + DY(J+1))
        TN=(T(I,J+1,1)*DY(J+2) + T(I,J+2,1)  *DY(J+1))/(DY(J+1)+DY(J+2))
        TS=(T(I,J-1,1)*DY(J)   + T(I,J,1)    *DY(J-1))/(DY(J) + DY(J-1))
        TE=(T(I+1,J,1)*DY(J+1) + T(I+1,J+1,1)*DY(J)  )/(DY(J) + DY(J+1))
        TW=(T(I-1,J,1)*DY(J+1) + T(I-1,J+1,1)*DY(J)  )/(DY(J) + DY(J+1))
           GP=GAMMAV(TP,PR,TSTAR)
           GN=GAMMAV(TN,PR,TSTAR)
           GS=GAMMAV(TS,PR,TSTAR)
           GE=GAMMAV(TE,PR,TSTAR)
           GW=GAMMAV(TW,PR,TSTAR)
         DN=2. * GP*GN / (DY(J+1)*GN + DY(J+1)*GP) * DX(I)
         DS=2. * GP*GS / (DY(J)*GS   + DY(J)*GP  ) * DX(I)
         DE=2. * GP*GE / (DX(I)*GE   + DX(I+1)*GP) * (DY(J)+DY(J+1))/2.
         DW=2. * GP*GW / (DX(I)*GW   + DX(I-1)*GP) * (DY(J)+DY(J+1))/2.
           AE(I,J)=DE*A(ABS(FE/DE)) + AMAX1(-FE,0.)
           AW(I,J)=DW*A(ABS(FW/DW)) + AMAX1(FW,0.)
```

```
      AN(I,J)=DN*A(ABS(FN/DN)) + AMAX1(-FN,0.)
      AS(I,J)=DS*A(ABS(FS/DS)) + AMAX1(FS,0.)
     TEAST=( (T(I+1,J,1)+T(I+1,J+1,1))/2. * DX(I)
     -      +(T(I,J,1)  +T(I,J+1,1)  )/2. * DX(I+1) )/(DX(I)+DX(I+1))
     TWEST=( (T(I-1,J,1)+T(I-1,J+1,1))/2. * DX(I)
     -      +(T(I,J,1)  +T(I,J+1,1)  )/2. * DX(I-1) )/(DX(I)+DX(I-1))
      GVN=GAMMAV(T(I,J+1,1),PR,TSTAR)
      GVS=GAMMAV(T(I,J,1),PR,TSTAR)
      GVE=GAMMAV(TEAST,PR,TSTAR)
      GVW=GAMMAV(TWEST,PR,TSTAR)
   B(I,J) = ( GVN/DY(J+1)*V(I,J+1)+GVS/DY(J)*V(I,J-1) ) * DX(I)/3.
     -     -2.*( GVN*(U(I,J+1)-U(I-1,J+1))-GVS*(U(I,J)-U(I-1,J)) )/3.
     -        +( GVE*(U(I,J+1)-U(I,J))-GVW*(U(I-1,J+1)-U(I-1,J)) )
    SPDXDY = ( -GVN/DY(J+1)-GVS/DY(J) ) * DX(I)/3.
       AP(I,J)=AE(I,J)+AW(I,J)+AN(I,J)+AS(I,J)-SPDXDY
     DV(I,J)=DX(I)/AP(I,J)
    VHAT(I,J)=(AE(I,J)*V(I+1,J)+AW(I,J)*V(I-1,J)+AN(I,J)*V(I,J+1)
     -         + AS(I,J)*V(I,J-1)+B(I,J))/AP(I,J)
 10 CONTINUE
    DO 20 I=1,NX
      DV(I,0)=0.
      DV(I,NY)=0.
    VHAT(I,0)=V(I,0)
 20 VHAT(I,NY)=V(I,NY)
    RETURN
    END
    SUBROUTINE PRESSURE(ERP,PDAM,IBP)
    COMMON/L1/DX(0:93),DY(0:50),NX,NY,NLE
    COMMON/L2/U(0:93,0:50),V(0:93,0:50),T(0:93,0:50,1:3),
   -          R(0:93,0:50),P(0:93,0:50),PPR(0:93,0:50)
    COMMON/L3/UHAT(0:93,0:50),DU(0:93,0:50),USTAR(0:93,0:50),
   -          UAP(93,50),UAE(93,50),UAW(93,50),
   -          UAN(93,50),UAS(93,50),UB(93,50),GRASH,RINFNON
    COMMON/L4/VHAT(0:93,0:50),DV(0:93,0:50),VSTAR(0:93,0:50),
   -          VAP(93,50),VAE(93,50),VAW(93,50),
   -          VAN(93,50),VAS(93,50),VB(93,50)
    COMMON/L5/AP(93,50),AE(93,50),AW(93,50),AN(93,50),
   -          AS(93,50),SC(93,50),SP(93,50),B(93,50)
    COMMON/L6/AA(0:93),BB(0:93),CC(0:93),DD(0:93),XX(0:93)
    REAL POF(0:93,0:50),PO(0:93,0:50),
   -     FFE,FFW,FFN,FFS,RHE,RHW,RHN,RHS,RESP,ERP,PDAM,
   -     FE,FW,FN,FS,DE,DW,DN,DS,GE,GW,GN,GS,GP
C----------EVALUATE COEFFICIENTS FOR INTERIOR CONTROL VOLUMES--------
     DO 10 I=1,NX
       DO 10 J=1,NY
         FFE=DX(I+1)/(DX(I)+DX(I+1))
         FFW=DX(I-1)/(DX(I)+DX(I-1))
         FFN=DY(J+1)/(DY(J)+DY(J+1))
         FFS=DY(J-1)/(DY(J)+DY(J-1))
          RHE=(R(I,J)*FFE+R(I+1,J)*(1.-FFE))
          RHW=(R(I,J)*FFW+R(I-1,J)*(1.-FFW))
          RHN=(R(I,J)*FFN+R(I,J+1)*(1.-FFN))
          RHS=(R(I,J)*FFS+R(I,J-1)*(1.-FFS))
         AE(I,J)=RHE*DU(I,J)*DY(J)
         AW(I,J)=RHW*DU(I-1,J)*DY(J)
         AN(I,J)=RHN*DV(I,J)*DX(I)
         AS(I,J)=RHS*DV(I,J-1)*DX(I)
         B(I,J)=(RHW*UHAT(I-1,J)-RHE*UHAT(I,J))*DY(J)
```

```
     -          +(RHS*VHAT(I,J-1)-RHN*VHAT(I,J))*DX(I)
          AP(I,J)=AE(I,J)+AW(I,J)+AN(I,J)+AS(I,J)
   10 CONTINUE
      CALL OLDS(POF,P,NX,NY)
      DO 80 IBAILOUT=1,IBP
      CALL OLDS(PO,P,NX,NY)
C--------------------SWEEP USING VERTICAL LINES----------------------
      DO 40 I=1,NX
       DO 20 J=1,NY
         AA(J)=AP(I,J)/PDAM
         BB(J)=AN(I,J)
         CC(J)=AS(I,J)
   20    DD(J)=AE(I,J)*P(I+1,J)+AW(I,J)*P(I-1,J)+B(I,J)
     -         +(1.-PDAM)/PDAM*AP(I,J)*POF(I,J)
      IF (I.EQ.1) THEN
C--------------SET PRESSURE ARBITRARILY=0 AT TOP LEFT POINT OF DOMAIN
        CC(NY)=0.
        AA(NY)=1.
        DD(NY)=0.
       ENDIF
      CALL TDMA(1,NY)
      DO 30 J=1,NY
   30 P(I,J)=XX(J)
   40 CONTINUE
C--------------------SWEEP USING HORIZONTAL LINES--------------------
      DO 70 J=1,NY
       DO 50 I=1,NX
         AA(I)=AP(I,J)/PDAM
         BB(I)=AE(I,J)
         CC(I)=AW(I,J)
   50    DD(I)=AN(I,J)*P(I,J+1)+AS(I,J)*P(I,J-1)+B(I,J)
     -         +(1.-PDAM)/PDAM*AP(I,J)*POF(I,J)
      IF (J.EQ.NY) THEN
C--------------SET PRESSURE ARBITRARILY=0 AT TOP LEFT POINT OF DOMAIN
        AA(1)=1.
        BB(1)=0.
        DD(1)=0.
       ENDIF
      CALL TDMA(1,NX)
      DO 60 I=1,NX
   60 P(I,J)=XX(I)
   70 CONTINUE
      CALL FINDDIF(P,PO,NX,NY,RESP,'PRESSURE  ',IDIF,JDIF)
      IF (ABS(RESP).LT.ERP) GO TO 90
   80 CONTINUE
   90 CONTINUE
      RETURN
      END
      SUBROUTINE USTARS(ERU,UDAM,IBU,PR,TSTAR)
      COMMON/L1/DX(0:93),DY(0:50),NX,NY,NLE
      COMMON/L2/U(0:93,0:50),V(0:93,0:50),T(0:93,0:50,1:3),
     -          R(0:93,0:50),P(0:93,0:50),PPR(0:93,0:50)
      COMMON/L3/UHAT(0:93,0:50),DU(0:93,0:50),USTAR(0:93,0:50),
     -          AP(93,50),AE(93,50),AW(93,50),
     -          AN(93,50),AS(93,50),B(93,50),GRASH,RINFNON
      COMMON/L6/AA(0:93),BB(0:93),CC(0:93),DD(0:93),XX(0:93)
      COMMON/L9/IBC,UBC(0:50),VBC(0:50),TBC(0:50,3)
      REAL USTAROF(0:93,0:50),USTARO(0:93,0:50),RESU,ERU,UDAM
```

```
      CALL OLDS(USTAROF,USTAR,NX,NY)
      DO 80 IBAILOUT=1,IBU
      CALL OLDS(USTARO,USTAR,NX,NY)
C-------------------SWEEP USING VERTICAL LINES----------------------
      DO 40 I=1,NX-1
       DO 20 J=1,NY
         AA(J)=AP(I,J)/UDAM
         BB(J)=AN(I,J)
         CC(J)=AS(I,J)
   20    DD(J)=AE(I,J)*USTAR(I+1,J)+AW(I,J)*USTAR(I-1,J)+B(I,J)
     -         + ( P(I,J) - P(I+1,J) ) * DY(J)
     -         + (1.-UDAM)/UDAM*AP(I,J)*USTAROF(I,J)
C-------------------IMPOSE BOUNDARY CONDITIONS----------------------
C--BOTTOM--
       IF (I.LE.(NLE-1)) THEN
         AA(0)=1.
         BB(0)=1.
         DD(0)=0.
        ELSE
         AA(0)=1.
         BB(0)=0.
         DD(0)=U(I,0)
        ENDIF
C--TOP--
         CC(NY+1)=0.
         AA(NY+1)=1.
         DD(NY+1)=1.
        CALL TDMA(0,NY+1)
        DO 30 J=0,NY+1
   30  USTAR(I,J)=XX(J)
   40  CONTINUE
C-------------------SWEEP USING HORIZONTAL LINES--------------------
       DO 70 J=1,NY
        DO 50 I=1,NX-1
          AA(I)=AP(I,J)/UDAM
          BB(I)=AE(I,J)
          CC(I)=AW(I,J)
   50     DD(I)=AN(I,J)*USTAR(I,J+1)+AS(I,J)*USTAR(I,J-1)+B(I,J)
     -         + ( P(I,J) - P(I+1,J) ) * DY(J)
     -         + (1.-UDAM)/UDAM*AP(I,J)*USTAROF(I,J)
C-------------------IMPOSE BOUNDARY CONDITIONS----------------------
C--LEFT--
         AA(0)=1.
         BB(0)=0.
         DD(0)=1.
C--RIGHT--
         CC(NX)=1.
         AA(NX)=1.
         DD(NX)=DX(NX)*UBC(J)/GAMMAV(T(NX,J,1),PR,TSTAR)
        CALL TDMA(0,NX)
        DO 60 I=0,NX
   60  USTAR(I,J)=XX(I)
   70  CONTINUE
       CALL FINDDIF(USTAR,USTARO,NX,NY,RESU,'U-STAR     ',IDIF,JDIF)
       IF (ABS(RESU).LT.ERU) GO TO 90
   80  CONTINUE
   90  CONTINUE
       RETURN
```

```
      END
      SUBROUTINE VSTARS(ERV,VDAM,IBV,PR,TSTAR)
      COMMON/L1/DX(0:93),DY(0:50),NX,NY,NLE
      COMMON/L2/U(0:93,0:50),V(0:93,0:50),T(0:93,0:50,1:3),
     -          R(0:93,0:50),P(0:93,0:50),PPR(0:93,0:50)
      COMMON/L4/VHAT(0:93,0:50),DV(0:93,0:50),VSTAR(0:93,0:50),
     -          AP(93,50),AE(93,50),AW(93,50),
     -          AN(93,50),AS(93,50),B(93,50)
      COMMON/L6/AA(0:93),BB(0:93),CC(0:93),DD(0:93),XX(0:93)
      COMMON/L9/IBC,UBC(0:50),VBC(0:50),TBC(0:50,3)
      REAL VSTAROF(0:93,0:50),VSTARO(0:93,0:50),RESV,ERV,VDAM
      CALL OLDS(VSTAROF,VSTAR,NX,NY)
      DO 80 IBAILOUT=1,IBV
      CALL OLDS(VSTARO,VSTAR,NX,NY)
C-------------------SWEEP USING VERTICAL LINES-----------------------
      DO 40 I=1,NX
       DO 20 J=1,NY-1
         AA(J)=AP(I,J)/VDAM
         BB(J)=AN(I,J)
         CC(J)=AS(I,J)
   20    DD(J)=AE(I,J)*VSTAR(I+1,J)+AW(I,J)*VSTAR(I-1,J)+B(I,J)
     -         + ( P(I,J) - P(I,J+1) ) * DX(I)
     -         + (1.-VDAM)/VDAM*AP(I,J)*VSTAROF(I,J)
C-------------------IMPOSE BOUNDARY CONDITIONS-----------------------
C--BOTTOM--
      IF (I.LE.NLE) THEN
        AA(0)=1.
        BB(0)=0.
        DD(0)=0.
       ELSE
        AA(0)=1.
        BB(0)=0.
        DD(0)=V(I,0)
       ENDIF
C--TOP--
       CC(NY)=1.
       AA(NY)=1.
       DD(NY)=0.
      CALL TDMA(0,NY)
      DO 30 J=0,NY
   30 VSTAR(I,J)=XX(J)
   40 CONTINUE
C-------------------SWEEP USING HORIZONTAL LINES---------------------
      DO 70 J=1,NY-1
       DO 50 I=1,NX
         AA(I)=AP(I,J)/VDAM
         BB(I)=AE(I,J)
         CC(I)=AW(I,J)
   50    DD(I)=AN(I,J)*VSTAR(I,J+1)+AS(I,J)*VSTAR(I,J-1)+B(I,J)
     -         + ( P(I,J) - P(I,J+1) ) * DX(I)
     -         + (1.-VDAM)/VDAM*AP(I,J)*VSTAROF(I,J)
C-------------------IMPOSE BOUNDARY CONDITIONS-----------------------
C--LEFT--
       AA(0)=1.
       BB(0)=0.
       DD(0)=0.
C--RIGHT--
       CC(NX+1)=1.
```

```
      AA(NX+1)=1.
      TMEAN=(T(NX,J,1)+T(NX+1,J,1))/2.
      DD(NX+1)=DX(NX)/2.*VBC(J)/GAMMAV(TMEAN,PR,TSTAR)
    CALL TDMA(0,NX+1)
    DO 60 I=0,NX+1
 60 VSTAR(I,J)=XX(I)
 70 CONTINUE
    CALL FINDDIF(VSTAR,VSTARO,NX,NY,RESV,'V-STAR    ',IDIF,JDIF)
    IF (ABS(RESV).LT.ERV) GO TO 90
 80 CONTINUE
 90 CONTINUE
    RETURN
    END
    SUBROUTINE PPRIME(ERPP,IBPP,ISKPP)
    COMMON/L1/DX(0:93),DY(0:50),NX,NY,NLE
    COMMON/L2/U(0:93,0:50),V(0:93,0:50),T(0:93,0:50,1:3),
   -          R(0:93,0:50),P(0:93,0:50),PPR(0:93,0:50)
    COMMON/L3/UHAT(0:93,0:50),DU(0:93,0:50),USTAR(0:93,0:50),
   -          UAP(93,50),UAE(93,50),UAW(93,50),
   -          UAN(93,50),UAS(93,50),UB(93,50),GRASH,RINFNON
    COMMON/L4/VHAT(0:93,0:50),DV(0:93,0:50),VSTAR(0:93,0:50),
   -          VAP(93,50),VAE(93,50),VAW(93,50),
   -          VAN(93,50),VAS(93,50),VB(93,50)
    COMMON/L5/AP(93,50),AE(93,50),AW(93,50),AN(93,50),
   -          AS(93,50),SC(93,50),SP(93,50),B(93,50)
    COMMON/L6/AA(0:93),BB(0:93),CC(0:93),DD(0:93),XX(0:93)
    REAL PPRO(0:93,0:50),FFE,FFW,FFN,FFS,RHE,RHW,RHN,RHS,
   -     FE,FW,FN,FS,DE,DW,DN,DS,GE,GW,GN,GS,GP,RESPP,ERPP
C----------EVALUATE COEFFICIENTS FOR INTERIOR CONTROL VOLUMES--------
    DO 10 I=1,NX
      DO 10 J=1,NY
        FFE=DX(I+1)/(DX(I)+DX(I+1))
        FFW=DX(I-1)/(DX(I)+DX(I-1))
        FFN=DY(J+1)/(DY(J)+DY(J+1))
        FFS=DY(J-1)/(DY(J)+DY(J-1))
         RHE=(R(I,J)*FFE+R(I+1,J)*(1.-FFE))
         RHW=(R(I,J)*FFW+R(I-1,J)*(1.-FFW))
         RHN=(R(I,J)*FFN+R(I,J+1)*(1.-FFN))
         RHS=(R(I,J)*FFS+R(I,J-1)*(1.-FFS))
        AE(I,J)=RHE*DU(I,J)*DY(J)
        AW(I,J)=RHW*DU(I-1,J)*DY(J)
        AN(I,J)=RHN*DV(I,J)*DX(I)
        AS(I,J)=RHS*DV(I,J-1)*DX(I)
        B(I,J)=(RHW*USTAR(I-1,J)-RHE*USTAR(I,J))*DY(J)
   -           +(RHS*VSTAR(I,J-1)-RHN*VSTAR(I,J))*DX(I)
        AP(I,J)=AE(I,J)+AW(I,J)+AN(I,J)+AS(I,J)
 10 CONTINUE
    DO 80 IBAILOUT=1,IBPP
    CALL OLDS(PPRO,PPR,NX,NY)
C-------------------SWEEP USING VERTICAL LINES-----------------------
    DO 40 I=1,NX
     DO 20 J=1,NY
       AA(J)=AP(I,J)
       BB(J)=AN(I,J)
       CC(J)=AS(I,J)
 20    DD(J)=AE(I,J)*PPR(I+1,J)+AW(I,J)*PPR(I-1,J)+B(I,J)
    IF ((I.EQ.NX).AND.(ISKPP.EQ.0)) THEN
C-------------SET P-PRIME ARBITRARILY=0 AT TOP RIGHT POINT OF DOMAIN
```

```
        CC(NY)=0.
        AA(NY)=1.
        DD(NY)=0.
       ENDIF
      CALL TDMA(1,NY)
      DO 30 J=1,NY
   30 PPR(I,J)=XX(J)
   40 CONTINUE
C--------------------SWEEP USING HORIZONTAL LINES----------------------
      DO 70 J=1,NY
       DO 50 I=1,NX
         AA(I)=AP(I,J)
         BB(I)=AE(I,J)
         CC(I)=AW(I,J)
   50    DD(I)=AN(I,J)*PPR(I,J+1)+AS(I,J)*PPR(I,J-1)+B(I,J)
      IF ((J.EQ.NY).AND.(ISKPP.EQ.0)) THEN
C--------------SET P-PRIME ARBITRARILY=0 AT TOP RIGHT POINT OF DOMAIN
        CC(NX)=0.
        AA(NX)=1.
        DD(NX)=0.
       ENDIF
      CALL TDMA(1,NX)
      DO 60 I=1,NX
   60 PPR(I,J)=XX(I)
   70 CONTINUE
      CALL FINDDIF(PPR,PPRO,NX,NY,RESPP,'P-PRIME    ',IDIF,JDIF)
      IF (ABS(RESPP).LT.ERPP) GO TO 90
   80 CONTINUE
   90 RETURN
      END
      SUBROUTINE CORVEL(PR,TSTAR)
      COMMON/L1/DX(0:93),DY(0:50),NX,NY,NLE
      COMMON/L2/U(0:93,0:50),V(0:93,0:50),T(0:93,0:50,1:3),
     -          R(0:93,0:50),P(0:93,0:50),PPR(0:93,0:50)
      COMMON/L3/UHAT(0:93,0:50),DU(0:93,0:50),USTAR(0:93,0:50),
     -          UAP(93,50),UAE(93,50),UAW(93,50),
     -          UAN(93,50),UAS(93,50),UB(93,50),GRASH,RINFNON
      COMMON/L4/VHAT(0:93,0:50),DV(0:93,0:50),VSTAR(0:93,0:50),
     -          VAP(93,50),VAE(93,50),VAW(93,50),
     -          VAN(93,50),VAS(93,50),VB(93,50)
      COMMON/L9/IBC,UBC(0:50),VBC(0:50),TBC(0:50,3)
      DO 10 I=1,NX-1
        DO 10 J=1,NY
   10     U(I,J)=USTAR(I,J)+DU(I,J)*(PPR(I,J)-PPR(I+1,J))
      DO 20 I=1,NX
        DO 20 J=1,NY-1
   20     V(I,J)=VSTAR(I,J)+DV(I,J)*(PPR(I,J)-PPR(I,J+1))
C------------ADJUST BOUNDARY VELOCITIES-----------------------------
      DO 30 J=1,NY
        TMEAN=(T(NX,J,1)+T(NX+1,J,1))/2.
        GV1=GAMMAV(T(NX,J,1),PR,TSTAR)
        GV2=GAMMAV(TMEAN,PR,TSTAR)
        U(NX,J)=(U(NX,J)+U(NX-1,J)+DX(NX)*UBC(J)/GV1)/2.
   30   V(NX+1,J)=(V(NX+1,J)+V(NX,J)+DX(NX)/2.*VBC(J)/GV2)/2.
      DO 40 I=1,NX
   40   V(I,NY)=V(I,NY-1)
      DO 50 I=0,(NLE-1)
   50   U(I,0)=U(I,1)
```

```
      RETURN
      END
      SUBROUTINE PHI(TAMB,DA,Q,E,FO,ERF,FDAM,M,TSTAR,IBF)
      COMMON/L1/DX(0:93),DY(0:50),NX,NY,NLE
      COMMON/L2/U(0:93,0:50),V(0:93,0:50),T(0:93,0:50,1:3),
     _         R(0:93,0:50),P(0:93,0:50),PPR(0:93,0:50)
      COMMON/L5/AP(93,50),AE(93,50),AW(93,50),AN(93,50),
     _         AS(93,50),SC(93,50),SP(93,50),B(93,50)
      COMMON/L6/AA(0:93),BB(0:93),CC(0:93),DD(0:93),XX(0:93)
      COMMON/L9/IBC,UBC(0:50),VBC(0:50),TBC(0:50,3)
      REAL TOL(0:93,0:50,3),TOLF(0:93,0:50,3),TSTAR,
     _     TAMB,DA,Q,E,ERF,FDAM(3),PEF,FO,PRESP,PRESC,ARRHEN,
     _     SCC,SPP,FFE,FFW,FFN,FFS,LE(3),YI(3),TONOFF,TE1,
     _     FE,FW,FN,FS,DE,DW,DN,DS,GE,GW,GN,GS,GP,REST
       TONOFF=0.
       IF (M.EQ.1) THEN
        PRESP=0.
        PRESC=Q
        TONOFF=1.
       ENDIF
       IF (M.EQ.2) THEN
        PRESP=-1.
        PRESC=0.
        ISPEC=3
        LE(M)=1.
        YI(M)=1.
       ENDIF
       IF (M.EQ.3) THEN
        PRESP=-FO
        PRESC=0.
        ISPEC=2
        LE(M)=1.
        YI(M)=0.
       ENDIF
C----------EVALUATE COEFFICIENTS FOR INTERIOR CONTROL VOLUMES---------
       DO 10 I=1,NX
         DO 10 J=1,NY
           FFE=DX(I+1)/(DX(I)+DX(I+1))
           FFW=DX(I-1)/(DX(I)+DX(I-1))
           FFN=DY(J+1)/(DY(J)+DY(J+1))
           FFS=DY(J-1)/(DY(J)+DY(J-1))
            FE=(R(I,J)*FFE+R(I+1,J)*(1.-FFE)) * U(I,J)   * DY(J)
            FW=(R(I,J)*FFW+R(I-1,J)*(1.-FFW)) * U(I-1,J) * DY(J)
            FN=(R(I,J)*FFN+R(I,J+1)*(1.-FFN)) * V(I,J)   * DX(I)
            FS=(R(I,J)*FFS+R(I,J-1)*(1.-FFS)) * V(I,J-1) * DX(I)
           GP=GAMMAT(T(I,J,1),M,TSTAR)
           GE=GAMMAT(T(I+1,J,1),M,TSTAR)
           GW=GAMMAT(T(I-1,J,1),M,TSTAR)
           GN=GAMMAT(T(I,J+1,1),M,TSTAR)
           GS=GAMMAT(T(I,J-1,1),M,TSTAR)
            DE=2. * GP*GE / (DX(I)*GE + DX(I+1)*GP) * DY(J)
            DW=2. * GP*GW / (DX(I)*GW + DX(I-1)*GP) * DY(J)
            DN=2. * GP*GN / (DY(J)*GN + DY(J+1)*GP) * DX(I)
            DS=2. * GP*GS / (DY(J)*GS + DY(J-1)*GP) * DX(I)
           AE(I,J)=DE*A(ABS(FE/DE)) + AMAX1(-FE,0.)
           AW(I,J)=DW*A(ABS(FW/DW)) + AMAX1(FW,0.)
           AN(I,J)=DN*A(ABS(FN/DN)) + AMAX1(-FN,0.)
           AS(I,J)=DS*A(ABS(FS/DS)) + AMAX1(FS,0.)
```

```
                ARRHEN=EXP(-E/T(I,J,1))
                PEF=DA*R(I,J)*R(I,J)
                 SPP=PRESP*PEF*T(I,J,ISPEC)*ARRHEN
                 SCC=PRESC*PEF*T(I,J,2)*T(I,J,3)*ARRHEN
               B(I,J)=SCC*DX(I)*DY(J)
               AP(I,J)=AE(I,J)+AW(I,J)+AN(I,J)+AS(I,J)-SPP*DX(I)*DY(J)
     10 CONTINUE
        CALL OLDS3(TOLF,T,NX,NY,M)
        DO 80 IBAILOUT=1,IBF
        CALL OLDS3(TOL,T,NX,NY,M)
C-------------------SWEEP USING VERTICAL LINES-----------------------
       DO 40 I=1,NX
        DO 20 J=1,NY
          AA(J)=AP(I,J)/FDAM(M)
          BB(J)=AN(I,J)
          CC(J)=AS(I,J)
     20   DD(J)=AE(I,J)*T(I+1,J,M)+AW(I,J)*T(I-1,J,M)+B(I,J)
      -          + (1.-FDAM(M))/FDAM(M)*AP(I,J)*TOLF(I,J,M)
C-------------------IMPOSE BOUNDARY CONDITIONS-----------------------
C--BOTTOM--
       IF (I.LE.NLE) THEN
         AA(0)=1.
         BB(0)=1.
         DD(0)=0.
        ELSE
         TE1=R(I,0)*V(I,0)*LE(M)*DY(1)*(1.-TONOFF)/
      -        ( GAMMAT(T(I,1,1),M,TSTAR)+GAMMAT(T(I,0,1),M,TSTAR) )
         AA(0)=1.+TE1
         BB(0)=1.-TONOFF
         DD(0)=TE1*YI(M)+T(I,0,1)*TONOFF
        ENDIF
C--TOP--
         CC(NY+1)=0.
         AA(NY+1)=1.
         DD(NY+1)=T(I,NY+1,M)
       CALL TDMA(0,NY+1)
       DO 30 J=0,NY+1
     30 T(I,J,M)=XX(J)
     40 CONTINUE
C-------------------SWEEP USING HORIZONTAL LINES---------------------
       DO 70 J=1,NY
        DO 50 I=1,NX
          AA(I)=AP(I,J)/FDAM(M)
          BB(I)=AE(I,J)
          CC(I)=AW(I,J)
     50   DD(I)=AN(I,J)*T(I,J+1,M)+AS(I,J)*T(I,J-1,M)+B(I,J)
      -          + (1.-FDAM(M))/FDAM(M)*AP(I,J)*TOLF(I,J,M)
C-------------------IMPOSE BOUNDARY CONDITIONS-----------------------
C--LEFT--
         AA(0)=1.
         BB(0)=0.
         DD(0)=T(0,J,M)
C--RIGHT--
         CC(NX+1)=1.
         AA(NX+1)=1.
         TMEAN=(T(NX,J,1)+T(NX+1,J,1))/2.
         DD(NX+1)=DX(NX)/2.*TBC(J,M)/GAMMAT(TMEAN,M,TSTAR)
       CALL TDMA(0,NX+1)
```

```
      DO 60 I=0,NX+1
   60 T(I,J,M)=XX(I)
   70 CONTINUE
      CALL FINDDIF3(T,TOL,NX,NY,REST,'PHI      ',M)
      IF (ABS(REST).LT.ERF) GO TO 90
   80 CONTINUE
   90 CONTINUE
      RETURN
      END
      SUBROUTINE DENS(TSTAR)
      COMMON/L1/DX(0:93),DY(0:50),NX,NY,NLE
      COMMON/L2/U(0:93,0:50),V(0:93,0:50),T(0:93,0:50,1:3),
     _          R(0:93,0:50),P(0:93,0:50),PPR(0:93,0:50)
      REAL TSTAR
      DO 10 I=0,NX+1
        DO 10 J=0,NY+1
   10     R(I,J)=TSTAR/T(I,J,1)
      RETURN
      END
      SUBROUTINE TDMA(N1,N2)
      COMMON/L6/AA(0:93),BB(0:93),CC(0:93),DD(0:93),XX(0:93)
      REAL PP(0:93),QQ(0:93)
C--THE TDM IS OF THE FORM AA(I)XX(I)=BB(I)XX(I+1)+CC(I)XX(I-1)+DD(I)--
C--FORWARD SUBSTITUTION--
      CC(N1)=0.
      BB(N2)=0.
      DO 10 I=N1,N2
        PP(I)=BB(I)/(AA(I)-CC(I)*PP(I-1))
   10   QQ(I)=(DD(I)+CC(I)*QQ(I-1))/(AA(I)-CC(I)*PP(I-1))
C--BACK SUBSTITUTION--
      XX(N2)=QQ(N2)
      DO 20 II=N1,N2-1
        I=N2-1+N1-II
   20   XX(I)=PP(I)*XX(I+1)+QQ(I)
      RETURN
      END
      SUBROUTINE WRITE1(X,TX,NX0,NXT,NFORMAT)
      REAL X(0:570)
      IF (TX.EQ.0.) TX=1.
      IF (NFORMAT.EQ.1) THEN
       WRITE(13,900) ((X(I)/TX),I=NX0,NXT)
       ELSE
       WRITE(13,905) ((X(I)/TX),I=NX0,NXT)
      ENDIF
C
  900 FORMAT(5(1X,F7.4))
  905 FORMAT(1P,5(1X,E12.5))
      RETURN
      END
C
      SUBROUTINE WRITE2(X,NX0,NXT,NY0,NYT,NFORMAT)
      REAL X(0:93,0:50)
      IF (NFORMAT.EQ.1) THEN
       DO 10 I=NX0,NXT
   10    WRITE(13,900) (X(I,J),J=NY0,NYT)
       ELSE
       DO 20 I=NX0,NXT
   20    WRITE(13,905) (X(I,J),J=NY0,NYT)
```

```
      ENDIF
C
  900 FORMAT(5(1X,F7.4))
  905 FORMAT(1P,5(1X,E12.5))
      RETURN
      END
C
      SUBROUTINE WRITE3(X,NX0,NXT,NY0,NYT,NFORMAT)
      REAL X(0:93,0:50,3)
       DO 5 M=2,3
       DO 5 I=NX0,NXT
       DO 5 J=NY0,NYT
        IF (X(I,J,M).LT.1.E-78) X(I,J,M)=0.
    5  CONTINUE
      IF (NFORMAT.EQ.1) THEN
       DO 10 M=1,3
       DO 10 I=NX0,NXT
   10    WRITE(13,900) (X(I,J,M),J=NY0,NYT)
      ELSE
       DO 20 M=1,3
       DO 20 I=NX0,NXT
   20    WRITE(13,905) (X(I,J,M),J=NY0,NYT)
      ENDIF
C
  900 FORMAT(5(1X,F7.4))
  905 FORMAT(1P,5(1X,E12.5))
      RETURN
      END
C
      SUBROUTINE WRITE4(X,NX0,NXT,NY0,NYT,NFORMAT)
      REAL X(0:570,2)
      IF (NFORMAT.EQ.1) THEN
       DO 10 I=NX0,NXT
   10    WRITE(13,900) (X(I,J),J=NY0,NYT)
      ELSE
       DO 20 I=NX0,NXT
   20    WRITE(13,905) (X(I,J),J=NY0,NYT)
      ENDIF
C
  900 FORMAT(5(1X,F7.4))
  905 FORMAT(1P,5(1X,E12.5))
      RETURN
      END
      SUBROUTINE FINDDIF(ARR1,ARR2,NX,NY,MAXDIF,VARNAME,IDIF,JDIF)
      REAL ARR1(0:93,0:50),ARR2(0:93,0:50),MAXDIF,LOCDIF
      CHARACTER VARNAME*10
      MAXDIF=0.
      IDIF=0
      JDIF=0
      DO 10 I=0,NX+1
        DO 10 J=0,NY+1
          LOCDIF=ARR1(I,J)-ARR2(I,J)
          IF (ABS(LOCDIF).GT.ABS(MAXDIF)) THEN
            MAXDIF=LOCDIF
            IDIF=I
            JDIF=J
          ENDIF
   10 CONTINUE
```

```
      WRITE(12,900) VARNAME,MAXDIF,IDIF,JDIF
  900 FORMAT('DELTA ',A,' = ',F9.5,' AT ',I3,', ',I3)
      RETURN
      END
C
      SUBROUTINE FINDDIF3(ARR1,ARR2,NX,NY,MAXDIF,VARNAME,M)
      REAL ARR1(0:93,0:50,3),ARR2(0:93,0:50,3),MAXDIF,LOCDIF
      CHARACTER VARNAME*10
      MAXDIF=0.
      IDIF=0
      JDIF=0
      DO 10 I=0,NX+1
        DO 10 J=0,NY+1
          LOCDIF=ARR1(I,J,M)-ARR2(I,J,M)
          IF (ABS(LOCDIF).GT.ABS(MAXDIF)) THEN
            MAXDIF=LOCDIF
            IDIF=I
            JDIF=J
          ENDIF
   10 CONTINUE
      WRITE(12,900) VARNAME,M,MAXDIF,IDIF,JDIF
  900 FORMAT('DELTA ',A,I2,' = ',F9.5,' AT ',I3,', ',I3)
      RETURN
      END
      SUBROUTINE OLDS(OLD,CURRENT,NX,NY)
      REAL OLD(0:93,0:50),CURRENT(0:93,0:50)
      DO 10 I=0,NX+1
        DO 10 J=0,NY+1
   10     OLD(I,J)=CURRENT(I,J)
      RETURN
      END
C
      SUBROUTINE OLDS3(OLD,CURRENT,NX,NY,M)
      REAL OLD(0:93,0:50,3),CURRENT(0:93,0:50,3)
      DO 10 I=0,NX+1
        DO 10 J=0,NY+1
   10     OLD(I,J,M)=CURRENT(I,J,M)
      RETURN
      END
      SUBROUTINE DAMPER(OLDVAL,NEWVAL,FRACT,NX,NY)
      REAL OLDVAL(0:93,0:50),NEWVAL(0:93,0:50),FRACT
      DO 10 I=0,NX+1
        DO 10 J=0,NY+1
   10     NEWVAL(I,J)=FRACT*NEWVAL(I,J)+(1.-FRACT)*OLDVAL(I,J)
      RETURN
      END
C
      SUBROUTINE DAMPER3(OLDVAL,NEWVAL,FRACT,NX,NY,M)
      REAL OLDVAL(0:93,0:50,3),NEWVAL(0:93,0:50,3),FRACT
      DO 10 I=0,NX+1
        DO 10 J=0,NY+1
   10     NEWVAL(I,J,M)=FRACT*NEWVAL(I,J,M)+(1.-FRACT)*OLDVAL(I,J,M)
      RETURN
      END
      FUNCTION CVMGT(AAA,BBB,CCC)
      REAL AAA,BBB
      LOGICAL CCC
      IF (CCC) THEN
```

```
          CVMGT=AAA
         ELSE
          CVMGT=BBB
         ENDIF
        RETURN
        END
        FUNCTION A(P)
C-------------"PECLET" FUNCTION PREFERRED IN SIMPLE ALGORITHM---------
        REAL X,P
        X=(1.-0.1*P)**5
        IF (X.GT.0.) THEN
          A=X
         ELSE
          A=0.
         ENDIF
        RETURN
        END
C
        FUNCTION GAMMAT(XXX,M,TSTAR)
C-----------------EVALUATES CONDUCTIVITY, GAMMAT, AT T=XXX------------
        REAL XXX,TSTAR
        GAMMAT=XXX/TSTAR
        RETURN
        END
C
        FUNCTION GAMMAV(XXX,PR,TSTAR)
C-----------------EVALUATES VISCOSITY, GAMMAV, AT T=XXX AND GIVEN PR--
        REAL XXX,PR,TSTAR
        GAMMAV=PR*XXX/TSTAR
        RETURN
        END
        SUBROUTINE SOLID(EPS,VFL,VFU,VF,VE0,UBUOY,
       -           THICK,ZZZ,TX,XODAMP,XNDAMP,ASW,IBEG,IRIGHT,MMAX,KSOL)
        COMMON/L1/DX(0:93),DY(0:50),NX,NY,NLE
        COMMON/L2/U(0:93,0:50),V(0:93,0:50),T(0:93,0:50,1:3),
       -           R(0:93,0:50),P(0:93,0:50),PPR(0:93,0:50)
        COMMON/L7/RSTAR,RS,CS,CP,SIG,T0,TL,XL,ES,TAU,ASTAR,TSTAR
        COMMON/L8/DXP(0:500),DYP(0:100),UPAR(2,0:100),VPAR(2,0:100),
       -           TPAR(2,0:100,3),TS(0:570,2),USPAR(0:570),VSPAR(0:570)
        REAL QR,RR,S,LN,C,XR,QYA,AA,BB,CC,DD,EE,FF,DHDX,ASTAR,
       -     QY(0:570),TOV(0:570),THICK(0:570),
       -     EPS,VFL,VFU,VF,VE0,UBUOY,ZZZ,TX,XODAMP,XNDAMP,ASW,UREF
        NX2=IBEG+IRIGHT-1
        RR=RS*CS/RSTAR/CP
        S=SIG*EPS*T0**3/RSTAR/CP
        LN=(1.-CP/CS)*TL/T0-XL/CS/T0
        C=CP/2./CS
        E=ES
        VFLINI=VFL
        VFUINI=VFU
        THKNEW=1.
        THKOLD=0.
C-----------------BEGIN MAIN ROUTINE-------------------
      DO 888 III=1,100
      IF (ABS(1.-THKOLD/THKNEW).LT.0.01) GOTO 999
      THKOLD=THKNEW
      VFL=VFLINI
      VFU=VFUINI
```

```
      MM=0
      DO 10 IK=NLE+1,NX2+1
   10 TOV(IK)=TS(IK,1)
      I=NLE+1
      QY(I)=(TS(I,2)+TS(I,1))*(TS(I,2)-TS(I,1))/DY(1)/TSTAR
      DO 20 I=NLE+2,NX2+1
      QY(I)=(TS(I,2)+TS(I,1))*(TS(I,2)-TS(I,1))/DY(1)/TSTAR
   20 CONTINUE
   30 VF=(VFL+VFU)/2.
      MM=MM+1
      IF (MM.GT.MMAX) THEN
      WRITE(*,*) 'MM EXCEEDED, VF = ',VF
      ZZZ=1.
      GO TO 999
      ENDIF
      UREF=VE0+UBUOY-VF
      XR=ASTAR/UREF
      R1=RR*VF/UREF
      S1=S/UREF
      THICK(NX2+1)=TAU/XR
      DO 40 J=NLE+1,NX2
      I=NLE+NX2-J+1
      DHDX=ASW/VF*( XNDAMP*EXP(-E/TS(I+1,1))+
     -              XODAMP*EXP(-E/TOV(I)) )/(XNDAMP+XODAMP)
       IF (I.LT.IBEG) DDX=(DX(I)+DX(I+1))/2.
       IF (I.GE.IBEG) DDX=DXP(I-IBEG+1)
       THICK(I)=THICK(I+1)-DHDX*DDX
       IF (THICK(I).LT.0.) THEN
       VFL=VF
       GO TO 30
       ENDIF
       QYA=(QY(I)+QY(I+1))/2.
       AA=R1*(THICK(I+1)*TS(I+1,1)/DDX-DHDX*(LN+C*TS(I+1,1)))
       BB=S1*(TS(I+1,1)**4+1.)
       CC=R1*(THICK(I)/DDX+DHDX*C)+2.*S1*TS(I+1,1)**3
       TS(I,1)=(QYA+AA+BB)/CC
       IF (TS(I,1).LT.1.) TS(I,1)=1.
   40 CONTINUE
      IF (ABS(THICK(NLE+1)).LT.(1.D-4*TAU/XR)) GO TO 50
      IF (THICK(NLE+1).GT.0.D0) THEN
      VFU=VF
      GO TO 30
      ENDIF
   50 CONTINUE
      TX=TAU/XR
      THKNEW=THICK(NLE+1)
  888 IF (KSOL.NE.0) GO TO 999
C
  900 FORMAT(1X,0P,I3,1P,4(1X,E12.5))
  905 FORMAT (2X,0P,I3,1P,1X,E12.5,1X,E9.2)
  999 WRITE(19,905) MM,VF,(THICK(NLE+1)/TX)
      CONTINUE
      RETURN
      END
      SUBROUTINE PARGRID(NF,IBEG,JTOP,IRIGHT,RDXP,DXPMIN,DXPMAX)
      COMMON/L1/DX(0:93),DY(0:50),NX,NY,NLE
      COMMON/L2/U(0:93,0:50),V(0:93,0:50),T(0:93,0:50,1:3),
     -          R(0:93,0:50),P(0:93,0:50),PPR(0:93,0:50)
```

```
      COMMON/L8/DXP(0:500),DYP(0:100),UPAR(2,0:100),VPAR(2,0:100),
     -          TPAR(2,0:100,3),TS(0:570,2),USPAR(0:570),VSPAR(0:570)
      IF (NF.EQ.1) GO TO 35
      NF=1
      FFC=1.
      DO 10 J=0,NY
   10 DYP(J)=DY(J)
      DO 20 J=NY+1,NY+1+JTOP
   20 DYP(J)=DY(NY)
      DO 30 I=IBEG,NX
   30 DXP(I-IBEG+1)=DX(I)/2.+DX(I+1)/2.
      DXP(NX+2-IBEG)=DXPMIN
      DO 33 I=NX+3-IBEG,IRIGHT
      DXP(I)=DXP(I-1)*RDXP
   33 DXP(I)=CVMGT(DXP(I),DXPMAX,DXP(I).LT.DXPMAX)
C----------SET INITIAL VALUES FOR PARABOLIC CALCULATION---------------
      IF (IBEG.EQ.NX+1) FFC=0.
   35 DO 40 J=0,NY+1
      UPAR(1,J)=(FFC*U(IBEG,J)+U(IBEG-1,J))/(1.+FFC)
      TPAR(1,J,1)=T(IBEG,J,1)
      TPAR(1,J,2)=T(IBEG,J,2)
   40 TPAR(1,J,3)=T(IBEG,J,3)
      VPAR(1,0)=V(IBEG,0)
      DO 50 J=1,NY
   50 VPAR(1,J)=(V(IBEG,J)+V(IBEG,J-1))/2
      VPAR(1,NY+1)=V(IBEG,NY)
      DO 60 J=NY+2,NY+1+JTOP
      UPAR(1,J)=UPAR(1,NY+1)
      VPAR(1,J)=VPAR(1,NY+1)
      TPAR(1,J,1)=TPAR(1,NY+1,1)
      TPAR(1,J,2)=TPAR(1,NY+1,2)
   60 TPAR(1,J,3)=TPAR(1,NY+1,3)
      CONTINUE
      RETURN
      END
      SUBROUTINE SETSUR(IBEG,JTOP,IRIGHT,ES,ASW,RS,
     -                  TSTAR,RSTAR,VF,VEL,ISR)
      COMMON/L1/DX(0:93),DY(0:50),NX,NY,NLE
      COMMON/L2/U(0:93,0:50),V(0:93,0:50),T(0:93,0:50,1:3),
     -          R(0:93,0:50),P(0:93,0:50),PPR(0:93,0:50)
      COMMON/L8/DXP(0:500),DYP(0:100),UPAR(2,0:100),VPAR(2,0:100),
     -          TPAR(2,0:100,3),TS(0:570,2),USPAR(0:570),VSPAR(0:570)
      IF (ISR.EQ.1) GO TO 25
      DO 10 I=NLE+1,IBEG
      TS(I,1)=T(I,0,1)
   10 TS(I,2)=T(I,1,1)
      DO 20 I=IBEG+1,IBEG+IRIGHT
      TS(I,1)=TS(IBEG,1)-(TS(IBEG,1)-1.)*(I-IBEG)/(1.*IRIGHT)
   20 TS(I,2)=TS(IBEG,2)-(TS(IBEG,2)-1.)*(I-IBEG)/(1.*IRIGHT)
   25 DO 30 I=IBEG,IBEG+IRIGHT
C*************************************************************
C********  NOTE!!! THE FOLLOWING LINE ASSUMES EQU. OF STATE  **
C************************  RHO=TSTAR/T  ************************
      VSPAR(I)=EXP(-ES/TS(I,1))*ASW*RS/TSTAR*TS(I,1)/RSTAR/VEL
   30 USPAR(I)=U(NX,0)
      CONTINUE
      RETURN
      END
```

```
      SUBROUTINE PARCA(IBEG,JTOP,IRIGHT,PR,
     -    TSTAR,GR,RINFNON,DA,Q,E,FO,IPAR,IDA,VEL,RSTAR,ASTAR)
      COMMON/L1/DX(0:93),DY(0:50),NX,NY,NLE
      COMMON/L6/AA(0:93),BB(0:93),CC(0:93),DD(0:93),XX(0:93)
      COMMON/L8/DXP(0:500),DYP(0:100),UPAR(2,0:100),VPAR(2,0:100),
     -          TPAR(2,0:100,3),TS(0:570,2),USPAR(0:570),VSPAR(0:570)
      COMMON/L9/IBC,UBC(0:50),VBC(0:50),TBC(0:50,3)
      REAL DENS(2,0:100),GAV(2,0:100),GAT(2,0:100),ALPH(0:100),
     -     BETA(0:100),WFPAR(0:100)
C***************DENSITY, DIFFUSION PROPERTIES CALCULATED************
      NYPAR=NY+JTOP
      DO 120 I=1,IRIGHT
C-------------------BEGIN CALCULATION-----------------------------
      DX1=DXP(I)
      DO 10 J=0,NYPAR+1
C*THE FOLLOWING LINES ASSUME EQUATION OF STATE AND DIFF. COEFF.'S***
      DENS(1,J)=TSTAR/TPAR(1,J,1)
      GAV(1,J)=PR*TPAR(1,J,1)/TSTAR
   10 GAT(1,J)=TPAR(1,J,1)/TSTAR
C--------------------COMPUTE U-VELOCITY---------------------------
      DO 20 J=1,NYPAR
      DYU=(DYP(J+1)+DYP(J))/2.
      DYL=(DYP(J)+DYP(J-1))/2.
      DY2=DYU+DYL
      DMUDY=(  (GAV(1,J+1)-GAV(1,J))*DYL/DYU
     -       +(GAV(1,J)-GAV(1,J-1))*DYU/DYL )/DY2
      RHOVEE=DENS(1,J)*VPAR(1,J)
      RU01=DENS(1,J)*UPAR(1,J)/DX1
      RU02=RHOVEE*DYL/DYU/DY2
      RU03=RHOVEE*DYU/DYL/DY2
      RU04=2.*GAV(1,J)/DY2/DYL
      RU05=2.*GAV(1,J)/DY2/DYU
      RU06=DYL/DYU/DY2*DMUDY
      RU07=DYU/DYL/DY2*DMUDY
      AA(J)=RU01-RU02+RU03+RU04+RU05+RU06-RU07
      BB(J)=     -RU02              +RU05+RU06
      CC(J)=           RU03+RU04          -RU07
   20 DD(J)=RU01*UPAR(1,J)+GR*(RINFNON-DENS(1,J))
C----------------SET BOUNDARY CONDITIONS FOR U-VELOCITY-------------
      AA(0)=1.
      BB(0)=0.
      DD(0)=USPAR(IBEG+I)
      CC(NYPAR+1)=0.
      AA(NYPAR+1)=1.
      DD(NYPAR+1)=UPAR(1,NYPAR+1)
      CALL TDMA(0,NYPAR+1)
      DO 30 J=0,NYPAR+1
   30 UPAR(2,J)=XX(J)
C--------------DETERMINE COEFFICIENTS FOR UPWIND SCHEME-------------
      DO 39 J=1,NY
      IF (VPAR(1,J+1).LT.0.) THEN
        ALPH(J)=1.
       ELSE
        ALPH(J)=0.
       ENDIF
      IF (VPAR(1,J-1).GT.0.) THEN
        BETA(J)=1.
       ELSE
```

```
          BETA(J)=0.
         ENDIF
      39 CONTINUE
C-----------------------COMPUTE T-----------------------------------
         DO 40 J=1,NYPAR
         DYU=(DYP(J+1)+DYP(J))/2.
         DYL=(DYP(J)+DYP(J-1))/2.
         DY2=DYU+DYL
         DMUDY=( (GAT(1,J+1)-GAT(1,J))*DYL/DYU
        -       +(GAT(1,J)-GAT(1,J-1))*DYU/DYL )/DY2
         RHOVEE=DENS(1,J)*VPAR(1,J)
         RU01=DENS(1,J)*UPAR(1,J)/DX1
         RU22=RHOVEE*ALPH(J)*2./DY2
         RU23=RHOVEE*(BETA(J)-ALPH(J))*2./DY2
         RU24=RHOVEE*(-BETA(J))*2./DY2
         RU04=2.*GAT(1,J)/DY2/DYL
         RU05=2.*GAT(1,J)/DY2/DYU
         RU06=DYL/DYU/DY2*DMUDY
         RU07=DYU/DYL/DY2*DMUDY
         WFST=Q*DA*TPAR(1,J,2)*TPAR(1,J,3)
        -       *DENS(1,J)*DENS(1,J)*EXP(-E/TPAR(1,J,1))
         AA(J)=RU01+RU23     +RU04+RU05+RU06-RU07+WFST*(2.-E/TPAR(1,J,1))
        -                                              /TPAR(1,J,1)
         BB(J)=     -RU22                +RU05+RU06
         CC(J)=     -RU24      +RU04                -RU07
      40 DD(J)=RU01*TPAR(1,J,1)+WFST*(3.-E/TPAR(1,J,1))
C-----------------SET BOUNDARY CONDITIONS FOR T-----------------------
         AA(0)=1.
         BB(0)=0.
         DD(0)=TS(IBEG+I,1)
         CC(NYPAR+1)=0.
         AA(NYPAR+1)=1.
         DD(NYPAR+1)=TPAR(1,NYPAR+1,1)
         CALL TDMA(0,NYPAR+1)
         DO 50 J=0,NYPAR+1
         IF (XX(J).GT.10.) XX(J)=10.
      50 TPAR(2,J,1)=CVMGT(XX(J),1.,XX(J).GT.1.)
         IF (I.EQ.1) THEN
           DO 51 J=0,NYPAR+1
C*THE FOLLOWING LINES ASSUME EQUATION OF STATE AND DIFF. COEFF.'S***
           GAV(2,J)=PR*TPAR(2,J,1)/TSTAR
      51   GAT(2,J)=TPAR(2,J,1)/TSTAR
         ENDIF
C-------------------CALCULATE NEW VALUES OF DENSITY-------------------
         DO 60 J=0,NYPAR+1
      60 DENS(2,J)=TSTAR/TPAR(2,J,1)
C-------------------COMPUTE YF-----------------------------------------
         DO 70 J=1,NYPAR
         DYU=(DYP(J+1)+DYP(J))/2.
         DYL=(DYP(J)+DYP(J-1))/2.
         DY2=DYU+DYL
         DMUDY=( (GAT(1,J+1)-GAT(1,J))*DYL/DYU
        -       +(GAT(1,J)-GAT(1,J-1))*DYU/DYL )/DY2
         RHOVEE=DENS(1,J)*VPAR(1,J)
         RU01=DENS(1,J)*UPAR(1,J)/DX1
         RU22=RHOVEE*ALPH(J)*2./DY2
         RU23=RHOVEE*(BETA(J)-ALPH(J))*2./DY2
         RU24=RHOVEE*(-BETA(J))*2./DY2
```

```
      RU04=2.*GAT(1,J)/DY2/DYL
      RU05=2.*GAT(1,J)/DY2/DYU
      RU06=DYL/DYU/DY2*DMUDY
      RU07=DYU/DYL/DY2*DMUDY
      RU08=-DA*TPAR(1,J,3)*DENS(2,J)*DENS(2,J)*EXP(-E/TPAR(2,J,1))
      AA(J)=RU01+RU23      +RU04+RU05+RU06-RU07-RU08
      BB(J)=     -RU22           +RU05+RU06
      CC(J)=     -RU24      +RU04          -RU07
   70 DD(J)=RU01*TPAR(1,J,2)
C-----------------SET BOUNDARY CONDITIONS FOR YF----------------------
C*******************ASSUMED LEF=LEO=1*********************************
      TE1=DENS(2,0)*VSPAR(IBEG+I)*DYP(1)/
     -   ( GAMMAT(TPAR(2,1,1),2,TSTAR)+GAMMAT(TPAR(2,0,1),2,TSTAR) )
      AA(0)=1.+TE1
      BB(0)=1.
      DD(0)=TE1
      CC(NYPAR+1)=0.
      AA(NYPAR+1)=1.
      DD(NYPAR+1)=TPAR(1,NYPAR+1,2)
      CALL TDMA(0,NYPAR+1)
      DO 80 J=0,NYPAR+1
   80 TPAR(2,J,2)=CVMGT(XX(J),0.,XX(J).GT.0.)
C-------------------COMPUTE YO-----------------------------------------
      DO 90 J=1,NYPAR
      DYU=(DYP(J+1)+DYP(J))/2.
      DYL=(DYP(J)+DYP(J-1))/2.
      DY2=DYU+DYL
      DMUDY=(  (GAT(1,J+1)-GAT(1,J))*DYL/DYU
     -       +(GAT(1,J)-GAT(1,J-1))*DYU/DYL )/DY2
      RHOVEE=DENS(1,J)*VPAR(1,J)
      RU01=DENS(1,J)*UPAR(1,J)/DX1
      RU22=RHOVEE*ALPH(J)*2./DY2
      RU23=RHOVEE*(BETA(J)-ALPH(J))*2./DY2
      RU24=RHOVEE*(-BETA(J))*2./DY2
      RU04=2.*GAT(1,J)/DY2/DYL
      RU05=2.*GAT(1,J)/DY2/DYU
      RU06=DYL/DYU/DY2*DMUDY
      RU07=DYU/DYL/DY2*DMUDY
      RU08=-FO*DA*TPAR(2,J,2)*DENS(2,J)*DENS(2,J)*EXP(-E/TPAR(2,J,1))
      AA(J)=RU01+RU23      +RU04+RU05+RU06-RU07-RU08
      BB(J)=     -RU22           +RU05+RU06
      CC(J)=     -RU24      +RU04          -RU07
   90 DD(J)=RU01*TPAR(1,J,3)
C-----------------SET BOUNDARY CONDITIONS FOR YO----------------------
C*******************ASSUMED LEF=LEO=1*********************************
      TE1=DENS(2,0)*VSPAR(IBEG+I)*DYP(1)/2./GAMMAT(TPAR(2,1,1),3,TSTAR)
      AA(0)=1.+TE1
      BB(0)=1.
      DD(0)=0.
      CC(NYPAR+1)=0.
      AA(NYPAR+1)=1.
      DD(NYPAR+1)=TPAR(1,NYPAR+1,3)
      CALL TDMA(0,NYPAR+1)
      DO 100 J=0,NYPAR+1
      IF (XX(J).GT.XX(NYPAR+1)) XX(J)=XX(NYPAR+1)
  100 TPAR(2,J,3)=CVMGT(XX(J),0.,XX(J).GT.0.)
C----------------------COMPUTE V-VELOCITY----------------------------
      VPAR(2,0)=VSPAR(IBEG+I)
```

```
      DO 110 J=0,NYPAR
      DYU=(DYP(J+1)+DYP(J))/2.
  110 VPAR(2,J+1)=(-UPAR(2,J+1)+DENS(1,J+1)/DENS(2,J+1)*UPAR(1,J+1))
     -             *DYU/DX1+DENS(2,J)/DENS(2,J+1)*VPAR(2,J)
C-----------------SET B.C.'S FOR ELLIPTIC REGION----------------------
      IF (IBC.NE.1) GO TO 114
      IF ((IBEG+I.EQ.NX+1).OR.((IBEG.EQ.NX+1).AND.(I.EQ.1))) THEN
        DO 113 J=1,NY
        GVAVE=(GAV(1,J)+GAV(2,J))/2.
        GTAVE=(GAT(1,J)+GAT(2,J))/2.
        UBC(J)=GVAVE*(UPAR(2,J)-UPAR(1,J))/DX1
        VBC(J)=GVAVE*(VPAR(2,J)-VPAR(1,J))/DX1
        TBC(J,1)=GTAVE*(TPAR(2,J,1)-TPAR(1,J,1))/DX1
        TBC(J,2)=GTAVE*(TPAR(2,J,2)-TPAR(1,J,2))/DX1
  113   TBC(J,3)=GTAVE*(TPAR(2,J,3)-TPAR(1,J,3))/DX1
      ENDIF
C---------------------SET TS(2) VALUES---------------------------
  114 TS(IBEG+I,2)=TPAR(2,1,1)
C---------------OPTIONALLY WRITE DATA-----------------------------
      IF (IPAR.EQ.1) THEN
        WRITE(31,900) (UPAR(2,J),J=0,NY+1+JTOP)
        WRITE(32,900) (VPAR(2,J),J=0,NY+1+JTOP)
        WRITE(33,900) (TPAR(2,J,1),J=0,NY+1+JTOP)
        WRITE(34,900) (TPAR(2,J,2),J=0,NY+1+JTOP)
        WRITE(35,900) (TPAR(2,J,3),J=0,NY+1+JTOP)
         IF (IDA.EQ.1) THEN
           PREF=DA*VEL*VEL*RSTAR/ASTAR
           DO 112 J=0,NY+1+JTOP
           WFPAR(J)=PREF*DENS(2,J)*DENS(2,J)*TPAR(2,J,2)*TPAR(2,J,3)*
     -              EXP(-E/TPAR(2,J,1))
           IF (WFPAR(J).LT.1.E-78) WFPAR(J)=0.
  112      CONTINUE
           WRITE(36,900) (WFPAR(J),J=0,NY+1+JTOP)
        ENDIF
      ENDIF
C---------------------RESET VALUES-------------------------------
      DO 116 J=0,NY+1+JTOP
      UPAR(1,J)=UPAR(2,J)
      VPAR(1,J)=VPAR(2,J)
      TPAR(1,J,1)=TPAR(2,J,1)
      TPAR(1,J,2)=TPAR(2,J,2)
  116 TPAR(1,J,3)=TPAR(2,J,3)
  120 CONTINUE
  900 FORMAT(1P,5(1X,E12.5))
      RETURN
      END
```

REPORT DOCUMENTATION PAGE

Form Approved
OMB No. 0704-0188

1. AGENCY USE ONLY (*Leave blank*)	2. REPORT DATE	3. REPORT TYPE AND DATES COVERED
	April 1993	Contractor Report

4. TITLE AND SUBTITLE

A Model of Concurrent Flow Flame Spread Over a Thin Solid Fuel

5. FUNDING NUMBERS

WU–674–22–05
G–NAG3–1046

6. AUTHOR(S)

Paul V. Ferkul

7. PERFORMING ORGANIZATION NAME(S) AND ADDRESS(ES)

Case Western Reserve University
Cleveland, Ohio 44106

8. PERFORMING ORGANIZATION REPORT NUMBER

E–7726

9. SPONSORING/MONITORING AGENCY NAMES(S) AND ADDRESS(ES)

National Aeronautics and Space Administration
Lewis Research Center
Cleveland, Ohio 44135–3191

10. SPONSORING/MONITORING AGENCY REPORT NUMBER

NASA CR–191111

11. SUPPLEMENTARY NOTES

Project Manager, Kurt Sacksteder, Space Experiments Division, NASA Lewis Research Center, (216) 433-2857. A similar version of this report was submitted by Paul V. Ferkul as a dissertation in partial fulfillment of the requirements for the degree of Doctor of Philosophy of Mechanical and Aerospace Engineering to Case Western Reserve University, Cleveland, Ohio.

12a. DISTRIBUTION/AVAILABILITY STATEMENT

Unclassified - Unlimited
Subject Category 29

12b. DISTRIBUTION CODE

13. ABSTRACT (*Maximum 200 words*)

A numerical model is developed to examine laminar flame spread and extinction over a thin solid fuel in low-speed concurrent flows. The model provides a more precise fluid-mechanical description of the flame by incorporating an elliptic treatment of the upstream flame stabilization zone near the fuel burnout point. Parabolic equations are used to treat the downstream flame, which has a higher flow Reynolds number. The parabolic and elliptic regions are coupled smoothly by an appropriate matching of boundary conditions. The solid phase consists of an energy equation with surface radiative loss and a surface pyrolysis relation. Steady spread with constant flame and pyrolysis lengths is found possible for thin fuels and this facilitates the adoption of a moving coordinate system attached to the flame with the flame spread rate being an eigenvalue. Calculations are performed in purely forced flow in a range of velocities which are lower than those induced in a normal gravity buoyant environment. Both quenching and blowoff extinction are observed. The results show that as flow velocity or oxygen percentage is reduced, the flame spread rate, the pyrolysis length, and the flame length all decrease, as expected. The flame standoff distance from the solid and the reaction zone thickness, however, first increase with decreasing flow velocity, but eventually decrease very near the quenching extinction limit. The short, diffuse flames observed at low flow velocities and oxygen levels are consistent with available experimental data. The maximum flame temperature decreases slowly at first as flow velocity is reduced, then falls more steeply close to the quenching extinction limit. Low velocity quenching occurs as a result of heat loss. At low velocities, surface radiative loss becomes a significant fraction of the total combustion heat release. In addition, the shorter flame length causes an increase in the fraction of conduction downstream compared to conduction to the fuel. These heat losses lead to lower flame temperatures, and ultimately, extinction. This extinction mechanism differs from that of blowoff, where the flame is unable to be stabilized due to the high flow velocity.

14. SUBJECT TERMS	15. NUMBER OF PAGES
Combustion; Flame spread; Microgravity combustion; Elliptic equations; Flame extinction	145
	16. PRICE CODE: A07

17. SECURITY CLASSIFICATION OF REPORT	18. SECURITY CLASSIFICATION OF THIS PAGE	19. SECURITY CLASSIFICATION OF ABSTRACT	20. LIMITATION OF ABSTRACT
Unclassified	Unclassified	Unclassified	